

Pontificia Universidad Católica del Perú
Escuela de Posgrado

Determination of the signals recorded by carpal vibrissae of rats during locomotion and forelimb touch down

Thesis to achieve the Degree of: Master of Science (M.
Sc.) In Mechatronics

Presented by: Sebastian Müller
Born am: 08.06.1991
Transit: Mechatronik
Matriculation number: 52116

Responsible Professor (TU Ilmenau): Univ.-Prof. Dr.-Ing. habil. Klaus Zimmermann
Responsible Professor (PUCP Lima): Prof. Dr. Jorge Hernan Alencastre Miranda
Supervisor (TU Ilmenau / PUCP Lima): M.Sc. Moritz Scharff

Registered on: 01.11.2019

Conceptual Formulation of the Master Thesis

of Mr. Sebastian Müller, BSc.

Topic: Determination of the signals recorded by carpal vibrissae of rats during locomotion and forelimb touch down.

The master thesis complements the current research activities at the Group of Biomechanics and Technical Mechanics Group of the Technische Universität Ilmenau, as well as the activities of the Section of Mechanical Engineering of the Pontifical Catholic University of Peru. The focus is on non-visual characterization of objects using tactile sensors, which are inspired by animal vibrissae.

The aim is to develop models of carpal vibrissae of rats which are used to characterize the contact between carpal vibrissae and surface during locomotion. The signals recorded by carpal vibrissae have an influence on the kinematics of legs during locomotion of rats. Combining motion studies, anatomic and mechanical properties of the carpal vibrissae in an inverse-dynamic model, the signals at the base of the carpal vibrissae can be determined by numerical simulation. This knowledge might lead to new approaches for passive sensor systems in robot locomotion or other tactile tasks.

Tasks of the master thesis are:

- to become acquainted with the corresponding literature;
- to set up a numerical simulation using method of multi-body dynamics;
- to include the motion trajectories of a forelimb of a rat (pre-existing experiments)
- to perform parameter studies to identify information about the "vibrissa-surface" contact;
- in addition: incorporate pre-curvature, conicity of the hair shafts, maybe a varying modulus of elasticity.

The master thesis shall be designed using LaTeX, all necessary files (LaTeX files, Matlab files, figures, pictures, drawings, literature files, ...) have to be put on a supplementing CD.

Date of issue: 01.11.2019

Responsible Professor (TU Ilmenau): Univ.-Prof. Dr.-Ing. habil. Klaus Zimmermann

Responsible Professor (PUCP Lima): Prof. Dr. Jorge Hernan Alencastre Miranda

Supervisor (TU Ilmenau / PUCP Lima): M.Sc. Moritz Scharff

Ilmenau, 9.10.19

Location, Date

K. Zimmermann

Signature of the responsible professor TU Ilmenau

Lima, 27 September 2019

Location, Date

J. Alencastre

Signature of the responsible professor PUCP Lima

Lima, 16. 10. 19

Location, Date

S. Müller

Signature of the student

Declaration

I certify that I have written the presented work independently by me. I have marked all passages that are taken literally or analogously from published or unpublished works of others as taken. All sources and aids that I have used for the work are indicated. The work has not yet been submitted to any other examination authority with the same contentor in essential parts. The following persons have been involved in this work in the manner described:

- The verification was done in cooperation with my fellow student Stefan Eckhardt.

Ilmenau, 22.06.2020

Sebastian Müller

Kurzfassung

Verschiedene Säugetiere, so auch Ratten, verfügen an ihren Pfoten über Tasthaare, die sog. karpalen Vibrissen. Untersuchungen der Fortbewegung von Ratten haben gezeigt, dass der Kontakt zwischen den karpalen Vibrissen und dem Untergrund Einfluss auf das Fortbewegungsverhalten der Tiere hat. Karpale Vibrissen bestehen aus einem Haarschaft und einem Follikel. Der Haarschaft ist lang, schlank, elastisch und im Follikel gelagert, in dem sich die Mechanorezeptoren befinden. Ausgehend von Vorarbeiten der Fachgebiete Biomechatronik und Technische Mechanik der Technischen Universität Ilmenau sowie der Section of Mechanical Engineering, Pontifical Catholic University of Peru, wurde ein mechanisches Modell einer karpalen Vibrisse erstellt. Zielsetzung der vorliegenden Arbeit ist es, die im Follikel wirkenden Kräfte und Momente während der Fortbewegung einer Ratte zu bestimmen. Aus den ermittelten Signalen sollen Rückschlüsse auf die Beschaffenheit des Kontaktes zwischen Haarschaft und Oberfläche gezogen werden. Hierzu wurde die in einer Vorarbeit ermittelte Bewegungsbahn einer Rattenpfote mit dem in dieser Arbeit erstellten mechanischen Modell kombiniert. Die daraus entstandene invers dynamische Analyse wurde im Mehrkörpersimulationsprogramm *ALASKA* durchgeführt. Da nicht alle Eigenschaften und Parameter des biologischen Vorbilds bekannt sind, wurden z.B. der Reibkoeffizient, die Lagerungseigenschaften oder die Materialeigenschaften des Haarschaftes variiert. Als Ergebnis der durchgeführten Parameterstudien konnten verschiedene Einflüsse bestätigt werden. Hierbei zeigen sich u. a. Effekte wie eine Änderung der Signalstärke sowie Änderungen in der Kontaktzeit.

Abstract

Various mammals, e.g. rats, have tactile hairs on their paws, the so-called carpal vibrissae. Studies of the locomotion of rats have shown that the contact between the carpal vibrissae and the ground have an influence on the locomotion behaviour of the animals. Carpal vibrissae consist of a hair shaft and a follicle. The hair shaft is long, slender, elastic and is located in the follicle. The follicle includes the mechanoreceptors. A mechanical model of a carpal vibrissa was designed on the basis of preliminary works from the Biomechatronics Group and Technical Mechanics Group of the Technische Universität Ilmenau and the Section of Mechanical Engineering, Pontifical Catholic University of Peru. The objective of the present work is to determine the forces and moments acting in the follicle during the locomotion of a rat. From the determined signals, conclusions could be drawn about the nature of the contact between hair shaft and surface. For this purpose, the in a preliminary work determined trajectory of a rat's paw was combined with the in this work created mechanical model. The resulting inverse dynamic analysis was performed in the multi-body simulation program *ALASKA*. Since not all properties and parameters of the biological model are known, e.g., the coefficient of friction, the support characteristics or the material properties of the hair shaft were varied. As a result of the parameter studies, various influences could be confirmed. Amongst other things, effects had been shown, such as a change in signal strength and changes in contact time.

Contents

1	Introduction	1	
2	Biological model	4	
	2.1	Vibrissae 5	
	2.1.1	Functions 7	
2.1.2	Occurrence of vibrissae in rats.....	9	
	2.2	Motion sequence 11	
	2.2.1	Skeletal structure 11	
2.2.2	Forelimbs and joint types.....	13	
	2.2.3	Muscles 15	
3	State of the art	18	
3.1	Application and functional principle of tactile sensors.....	18	
3.2	Model of an artificial vibrissae.....	19	
3.3	Coulomb's friction theory.....	22	
3.4	Simulation methods.....	23	
	3.4.1	Finite element method 24	
	3.4.2	Multibody systems 25	
	3.4.3	Conclusion 26	
4	Objectives	27	
5	Model structure	29	
	5.1	Motion analysis 30	
	5.1.1	Pedipulator 30	
	5.1.2	Motion Trajectory 31	
5.2	Model parameters.....	31	
	5.2.1	Abstraction levels of the model.....	33

5.3	Modelling of the beam/vibrissae.....	34
5.4	Clamping of the beam/vibrissae	35
5.5	Trajectory presetting of the beam/vibrissae	36
5.6	Verification of the simulation models.....	37
6	Results	47
6.1	Reproducibility of motion	47
6.2	Surface scanning with fixed clamping.....	49
6.2.1	Variation of the coefficient of friction	53
6.2.2	Variation of object distance	55
6.2.3	Variation of fixing angle	57
6.2.4	Variation of surface slope.....	59
6.2.5	Variation of Young’s Modulus	61
6.3	Surface scanning with elastic bearing	62
6.3.1	Variation of spring stiffness	64
6.3.2	Variation of the coefficient of friction	66
6.3.3	Variation of object distance	67
6.3.4	Variation of fixing angle	69
6.3.5	Variation of surface slope.....	70
6.3.6	Variation of Young’s Modulus	71
	6.4 Conclusion	72
7	Summary and Outlook	74
	Bibliography	83
A	Bearing reactions for directional and angular forces	88
B	Muscles of the front extremity and their function	90

List of symbols

Symbol	Meaning
A	Cross-sectional area of the beam
a	Acceleration
\dot{C}	Vector of constraints
\dot{C}_q	Derivation of the constraints by generalized coordinates
c	Spring stiffness
c_x	Spring stiffness in x direction
c_y	Spring stiffness in y direction
D	Damping matrix
D_R	Proportionality factor between stiffness matrix and Damping matrix
d_x	Damping term in x direction
d_y	Damping term in y direction
E	Young's modulus
\vec{F}	Force vector
F_N	Normal force
F_R	Friction
F_{Ri}	Directional stability
F_{Wi}	Angular Force
F_x	Bearing force in x direction
F_y	Bearing force in y direction
G	Sliding modulus
\dot{g}	Gravitational constant
I_z	Equatorial moment of inertia
J	Inertial matrix
K	Stiffness matrix
K	Contact point between beam and object

Symbol	Meaning
L	Length of beam
M	Mass matrix
\dot{M}	Moment vector
M_z	Bearing torque about z axis
m	Mass
\dot{u}	State vector of the MKS system equation
\dot{P}	Outside forces
\dot{q}	Generalized coordinates
R	Outer radius of beam
R_k	Radius of circle
R_i	Inner radius of beam
S_1	Force application point
$Trans$	Path of translational scanning
$TransVel$	Translational scanning speed
$TransAcc$	Translational scanning acceleration
t	time
t_{end}	End Time
t_{Step}	StepTime
t_{step}	Time of acceleration process
$g(x)$	Object contour
g_1	Object contour of circle
g_2	Object contour from the ramp
q	Relative distance to contact surface
v	Speed
$x_{Abstand}$	Shift in x direction
x_E	x -Coordinate clamping of the beam
x_{g1}	x -Coordinate of the circle point
x_{g2}	x -Coordinate of the ramp contour
x_k	Center position in x -coordinate
x_{Kp}	x -Coordinate of the contact point
x_{cut}	x -Coordinate of first contact
x_v	Control value for object scanning
y_E	y -Coordinate clamping of the beam
y_k	Center position in y -coordinate
y_{Kp}	y -Coordinate of the contact point
α	Force application angle
$\alpha_{g2,an}$	Angle of slope of ramp contour
$\alpha_{g2,ab}$	Angle of slope of ramp contour
β	Fixing angle of the beam
ϕ	Angle of surface slope
$\dot{\lambda}$	Langrange multiplier

Symbol	Meaning
ρ	Density
μ	Coefficient of friction
μ_{kin}	Coefficient of sliding friction
μ_{sta}	Coefficient of static friction
ν	Cross-contraction number
$\dot{\omega}$	Angular velocity



CHAPTER 1

Introduction

In order to find new innovations and approaches to solutions, the proverbial view must be taken beyond the horizon in the sense of treading previously unknown ground. Thanks to technical progress, it is possible to completely reassess and use knowledge from nature. The structures and principles that have emerged in the course of evolution can be used to solve technical challenges through scientific evaluation.

In this respect, however, the inspiration of biology alone is not enough. Rather, the biological phenomena must be analysed and understood in detail before technology can make use of the knowledge gained. An exact copy of the natural model into technology is not intended [Bau89].

The physical principle of action is to be interpreted by forming a model with technical terms and to be elucidated with the respective methods of technical science. In this way, biological principles of action are transferred to technology. By means of this abstraction and the creation of models of biological functions, natural systems can be understood. From such an interdisciplinary science, biological knowledge, i.e. biomechanics, has developed further into biomechatronics in recent years. However, this also results in an increased need for control in order to operate these biomechatronic components with each other. This increased need for control results in increasing sensorisation. Modern technical devices in particular are

dependent on a variety of information in order to be able to perform their tasks correctly. Such information does not only refer to the own state and position of the device, but also to information from the environment. Meanwhile, sensors can be found in all components of highly integrated mechatronic systems. The increase in performance is possible through conclusions from biology and the further development of numerical simulation programs [Sen97]. Modern simulation techniques enable the saving of time, development costs and resources. Mechanical motion sequences and other technical processes can be mathematically reproduced with the help of computers. Computer simulations make it possible to adequately meet the demands for shortened development and test phases. A shortened development time is thus made possible by sophisticated simulation tools. The industry, for example, makes use of these elements in many areas - whether construction, design or production [Sen97].

New types of measuring devices can be tactile sensors that make it possible to detect objects. They are of particular importance if, for example, sensor systems with optical processes fail or their use is restricted. The origin of tactile sensor technology is derived from nature, as shown in Fig. 1.1. This sensor technology is often associated with rodents, dogs and cats. For example, in biology the whiskers of a cat are also called vibrissae or sinus hairs. These are specialised in the perception of tactile stimuli and are also found in rodents. The sinus hairs are usually found in specific places (see figure 2.5). These are anchored in the skin and the underlying tissue. The best known type of tactile hairs are the whiskers (mystacial vibrissae) on the muzzle of the animals. On the paws of the animals there are the so-called carpal vibrissae, which enable e.g. rats to orientate themselves during locomotion.

Research is currently being conducted in the field of biomechatronics with regard to sinus hairs, but the exact functions of the carpal vibrissae at the corresponding points have not yet been fully clarified.

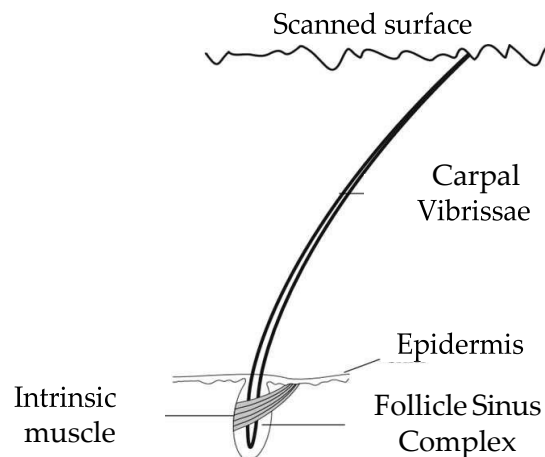


Figure 1.1: Schematic drawing of a vibrissa on a rough surface [SWZ⁺14].

The aim of this work is to develop a technical model from a biological model of a carpal vibrissa. The modelled carpal vibro-vibrissae should follow a recorded trajectory. The trajectory simulates the movement of a rat ankle to which the hair is attached (see figure 5.1). This trajectory was derived from the natural model of the front limb of a rat. The resulting kinematics, i.e. the local change of the body points to be observed over a certain period of time, was described in a previous research paper entitled „Kinematics of spatial guidance of carpal vibrissae“ [Ber14] at the TU Ilmenau made by Mrs Van den Berg in the department of biomechatronics. The knowledge gained from this work forms the basis of the present paper. Based on this trajectory, these results are to be implemented in the present work in a multi-body simulation program (*ALASKA*) for an inverse-dynamic model. From this, information about the surface condition by means of a carpal vibrissa is to be obtained. In order to be able to describe the motion sequence, the biological model of a rat and its properties will be investigated first. Special emphasis will be put on the bone structure, the structure of the muscles of the front extremities and the structure of the sinus hair, especially the capillary vibrissae. These are implemented in the computer environment (*ALASKA*). Various parameter studies are then carried out. From the knowledge gained from these studies it will be possible to draw conclusions for the use of passive sensor systems.

Biological model

Rats are often used as model organisms in biological analyses and experiments. Due to their similarity to other mammals, rats are widely used in biomedical research [LM10]. In addition, they can adapt to many different experimental conditions and are therefore suitable for repeated experiments. Another advantage, in terms of motion analysis, is the ability of rats to move on any surface. This provides, among other things, the possibility of varying the substrates during locomotion in order to observe the behavior of carpal sinus hairs during a step cycle of a rat [BCD⁺17].

In order to be able to evaluate and assess the foreleg and the incoming signals of the carpal vibracles metrologically, the basics for the general understanding of biology are now presented. Thus it is possible to use the abstraction of the biological view for the technical aspect. This in turn is necessary to develop new approaches for passive sensor systems in robot locomotion or other tactile tasks.

The bone structure, the movement of the front extremity and the respective hair characteristics are described below. Furthermore, the nature of a vibrissa from the tip of the hair to its rooting in the follicle-sinus-complex (FSC) is explained in more detail.

2.1 Vibrissae

Vibrissae are special tactile hairs that occur in a variety of mammals (e.g. rats, seals, cats, etc.). In figure 2.1 the mystacial vibrissae (left) and the carpal vibrissae (right) are shown using the example of a rat. They are used for orientation and perception of objects and their properties in the animals habitat.



Figure 2.1: Occurrence of vibrissae in rats; left: snout of a rat with mystacial vibrissae; right: anterior extremity of a rat with carpal vibrissae [LM10, ARF95]

Vibrissae basically consist of the cuticle, cortex and medulla layer. Although the medulla is hollow, the vibrissae in mechanical models are often regarded in the literature as solid material [Har15]. Vibrissae are conically shaped (see figure 2.2). This results in varying stiffness over the length of the hair [VCK⁺12].

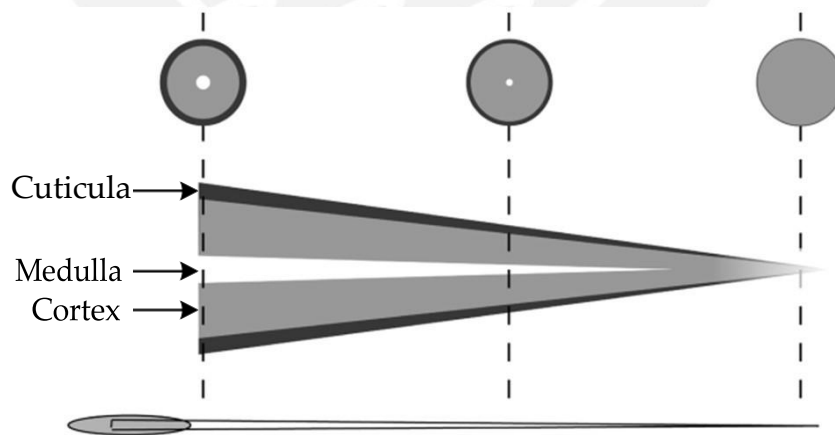


Figure 2.2: Morphology of a vibrissa according to [VCK⁺12].

Furthermore, vibrissae have an intrinsic curvature, which is usually simplified by quadratic or parabolic functions implemented in the different calculation models [Har15].

Vibrissae differ from other hairs by the respective depth of rooting, their thickness and length (see fig. 2.4). They consist of dead epidermal cells, which means that vibrissae do not have any stimulus receptors and only act as a transmitter of stimuli. They are deeply embedded in the surrounding tissue by the hair root. The anchoring is reinforced by the fibre bands which are located in the epidermis (see figure 2.3) and embedded in capsules, the so-called blood sinus. They consist of a sponge-like erectile tissue (cavernous sinus) in the lower area and an open ring sinus in the upper area. These areas are filled with blood. This leads to the hypothesis that the animals are able to variably adjust the elasticity of the anchorage by a change in blood pressure [Car09, Sch03]. The blood-filled tissue and the actual hair are summarized in the literature on FSC.

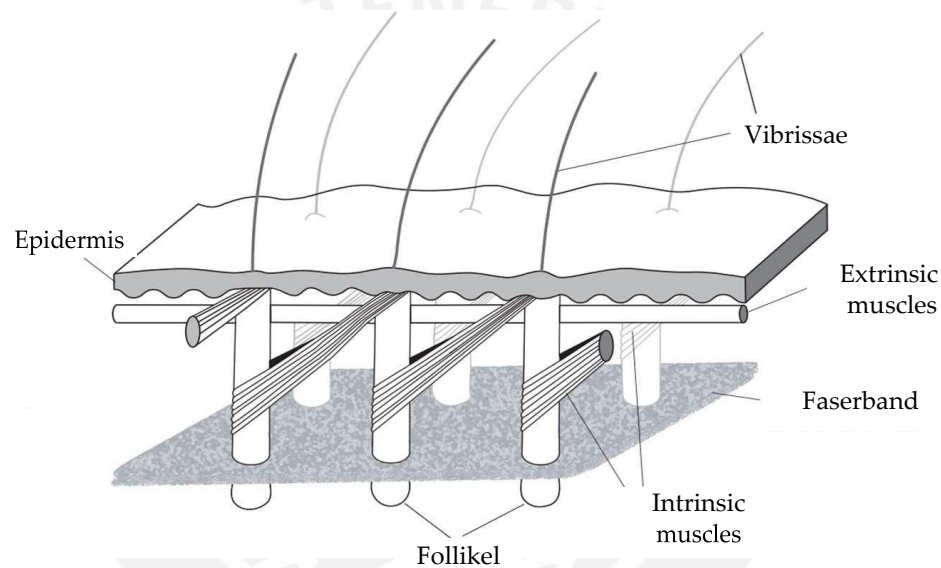


Figure 2.3: Vibrissae complex according to [BAW⁺17].

The evaluation of the forces and moments resulting from a deformation are recorded in the mechanoreceptors. These are located in the root area of the sinus hairs (see fig. 2.4) and convert the perceived mechanical stimuli into electrical impulses. These are transmitted to the central nervous system (ZNS), where the information is processed [Smi09].

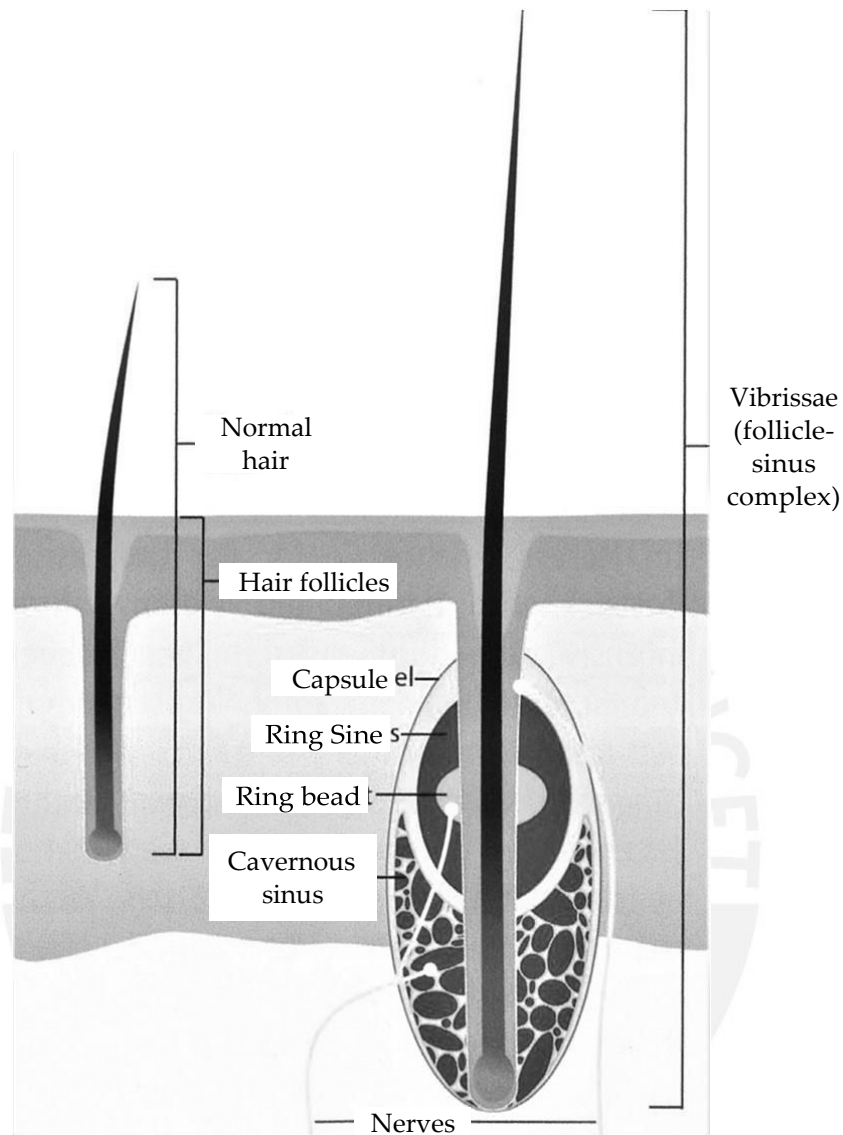


Figure 2.4: Comparison of an ordinary hair and a follicle-sinus-complex according to [Wel18].

2.1.1 Functions

Depending on the body part in the root area, an FSC can be enclosed by a muscle loop, which initiates an oscillating movement of the vibrissa by specific contraction [Car09]. During such a movement, the vibrissae are moved forward or backward by the intrinsic muscle. Both the frequency and amplitude can be adjusted accordingly [Car09]. This possibility of rodents to actively move their tactile hairs results in different scanning possibilities [Car09, MGA⁺11]:

- Passive scanning: in this state the rat's vibrissae are not actively moved, a vibrissae deformation occurs only due to external forces [Car09];
- twitching: the vibrissae are moved at a frequency of 7-12 Hz [MGA⁺11];
- Active scanning: rhythmic movements with a large amplitude and a frequency of 5-15 Hz appear to find objects (e.g. food) [Car09];
- Foveal Whisking: the vibrissae are stretched forward by muscle contraction and oscillate with a low amplitude at a frequency of 15-25Hz, serves to perceive immobile objects [BK03].

When exploring, five different tasks and functions can be realized. These are explained in detail in the table 2.1 [BK03]:

Table 2.1: Functions of the vibrissae.

Function	Description
Localization	With the help of vibrissae it is possible for the animals to recognize the relative position of objects/gaps to the body at any time [AK11].
Object Sizes	Rats can determine the size of objects to within a few millimeters using their vibrissae [KMB ⁺ 01].
Detection of objects	rats mainly use the microvibrissae for object detection, while the macrovibrissae are more suitable for spatial Orientation serve [BPM96].
Surface structures	rats can detect surface structures of up to 30 μm size and 90 μm intervals, which is comparable to the sensitivity of a human finger [CS90].
Distances	rats can estimate distances of objects up to 160 mm [HM86] by their vibrissae alone.

For interactions with the environment, several functions listed in the table 2.1 can be combined. The functions of the vibrissae are sometimes supplemented or completely taken over by other senses.

2.1.2 Occurrence of vibrissae in rats

Vibrissas are found on various parts of the rat's body, such as the underside of the legs, the side of the body, above the eyes, and to varying degrees around the muzzle of the animal [SK87].

Probably the best known tactile hairs are the mystacial vibrissas - a subgroup of the vibrissas, which occur more frequently in the snout region (mystacial) of the animals. There is also a subgroup of vibrissae on the paws, these are called carpal vibrissas. In figure 2.5 further examples of tactile hairs of a rat are shown [Kla99]. In the following, mystacial vibrissas (as the best known sinus hair of this group) and the carpal vibrissas are presented. Due to their lack of relevance for this work, a detailed description of the other types of vibrissae is not given.

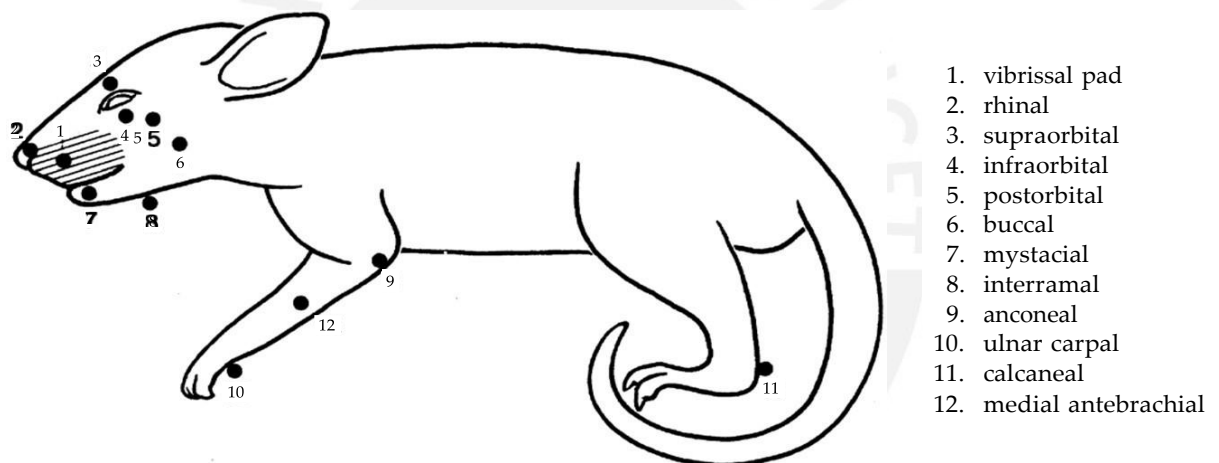


Figure 2.5: Occurrence of sinus hairs in a rat after [Kla99].

Mystacial vibrissas

In the snout area of the rat, the figure 2.5 shows an accumulation of vibrissas. The arrangement of these hairs follows a certain pattern in many species. The so-called vibrissal pad (see figure 2.6), this is divided into characteristic rows and columns. The differences in the lengths of the vibrissal pads (macro and micro vibrissae), which occur in the muzzle area, are used to perform various tasks, such as spatial orientation and object recognition [VCK⁺12].

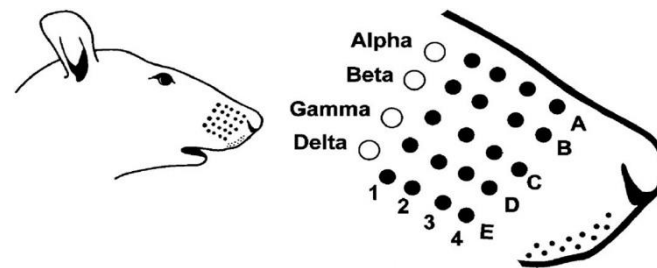


Figure 2.6: Arrangement of the mystacial vibrissae [VCK⁺12].

Carpal Vibrissae

Other important sinus hairs are the carpal vibrissae, which are located on the front extremities of the rat. Rodents have three of these tactile sensors per anterior limb (see fig. 2.7). The carpal vibrissae are approximately 5-10 mm long and can be distinguished, also optically, very well from other fur hairs [ARF95]. Furthermore, the carpal and mystacial vibrissae differ in that the mystacial vibrissae have a higher sensitivity. Furthermore, carpal vibrissae cannot be actively moved. There are no significant differences in the structure of the actual vibrissae and their embedding in the skin [ARF95]. On closer examination, however, there are differences in the carpal vibrissae:

- fewer mechanoreceptors than in the mystacial vibrissae and thus reduced sensitivity [GIY73, SWZ⁺14];
- deviations in the typical FSC pattern [SWZ⁺14];
- a reduced formation of the medulla layer [SWZ⁺14];
- no direct connection to the nerve endings of the inner conical body [SWZ⁺14].

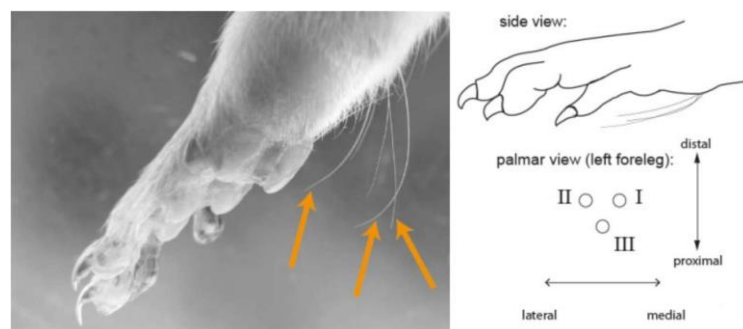


Figure 2.7: Carpal vibrissae of a rat [SWZ⁺14].

2.2 Motion sequence

In order to be able to make a statement about the behavior of capal vibrissae of a rat during locomotion, it is necessary to know information about the different gaits. For this reason, various methods of locomotion and the associated movement sequences are described below in Table 2.2 [Sch01]:

Table 2.2: Types of locomotion of a rat [Sch01].

Type of Movement	Description
Crawling	the rat lies on its side or belly, pulling with its front legs and pushing with its hind legs
Walking	forward or backward; one or two extremities are lifted one after the other and led sideways to the front; the body has a small distance to the ground; tail is pulled behind or carried horizontally; stride length during normal walking $\Delta x \approx 5 - 6 \text{ cm}$
Tripping	walking movement; hind limbs are more extended than front limbs; tail does not touch the ground
Trot	diagonal gait; when trotting, two or four limbs alternately without ground contact; tail without ground contact; head always in direction of movement
Running	fastest way of locomotion; increase in stride size by bending the back and stretching the extremities; tail without ground contact; head straight ahead
Bounce	shape of the race, with lower speed and stride size
Jumping	the back is bent, the rear extremities are first bent and then quickly stretched out; after a jump the rat lands on the front extremities
Stroll	mix of tripping and bouncing; variable speed; sudden changes of direction and sideways jumps possible; ends abruptly
Swimming	same movement as walking, but in water; diving is also possible
Climbing	locomotion, walking, running or hanging on inclined, vertical or horizontal planes; tail in object contact or used for balancing

2.2.1 Skeletal structure

In the following, the most necessary basics about the skeletal structure of the musculoskeletal system of rats will be described in order to be able to carry out an investigation based on a measured trajectory within the scope of this work.

The locomotor system of rodents is divided into the passive and active locomotor system [LM10]:

- Active locomotor system: serves the movement, consists of the skeletal muscles and other auxiliary components (e.g. tendons and fasciae);
- Passive locomotor system (supporting apparatus): serves to support or shape the body and consists of the skeleton (e.g. bones and joints).

To describe the musculoskeletal system, the anatomy of the animal is first described, see figure 2.8.

The spinal column of the rat comprises seven cervical vertebrae, 13 thoracic vertebrae, seven lumbar vertebrae, the sacrum, and a large number of caudal vertebrae. The shoulder girdle consists of the scapula and a collar bone. The front leg of a rat has four fingers; the hind leg ends with five toes [LM10].

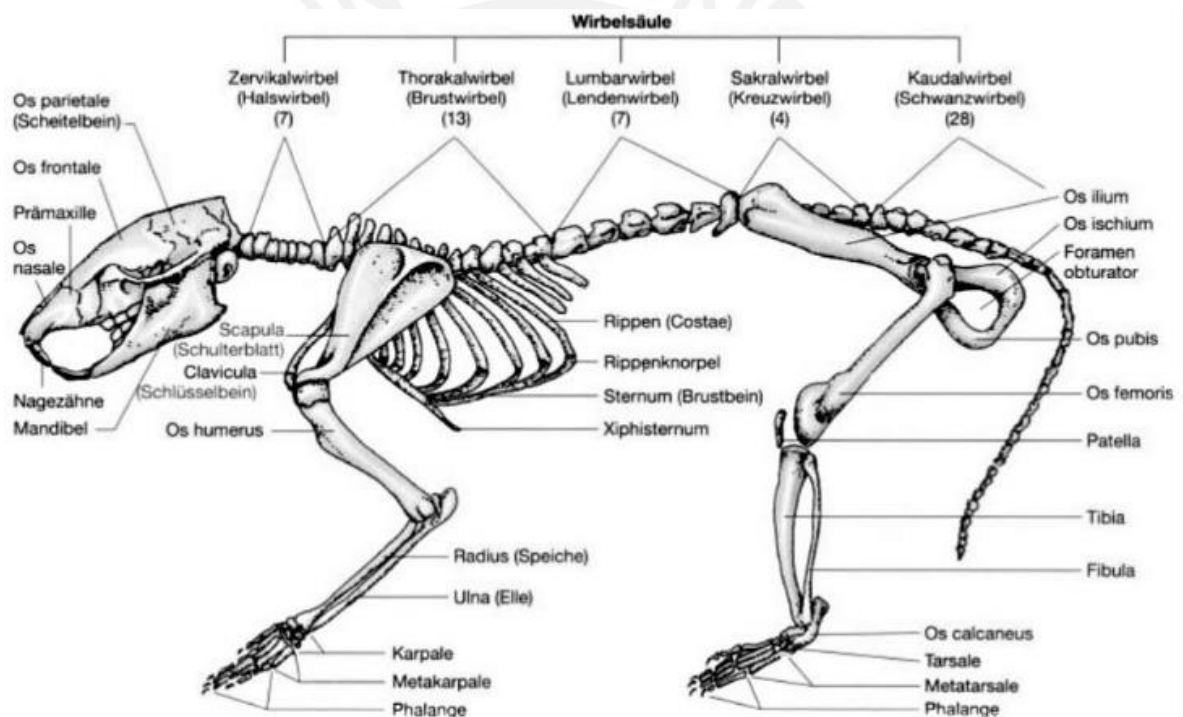


Figure 2.8: Skeletal structure of a rat [LM10].

The term „extremities“ comes from Latin (*extremitates corporis*) and means „limbs, body appendages of animals and humans, which primarily serve the locomotion and are usually attached laterally to ventrally to the trunk“. Extremities are generally subdivided into several sections that can move against each other and against the trunk, and are used as levers with a supporting, pushing or rowing function during locomotion (biomechanics) [Leh99].

2.2.2 Forelimbs and joint types

In addition to the skeletal structure, it is also necessary to be able to reproduce the motion sequence for the examination of carpal vibrissae. For this reason, the characteristics and functions of the front extremities and their joints are described below.

Joints are the connection points between two or more bones. The shape of the joint determines its function and thus the degree and direction of possible movements. For example, the ball-and-socket joint of the shoulder allows rotations forwards and backwards, inwards and outwards, as well as lateral movement of the front extremities. In contrast, the hinge joints, e.g. on the forearm, fingers and toes, can only be bent (Flexion) and stretched (Extension) [MH73].

The components of the joint provide stability and reduce the risk of injury under constant load. The bone ends that form the joint are covered with cartilage. Cartilage is a hard, resistant protective tissue made of collagen, water and proteoglycans that reduces friction during movement [MH73].

Figure 2.9 shows the joint types required for the examination of the anterior extremity. The corresponding degrees of freedom can be found in table 2.3 [BETV11].

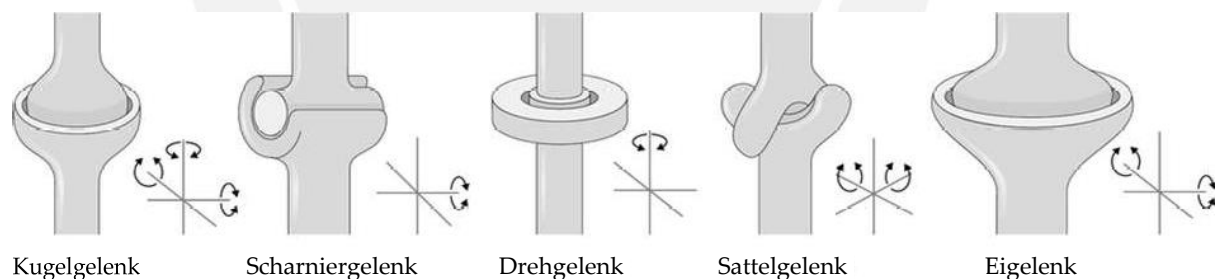


Figure 2.9: Joint types according to [BETV11].

Table 2.3: Degrees of freedom according to [MF11].

Articulation	Degrees of freedom
Swivel joint	1
Hinge joint	1
Saddle joint	2
Egg joint	2
Ball joint	3

The basic function of the extremities of rats is to walk and grasp objects. The individual sections of the front extremities of rodents are designed to be as similar as possible to the arms of humans (see fig. 2.10). The front limbs consist of shoulder blade, upper arm and a forearm composed of ulna and radius. This is followed by the carpus, which consists of several smaller bones [FSS⁺02].

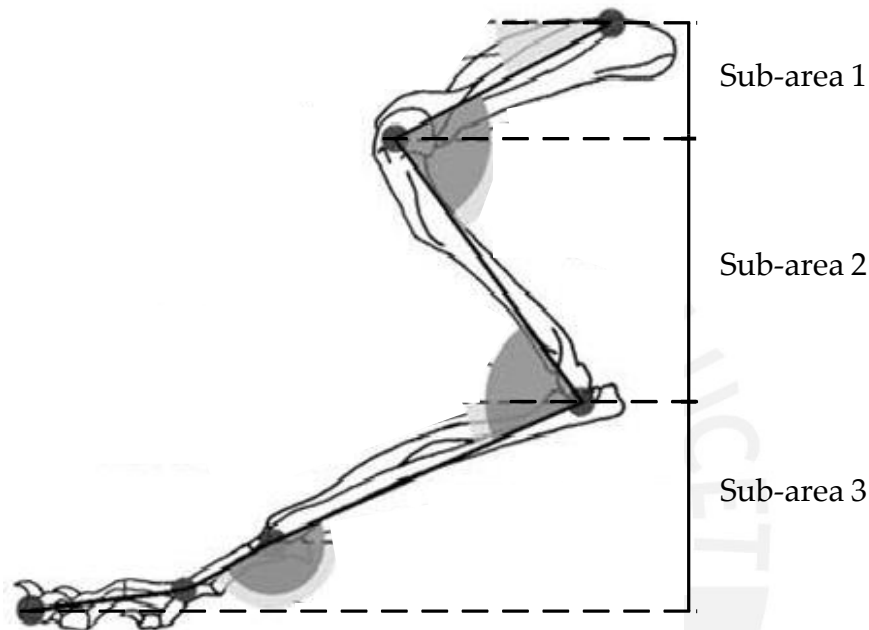


Figure 2.10: Forelimb of a rat after [FSS⁺02].

Subarea 1 consists of the shoulder blade and collarbone. The scapula is connected to the sternum by a ball joint, which is of existential importance for locomotion. The clavicle acts as a connecting element between the scapula and the sternum and stabilizes the shoulder during various movements [Jen74]. At the lower end of the scapula is the joint receiver of the shoulder joint, which enables movement of the front extremity through extension and flexion.

The humerus belongs to section 2 of the anterior extremity. This connects the shoulder joint and ends in the elbow joint, which is divided into two partial joints. On the one hand there is the joint connection of the humerus to the ulna, which is constructed as a hinge joint, and on the other hand there is the connection by means of a swivel joint to the radius [FSS16].

In section 3, which simulates the forearm, ulna and radius run parallel to each other and meet at the coupling point to the paw, the wrist. Mechanically, the proximal joint is seen as an egg joint. The distal joint, on the other hand, is declared a hinge joint. By means of these two joints the rat is able to rotate the sole of the foot [AAC⁺17].

The last limb of the front extremity is the paw. It is connected to the forearm and consists of hand and finger bones. The carpal vibrissae which are necessary for the recognition of objects and their characteristics are also attached to the paw [FSS16, HVN⁺14].

2.2.3 Muscles

As a third part of the body necessary for movement, the function of muscles is briefly explained below.

Muscles are structures consisting of muscle fibres, which are attached to the joints by means of tendons and produce movement through contractions.

The muscle fibers are composed of several muscle fiber bundles. Several bundles are surrounded by connective tissue (fascia). The muscle fibre strands are traversed by small vessels that supply the tissue with oxygen and glucose [Hic08].

With each movement, several muscles are always working (simultaneously or consecutively). When a movement is performed, muscles contract. The contracting muscle is called the agonist, the corresponding antagonist is called the antagonist. Muscles can shorten to a maximum of half their initial length and cannot return themselves to their initial position; this requires the antagonist. [Hic08]

In figure 2.11 various muscle strands are shown and described in detail. A detailed description of the individual muscles is available in [Ber14]. A summary of the muscle bundles of the forelimbs is added in A.

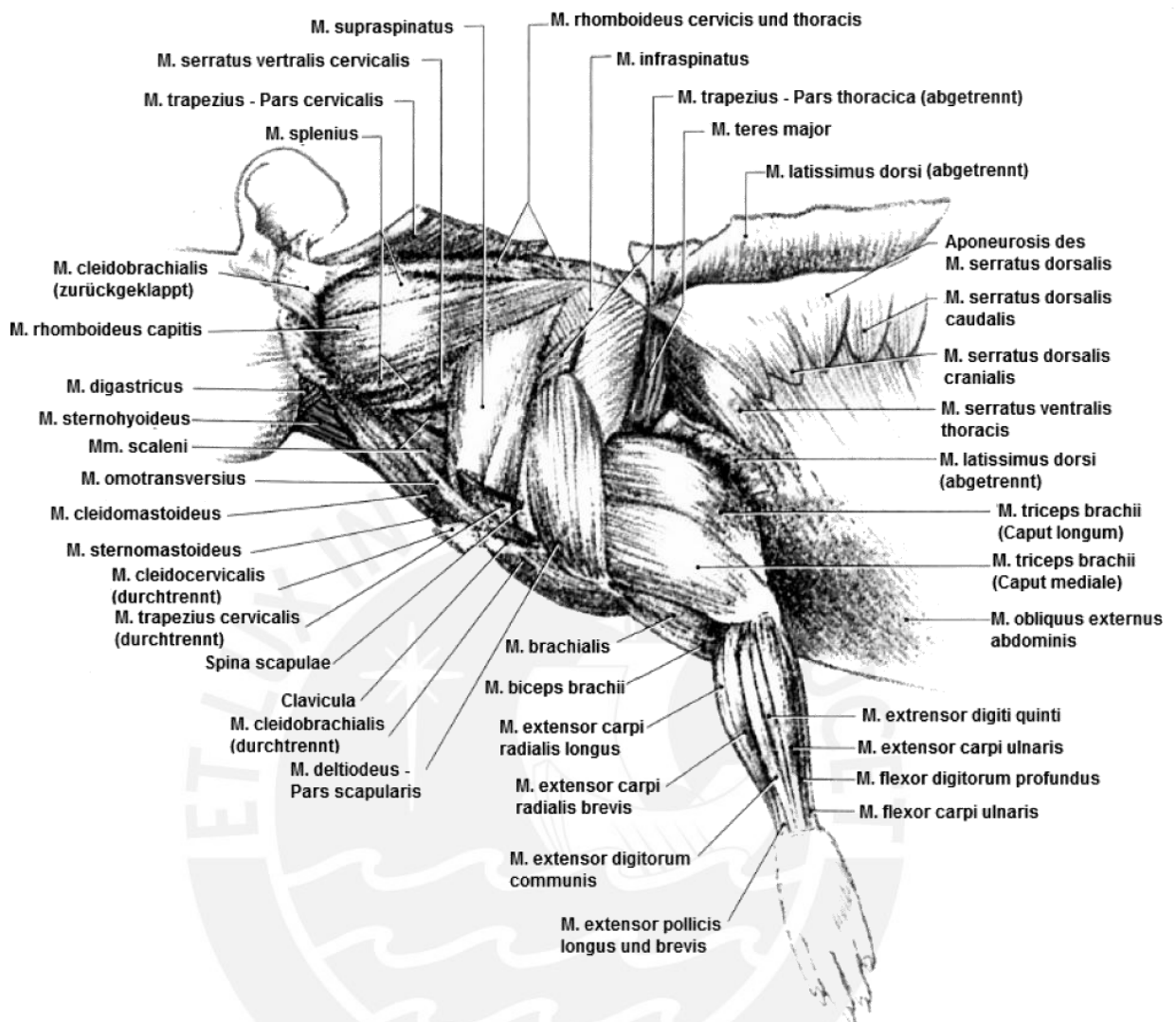


Figure 2.11: Muscles of the front extremity [WHF97].

In the following, important features of biology are summarized, which are needed for this work:

- Vibrissae are long, slender, elastic tactile hairs and can be found on the extremities, among others [Kla99].
- Vibrissae act as transmitters of stimuli because they have no receptors [Kla99].
- The receptors of the vibrissae are located in the follicle-sinus-complex, in which the hairs are elastically supported [Kla99].
- Vibrissae are used to scan the object and determine the object properties [PMG11].
- Rats possess the ability to perform various types of movement [Sch01].
- The extremities of rats can be divided into three areas and are coupled together by different joint types [BETV11, MF11].
- Various muscles are required for locomotion, which change the relative position between individual bones [WHF97].

State of the art

The following explanations are intended to explain the application and functions of tactile sensors in more detail. Within this framework, a beam model is presented, taking into account the basics of technical mechanics, and possible simulation methods, such as the finite element method and multi-body system theory, are considered.

independently

3.1 Application and functional principle of tactile sensors

Tactile measurement technology is based on contact between a test surface and the tactile stimulus transducer of the sensor. It is a measuring method which can non-destructively determine the shape, position and dimensions of the scanned material parts and surfaces. Depending on the design of the corresponding tactile system, the accuracy of the measurements is in the range of micro- to nanometers [Sk111].

The functional principle of tactile sensors can be divided into two main levels of abstraction. On the one hand, there are sensors which only detect contact with the object to be measured, but do not provide any information about the strength or other properties of the contact. On the other hand, there are sensors which can detect the strength and direction of the contact by means of force and moment sensors and thus provide more precise information about the contact.

The information obtained from tactile sensors can be used, among other things, for collision monitoring between machine and objects or people. Furthermore, it is possible to detect surfaces with this type of sensor and thereby obtain information (e.g. roughness) about them [Elk16].

Tactile sensors are also used in the following areas [Dru18]:

- Scanning of objects;
- pressure measurement;
- three-dimensional shape recognition;
- roughness measurement.

Sensors, which can also detect the strength and direction, often use a probe which is in contact with the test object and measure the reactions at the clamping of the probe.

3.2 Model of an artificial vibrissae

In the following, models will be presented which simulate a vibrissae under consideration of large deformations. In the literature, vibrissae are often depicted in first approximation as cylindrical bending beams. For the calculation of deformation states of the vibrissa, the following parameters are required [KS09]:

- geometries;
- material properties;
- loads.

In the literature there are various basic models for mathematically representing a vibrissae [KS09]:

- **Rigid body model:** In the rigid body model, the body is regarded as rigid. This model is primarily used in control engineering due to the possibility of controlling and stabilizing the bearing point. Here the beam is regarded as not flexible.
- **continuum model:** In the continuum model, the bodies are regarded as deformable, which makes it possible to calculate displacements of individual points. This model makes it possible to simulate large deformations of the beam under the condition of the nonlinear Euler-Bernoulli theory. It is also usually applied with free or elastic support, with and without pre-bending.

The modulus of elasticity (Young's modulus) E , the moment of inertia I_z , the sliding modulus G and the cross-sectional area A are required to calculate the bending stiffness.

For the description of an Euler-Bernoulli beam, the cross-section is flat after deformation if it was perpendicular to the neutral phase in the unloaded state. This is no longer the case with extended beam theory (e.g. with Timoshenko beams). Here the cross-sectional plane can rotate around the shear axis [KS09].

In order to represent the deformation of the beam model as accurately as possible, two levels of abstraction are distinguished [KS09]:

- Step 1: Determination of forces and moments using linear beam theory.
- Step 2: Determination of the forces and moments at the deformed beam (deformable model) by considering a nonlinear beam theory.

In the following example models, the Young's modulus E and the moment of inertia I_z are considered constant over the cross-section. The model consists of a clamped beam of length L (see figure 3.1 and 3.2). A force F is impressed at the end of the beam.

Step 1: Linear deformable model

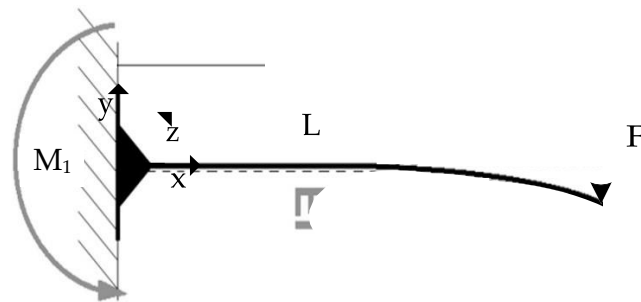


Figure 3.1: Deformed beam with linear mathematical model.

$$M_1 = F \cdot L \quad (3.1)$$

Step 2: Nonlinear deformable model

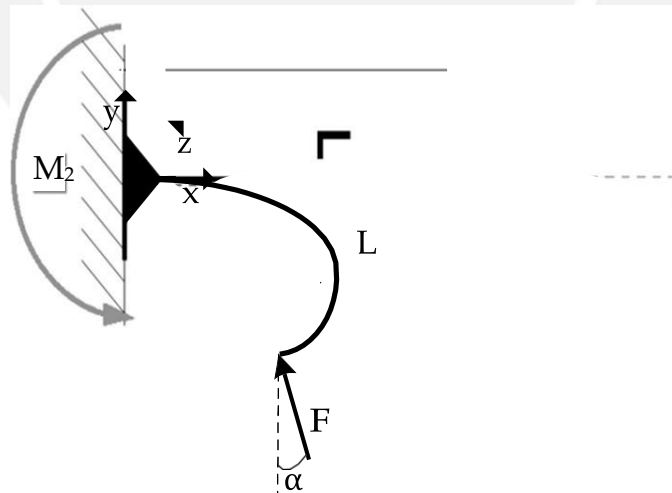


Figure 3.2: Deformed beam with non-linear mathematical model.

$$M_2 = L \cdot (F \cdot \cos(\alpha)) \quad (3.2)$$

3.3 Coulomb's friction theory

When an artificial vibrissae comes into contact with an object, frictional effects occur at the point of contact. The theoretical principles are explained below.

Friction always occurs when two surfaces are in contact. The friction coefficient is used to describe friction. This represents the ratio between normal force F_N and friction force F_R when two surfaces come into contact. Since it is a ratio, it is dimensionless. Basically two types of friction are distinguished [GHSW19]:

$$F_R = \mu \cdot F_N \quad (3.3)$$

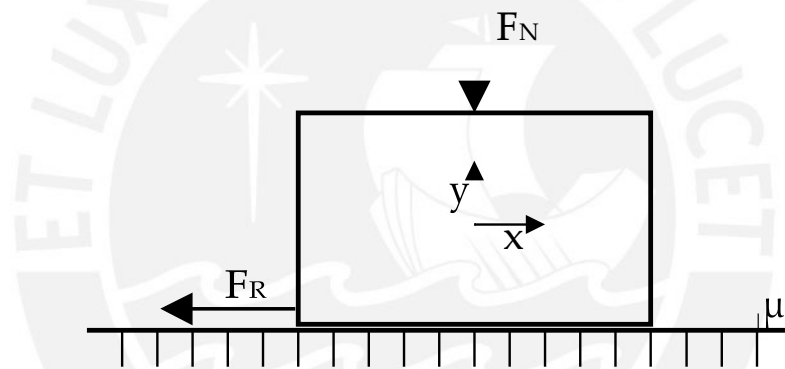


Figure 3.3: Schematic representation of Coulomb friction [GHSW19].

- **Static friction:** describes friction effects between two surfaces without relative velocity between the surfaces (Often the maximum forces occur with this type of friction)
- **Kinetic friction:** describes frictional effects between two surfaces during relative movement of the surfaces.

Figure 3.4 shows an exemplary characteristic curve of a force over time. The figure shows the occurrence of static and sliding friction [GHSW19].

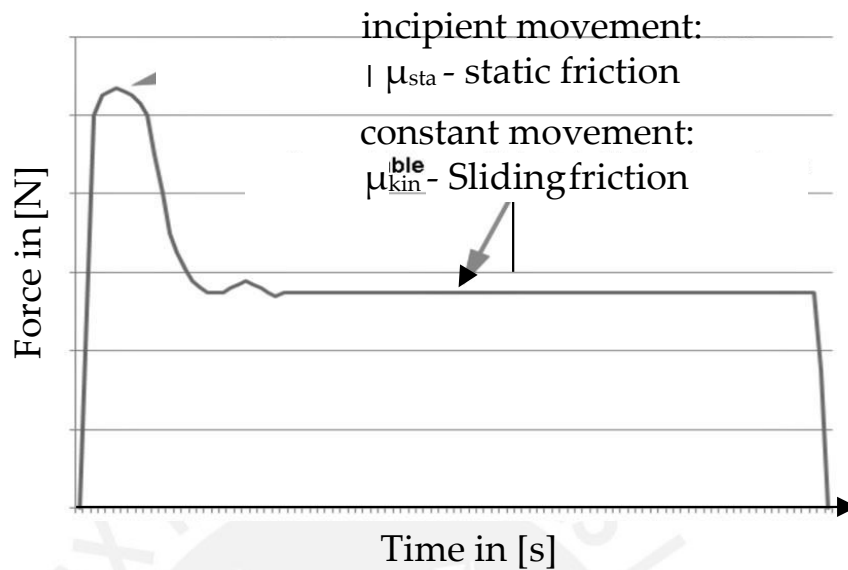


Figure 3.4: Graphical representation of static and sliding friction.

3.4 Simulation methods

Today, numerical calculation methods are indispensable. Modern simulation techniques save time and development costs. With the help of computers with their ever faster and more powerful processors, mechanical motion sequences and many other technical relationships can be represented much faster and graphically precise [Sen97, Kle03]. However, depending on the accuracy of the simulation model, an exact statement about the real component behaviour cannot necessarily be made.

Sophisticated simulation tools are now available in many technical fields, which enable effective work. The most important and therefore most frequently used are process simulation (simulation of production processes), graphical 3D simulation (e.g. CAD), numerical methods (e.g. ODE45), Finite Element Method (FEM) and the multi-body simulation (MKS). The latter two are applied in the simulation of mechanical systems and processes and are presented in this thesis [Sen97].

Simulations can be divided into the following categories based on the specifications [Eng17]:

- forward simulation: A model in which forces and moments act in a time-dependent manner is integrated over time to synthesize motion or behavior in interaction;
- inverse dynamics: a motion sequence is assumed to be known (e.g. measurement) and through the analysis, the effective internal and possible external forces and moments are calculated.

3.4.1 Finite element method

The Finite Element Method (FEM) is a frequently used tool in the engineering world. With this simulation method it is possible to calculate linear and non-linear calculations in the field of statics and dynamics by simultaneously solving differential equation systems. With this method, e.g. the vibrissa behaviour of materials and also the mechanical stress are analysed and examined by means of substitute models [Sen97]. Furthermore, interdisciplinary calculations, such as z. B. magnetic fields, temperature distributions etc. can be solved [Bra16].

Function

FEM calculations decompose a component into a grid, which consists of finite elements. Simple basic equations are applied to each individual element of the mesh in order to enable a simulation of the entire component [Bra16].

To obtain the result, the following sub-steps must be completed: Data input or modeling, creation (construction of the element stiffness matrix and element load vectors, the system stiffness matrix and the load vector), calculation, evaluation and interpretation of the results [Bra16].

The FEM calculations are represented by linear systems of equations of the 2nd order as follows:

$$\mathbf{M}\ddot{\mathbf{u}}(t) + \mathbf{D}\dot{\mathbf{u}}(t) + \mathbf{K}\mathbf{u}(t) = \dot{\mathbf{P}}(t) \quad (3.4)$$

The system of equations includes mass matrix \mathbf{M} , damping matrix \mathbf{D} and stiffness matrix \mathbf{K} of the system. $\dot{\mathbf{P}}(t)$ represents the vector of the external forces acting on the system. The vector \mathbf{u} describes the states (displacement, velocity, acceleration, etc.) of the system [Bra16].

3.4.2 Multibody systems

The main difference between FEM and MKS lies not only in the actual methodology but also in the different areas of application. As already explained, the FEM is mainly used for static and dynamic calculations and in flow simulation [Bra16]. The MKS method is mostly used for dynamic problems with large non-linear movements in the time domain [RS17]. MKS programs use mechanical models which are converted into equations of motion. For this purpose, the program provides a large number of basic components (masses, joints, springs etc.), force laws (impulse theorem, rotational impulse theorem etc.) and motion specifications [SH16].

System equation

A body basically has six independent movement possibilities (degrees of freedom). The joints in an MKS simulation represent constraints that restrict the degrees of freedom in the movement possibilities of the body and thus exert constraining forces on the body. They determine the kinematics of the system, while the physical bonds determine the dynamic behaviour. For example, the simulation of elastic coupling assumes that the bodies are not connected by blocking degrees of freedom, but that each relative movement of the bodies causes a defined force. The relationship between relative motion and force effect can be described in z. B. by functional expressions or characteristic curves [RS17].

The equations of motion can be formulated e.g. with the Newton-Euler approach by the equilibrium of forces and moments [RS17]:

$$\dot{\vec{F}} = m \cdot \dot{\vec{a}} \quad (3.5)$$

$$\dot{\vec{M}} = \mathbf{J} \cdot \dot{\vec{\omega}} + \vec{\omega} \times \mathbf{J} \cdot \vec{\omega} \quad (3.6)$$

The inertia matrix \mathbf{J} and the moment vector \vec{M} refer in the present case to the center of gravity of the bodies. The vector $\vec{\omega}$ describes the angular velocity of the individual centers of gravity of the bodies and the force vector \vec{F} the forces acting on each individual body.

Simulation programs for solving MKS automatically create the system of equations from the geometrically defined model and the constraints. They then calculate the dynamic and kinematic system behaviour in the specified time range. As a result, all motion quantities as well as internal and external forces are available; it is also possible to additionally animate the motion sequence [SH16].

MKS is a kinematic chain of several rigid bodies formed by constraining conditions. The corresponding equations of motion are derived from the 2nd Newtonian axiom and are summarized in matrices:

$$\mathbf{M}(q)\ddot{q} - \dot{Q}_v + \dot{C}_q^T \dot{\lambda} = \dot{F} \quad (3.7)$$

The equation contains the generalized coordinates q , the mass matrix $\mathbf{M}(q)$ and the constraints C . \dot{C}_q is the derivative of the constraints on the generalized coordinates. $\dot{\lambda}$ in this formulation of the equations of motion denotes the Lagrangian multipliers¹ [WF19].

3.4.3 Conclusion

FEM and MKS are of great importance and great benefit for simulations in the field of structural and continuum mechanics as well as vibrissa engineering. The reason for this is the simplified design of components according to their load.

The MKS method is predestined for determining and optimizing the movements of interconnected rigid and/or elastic bodies.

A vibrissae can be modelled as beams; it is possible to model them from single coupled beam elements in order to calculate large deformations using MKS. Furthermore, it is possible to specify motion sequences in MKS. This can be used, among other things, to simulate the path of motion of a rat and thus to draw conclusions about various frictional effects during contact between carpal vibrissae and a surface. For these reasons, an MKS is carried out in the program *ALASKA* in the following.

¹Lagrangian multipliers λ usually represent forces or moments resulting from the constraints. Thereby they have a blocking effect of the degrees of freedom without doing work [WF19].

Objectives

Currently, research teams in biology and technology are working on the analysis and synthesis of mammalian environmental perception using vibrissae (special tactile hairs). By using this complex sensory organ, rats and mice, for example, are able to detect object distances, contours or surface conditions with just a few touches.

In the context of the present work the focus is on the development and investigation of a biologically inspired mechanical model for object sensing by means of artificial vibrissae. For this purpose, the scanning procedure is extended by friction and dynamic effects according to the biological model. The artificial vibrissae are modelled by a cylindrical Euler-Bernoulli beam, which is clamped or elastically mounted on one side and is guided along an object or surface for the purpose of scanning by specifying a trajectory of motion.

At first a mechanical model for the simulation of a vibrissa movement along a surface in the program *ALASKA* is to be developed. Subsequently, different influences of friction parameters on the bearing reactions of the vibrissae will be investigated. In order to generate results that correspond to the natural model, a measured motion sequence of the front extremity of a rat will be used as a model of the trajectory during the simulation. For this purpose, the following main topics will be treated:

- Development of a vibrissae model for object scanning taking into account biological properties by means of a motion trajectory.
- Determination of relevant parameters for the investigation of frictional influences during object scanning.
- Implementation of the model in the multibody simulation program *ALASKA* with integration of the motion trajectory of [Ber14].
- Simulative investigation of the influences of friction, object distance and variation of the clamping or elastic support (mounting angle etc.).



Model structure

In this chapter, the motion analysis and the procedure for building the model are presented. This is because before the actual simulation, the model is built. For this purpose it is necessary to transfer the reality into a simplified model. A good model is always a compromise between simplification and complexity. A higher model complexity leads to better results, but also to an increase in the number of parameters and simulation time.

On the one hand, model equations for simple systems are faster and easier to declare. On the other hand, especially in biomechanics it is difficult to assign a suitable value to each free parameter. Due to the very limited measurement possibilities on living objects, approximate assumptions often have to be made. As a result, the accuracy of the model does not necessarily increase with an increasing number of parameters. However, a too strong simplification leads to the non-consideration of essential properties, which also weakens the informative value of the simulation results.

The aim of these model analyses is to design a realistic simulation model that simulates a single vibrissae with the necessary mounting. With the simulated vibrissae sensor, various test scenarios are run through in the multi-body simulation program *ALASKA/ModellerStudio 9.7.2* and checked for correctness. First, a beam clamped on one side is modelled. This is used to perform various tests and comparisons. After the verification phase the beam

model is provided with a trajectory. The beam is guided along a surface for scanning under variation of different parameters. The results are processed and visualized in *MATLAB*.

5.1 Motion analysis

For an investigation of carpal vibrissae of a rat during locomotion it is necessary to know and subsequently reproduce the motion sequence of the rat and in particular the path of the rooting of the vibrissae. However, it is difficult to obtain information because of the small front extremities and the very small carpal vibrissae. A pedipulator was used to gain insights into the walking parameters and tactile information of carpal vibrissae. Due to this approach it is possible to visualize the behavior and to obtain the verification of the individual movement elements of a front extremity [Ber14, HVN⁺14].

5.1.1 Pedipulator

The pedipulator is a so-called walking device for the analysis of various movement parameters [IB03]. In order to visualize the behavior of carpal vibrissae during a step cycle, the data of a pedipulator were evaluated in the work of [Ber14]. The pedipulator is used as a mechanical aid. A dissected front extremity of a rat is attached to the pedipulator. The rat leg is guided on a two-dimensional trajectory by a gear. Thus, the natural movement of the rat's front limb is simulated over a longer period of time at continuous speed. In addition, the pedipulator allows focusing on the exact contact point between carpal vibrissae and the substrate without any restrictions.

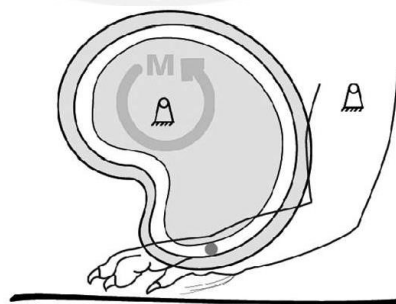


Figure 5.1: Schematic structure of the pedipulator [HVN⁺14].

The two-dimensional movement trajectory of the front extremity created by [Ber14] is implemented in the program *ALASKA* for the simulations to be performed.

5.1.2 Motion Trajectory

The movement trajectory should be modelled on the natural model. Therefore a large number of experiments were carried out. The foot that was not fixed could not be correctly positioned like the natural model, which led to a falsification of the trajectory. Thereupon, the foot of the extremity was severed with the aim of describing the movement as accurately as possible. The raw data was collected from several movement cycles and post-processed. The combination of the individual analyses resulted in the trajectories for the individual joint points of the rat as shown in Figure 5.2. Point 3 and the corresponding movement trajectory depicted the wrist and are used as a basis for the investigations carried out in this work. This is based on the rooting of the carpal vibrissae in the wrist [Ber14].

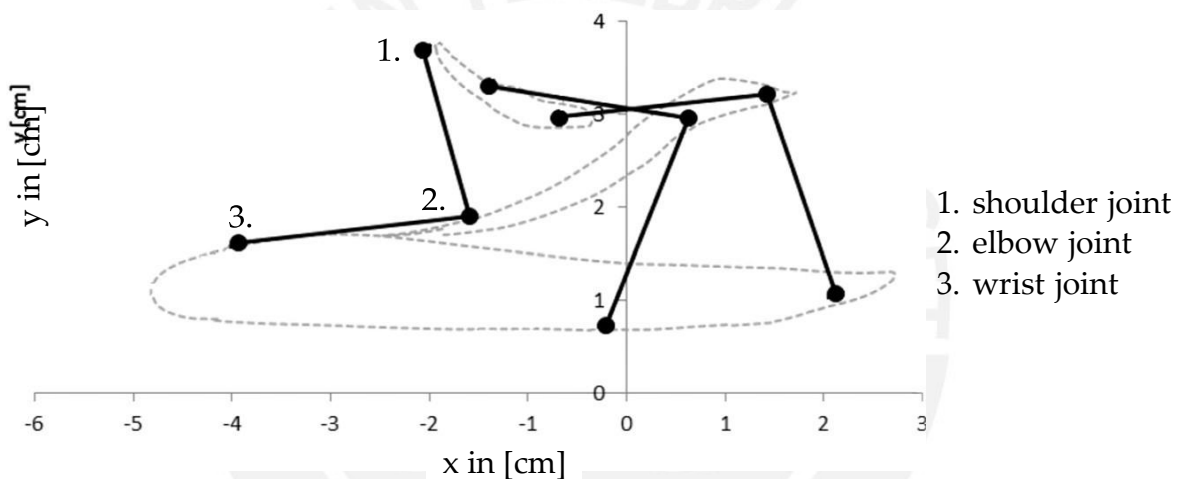


Figure 5.2: Trajectory recording according to [Ber14].

5.2 Model parameters

Basically in this thesis a two-dimensional problem (plane problem) is considered. The simulation times depend on the number of steps, the stiffness and also the abstraction of the system. In order to obtain as little or no dynamic effects as possible, movements are simulated at low speeds. A quasi-static simulation is not used due to the increasing simulation effort. Furthermore, the acceleration due to gravity is neglected. Furthermore the model is designed as a multi-body model and has the possibility to realize a contact only at the tip of the simulated vibrissae. Further contact points would increase the simulation effort considerably and do not bring any gain in the first approximation.

The most important settings of the simulation in the program *ALASKA* are listed below:

Basic settings for the simulations:

- Gravity: $\vec{g} = (\mathbf{0}, \mathbf{0}, \mathbf{0}) \frac{m}{s^2}$
- StepTime: $t_{Schritt} = \mathbf{0,001} s$
- Integrator: LSODEStiff
- Number of intermediate steps: EvalRate = 100

Basic settings for the beam:

For the parameter selection of the beam or the vibrissae the values of [SBH⁺10, Car09] and *ALASKA* [Mec19] by their specific properties:

- Beam type: TPlanarJointBeam
- Density: $\rho = 1140 \frac{kg}{m^3}$
- Transverse contraction number: $\nu = \mathbf{0,3}$
- Young's modulus¹: $E = \mathbf{8,0 - 10^9} \frac{N}{m^2}$
- Sliding module²: $G = \frac{E}{2 \cdot (1+\nu)} = \mathbf{3,07692 - 10^9} \frac{N}{m^2}$
- Length: $L = \mathbf{0,008} m$
- Outer radius: $R = \mathbf{0,0001} m$
- Inner radius: $R_i = \mathbf{0} m$
- DampingRation³: $D_R = \mathbf{0,1}$

¹Young's modulus provides information about the linear-elastic behaviour of the proportional relationship between stress and strain during the deformation of a solid body [Car09].

²Sliding module provides information about the linear-elastic deformation of a component due to a shear force or shear stress [Mec19].

³Proportionality factor between damping and and stiffness matrix [Mec19].

5.2.1 Abstraction levels of the model

The number of beam elements used has an influence on the accuracy of the simulation, but also on the simulation time. For this reason it has to be tested, which number of elements is reasonable to keep the simulation times within limits. Therefore, the number of individual beam elements was varied in the range of one to twelve, which in sum result in the beam in its entire length. Figure 5.3 shows the deformation of the beams at a directional force of 1 N with variation of the number of elements. It is easy to see that a small number of bars has a discontinuous course. This is due to the larger distances between the modulated joints of the beam elements. With an increase in the number of beam elements the course becomes smoother and has a smaller deviation from the numerical simulation of [Eck20]. From a bar number of five elements (green curve) the difference between adjacent curves is hardly recognizable. For this reason, the following modulation is continued with five bar elements.

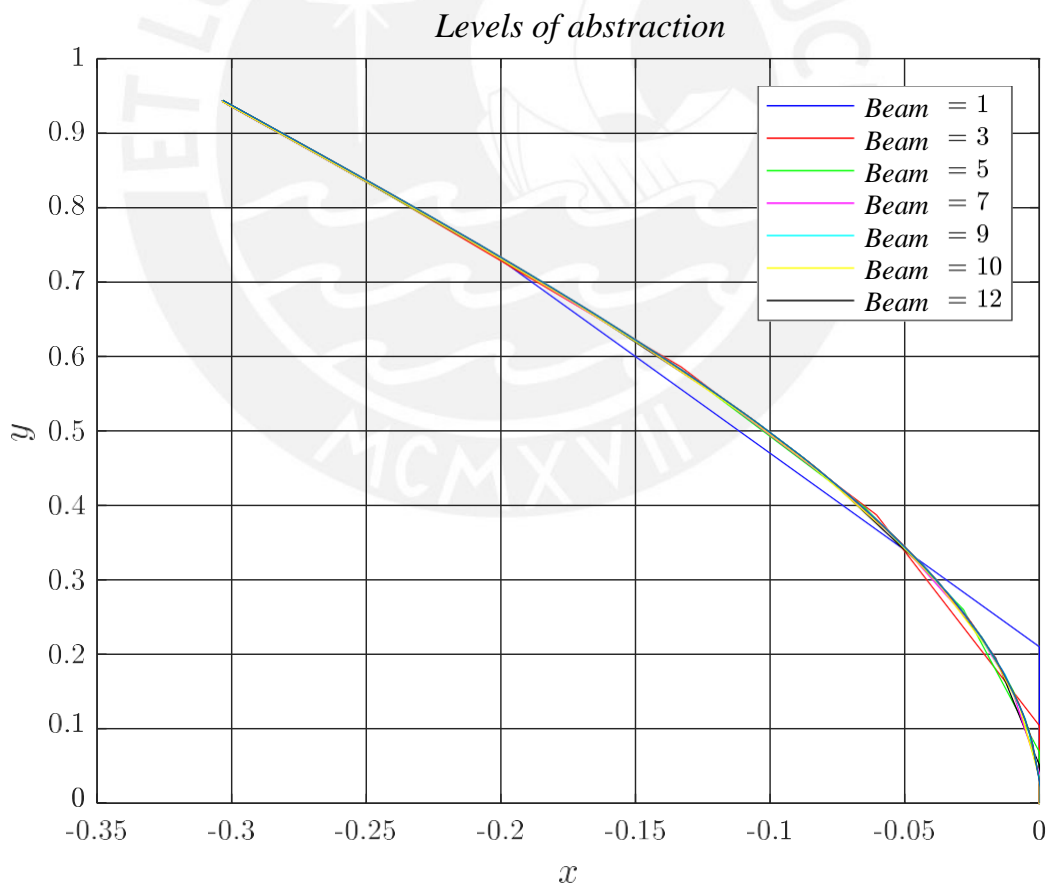


Figure 5.3: Abstraction level of the beam from one to twelve partial elements.

5.3 Modelling of the beam/vibrissae

In the first step, a simple model was created in the simulation environment, which consists of a clamp and a beam made of steel. A force is applied to this beam. The beam is connected to the fixture via the initial coordinate systems (BFR) using the joint option „Fixed“.

In figure 5.4 a „TPlanarJointBeam“ is shown. This beam consists of four rigid body elements, which are connected with thrust and pivot joints. Both the two swivel joints and the one thrust joint can have resilient and damping properties. The slip joint models the extension and the two swivel joints model the bending of the beam.

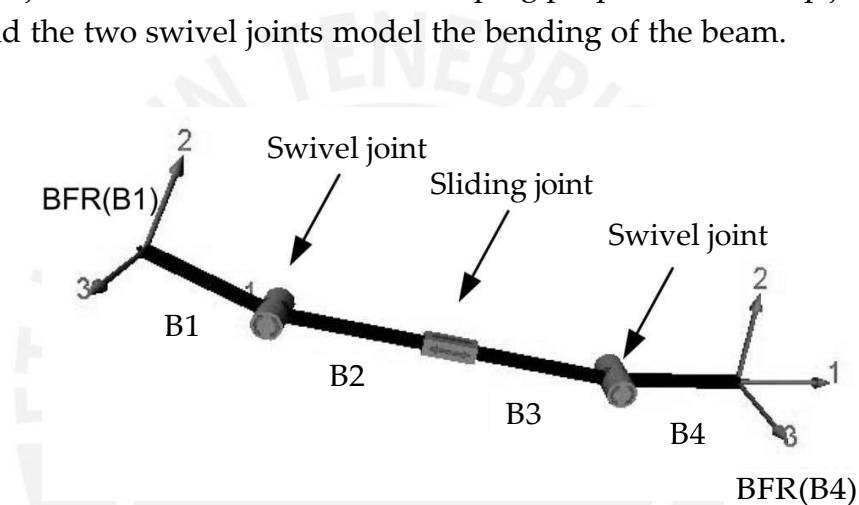


Figure 5.4: Representation of the structure of a TPlanarJointBeam [Mec19].

The joint beam elements are coupled to form a multi-body system by connecting the initial coordinate systems (BFR(B1) and BFR(B4)) of adjacent elements using the program function „Fixed“.

The calculation of internal forces and deformations is based on the assumptions of Euler-Bernoulli theory. This theory states that the beam cross-sections after deformation are perpendicular to the neutral fibre, whereby the shear force thrust component is neglected. However, this theory only provides sufficient accuracy for slender beams. A corresponding degree of slenderness - ratio of beam length to cross-sectional dimensions at least 10 to 1 - must be ensured [Mec19].

5.4 Clamping of the beam/vibrissae

In this work, a vibrissae shall be represented as realistically as possible and entered into a multi-body program as a beam. Since the vibrissae of a rat are anchored in the skin and can only be considered as restraints in the first approximation, the system is provided with a restraint in the first experiments and verified. This should result in the best possible application of the system to reality. After the first approximation, the clamping is replaced by a spring-damper circuit.

For the first tests, the beam is subjected to a directional or angular force. For this purpose, the end which is not subjected to the force is clamped. This results in two possibilities. On the one hand, there is the option of clamping which does not allow any movement - this is realized with the joint option „Fixed“. This clamping is fixed in the coordinate origin and is firmly connected to the beam (see figure 5.5).

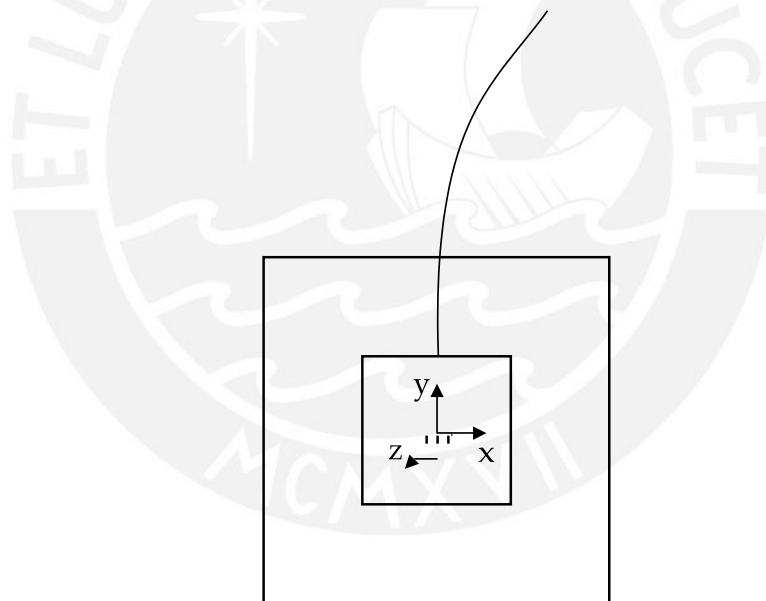


Figure 5.5: Rigid vibrissae clamping, which does not allow any movement.

Another possibility which can reproduce the elasticity of the natural tissue is an elastic restraint in the program *ALASKA*. This is executed as „Bushing“. The element „Bushing“ (see fig. 5.6) offers both an elastic and a damping property for all six degrees of freedom. For the modeled plane problem it is necessary to set the spring stiffnesses and damping terms for a translation in x direction (in *ALASKA* 1-direction) and y direction and a rotation around the z axis. The parameters of the other directions have no influence in a

two-dimensional simulation, but must be assigned a value in the program. For the following simulations, the parameters from [SBH⁺10] were chosen as follows:

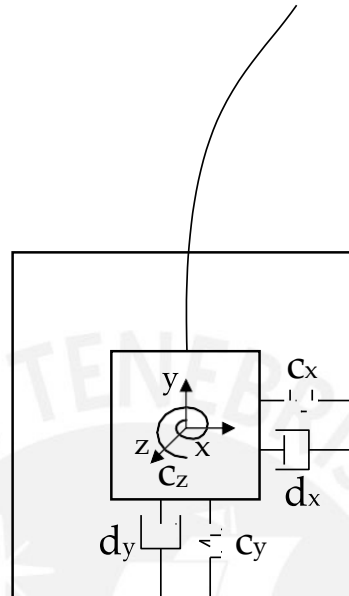


Figure 5.6: Vibrissae clamping in the form of a 2D bushings.

In this program option, the stiffnesses and the damping terms must be entered for each direction of movement. These were selected as follows:

- $DStiffness = (0,3 \frac{N}{m}, 1 \frac{N}{m}, 10 \frac{N}{m}, 10 \frac{Nm}{rad}, 10 \frac{Nm}{rad}, 10 \frac{Nm}{rad})$
- $DDamping = (3 \frac{Ns}{m}, 10 \frac{Ns}{m}, 100 \frac{Ns}{m}, 100 Nm s, 100 Nm s, 100 Nm s)$

5.5 Trajectory presetting of the beam/vibrissae

In order to be able to carry out an analysis taking into account the natural motion sequence, a motion specification of the clamping or elastic support of the beam must be made.

The data for a movement of a rat leg were collected from an already existing work by [Ber14]. The data was saved as an XML file and contains the x and y position. This dataset contains a motion cycle of a front limb of a rat. The recorded point is located on the wrist, to which the tactile hair is attached. The point has a relative distance $q = 0.0005m$ to the ground, which has a surface slope of $\phi = 0$ measured from point $x_{Abstand} = -0.009m$. Furthermore, an angle of the beam of $\beta = 170^\circ$ is assumed (see fig. 5.7). Furthermore, the figure shows

different exemplary contact points K at different times t .

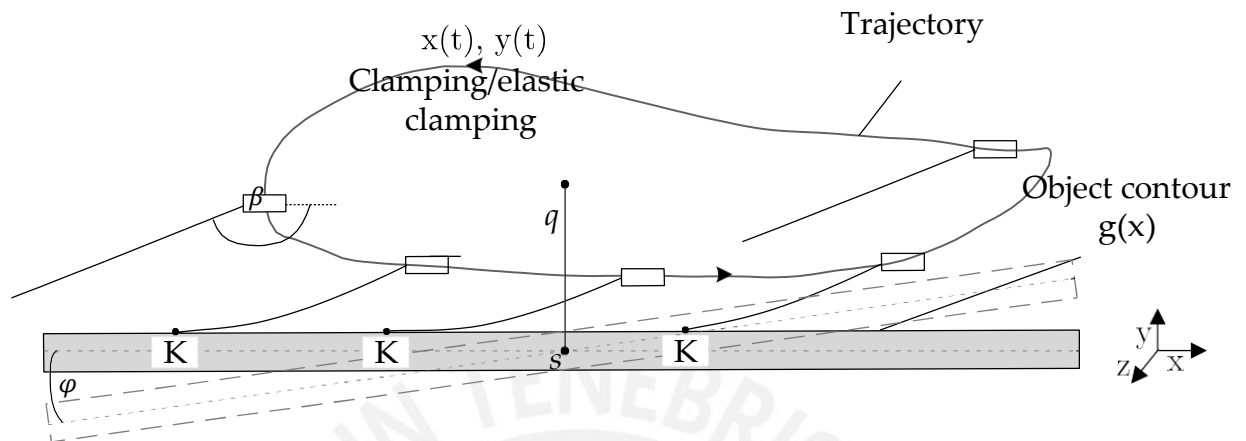


Figure 5.7: Sequence of the movement path with exemplary representation of different contact points.

5.6 Verification of the simulation models

The simulation results of the present master thesis have to be verified to check the correctness. Parallel to the present work, Mr. Stefan Eckhardt is also researching the forces on vibrissae in the context of his master thesis at the TU Ilmenau / PUCP Lima. Under the title „Contribution to artificial tactile sensors for object contour recognition using coupled technical vibrissae“ [Eck20] the author uses the program *MATLAB R2015b* to collect data. However, Mr. Eckhardt performs static simulations numerically. In *ALASKA/ModellerStudio 9.7.2*, however, dynamic effects are considered. In order to accurately estimate deviations and effects, the MKS analysis was performed with small changes in force and positions over time.

The comparison of the simulation results of the two programs used (*ALASKA* and *MATLAB*) is therefore suitable for verifying the simulation model. In order to create an approximately comparable basis for analysis, the following parameters are represented dimensionless according to [Ste13]:

$$\begin{aligned}
 \text{[Lengths]} &:= L \\
 \text{[Forces]} &:= \frac{EI_z}{L^2} \\
 \text{[Moments]} &:= \frac{EI_z}{L}
 \end{aligned} \tag{5.1}$$

For the comparison a single vibrissae was first subjected to a directional or angular force [Zen14]:

- The **directional force** always maintains its original direction - regardless of how the beam deforms (see fig. 5.8 (a)).
- In turn, the **angular force** maintains its relative angle to the top of the beam (see figure 5.8 (b)).



Figure 5.8: Clamped bending beam with force imprint at the end of the beam:

- (a) directional force F_{Ri}
 (b) angular force F_{Wi} .

In these simulations, it should be possible to compare the forces and moments in the restraint and the deformation in different states. Therefore, different dimensionless force amounts (1, 3, 5, 7, 10) and different force introduction points (30%, 50%, 70% and 100% of the beam) were considered.

Subsequently, a vibrissae in the sense of an object scanning was carried out.

The deformation of the vibrissae model is calculated using *ALASKA* in discrete points. These are shown in the following graphics by red crosses. The results are shown as a solid blue line using *MATLAB*.

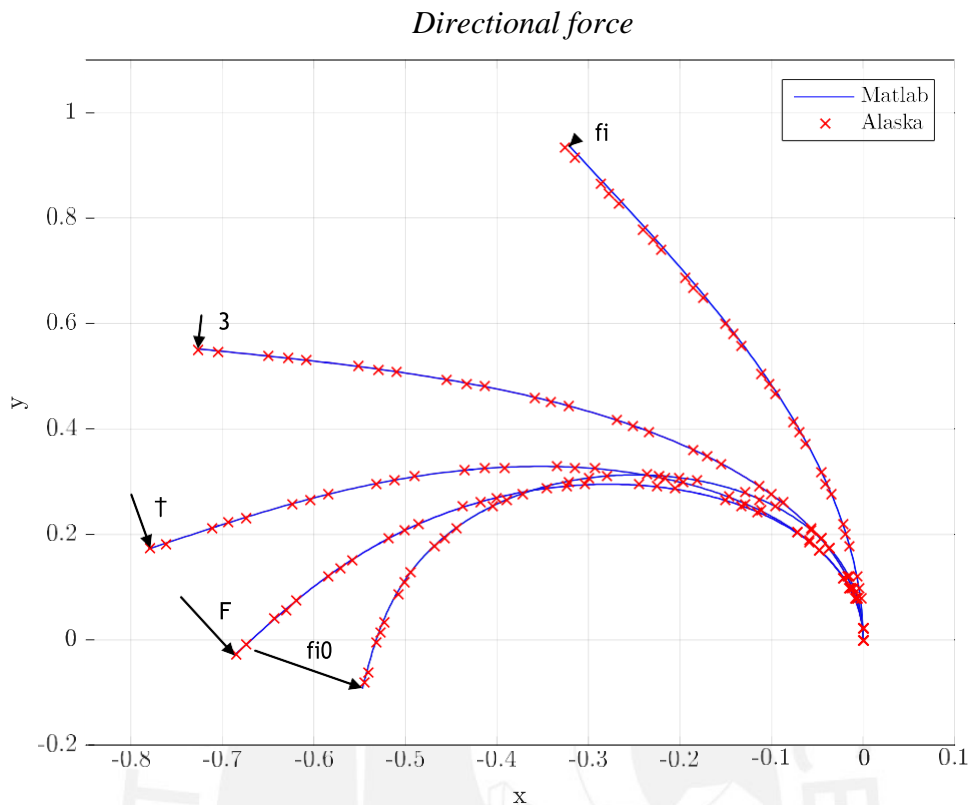


Figure 5.9: Deformation with angular force, force amplitude varied.

Figure 5.9 shows the deformations of a vibrissae with a variation of the amplitude of the angular force. In Figure 5.10 the point of force application has been varied. Qualitatively, the deformation is plausible in both cases.

Since the y -component is small in terms of amount in the case of the angular force application, the beam overlaps with **10** in the case of the dimensionless amount of the force, the beams **3**, **5**, **7** as shown in figure 5.9. If the deformation is even greater, the beam would twist in.

For a load of **10**, the beam deforms the most. Under this load, the direction of the angular force has rotated by nearly 180° .

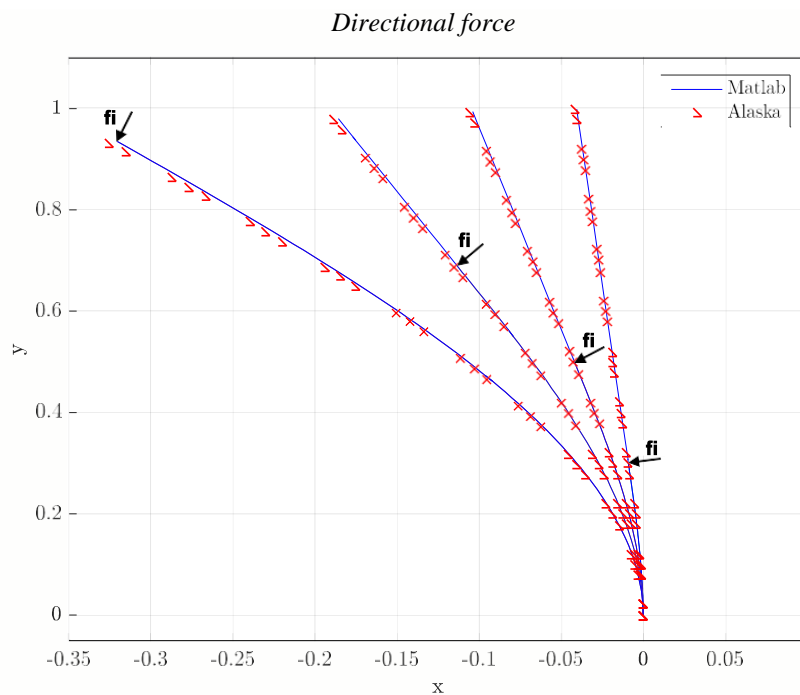


Figure 5.10: Deformation with the angular force, point of force application varied.

In figure 5.11 and 5.12 a directional force has been imprinted. This force has only an x-component. Therefore, the force vector is above the tangent of the beam.

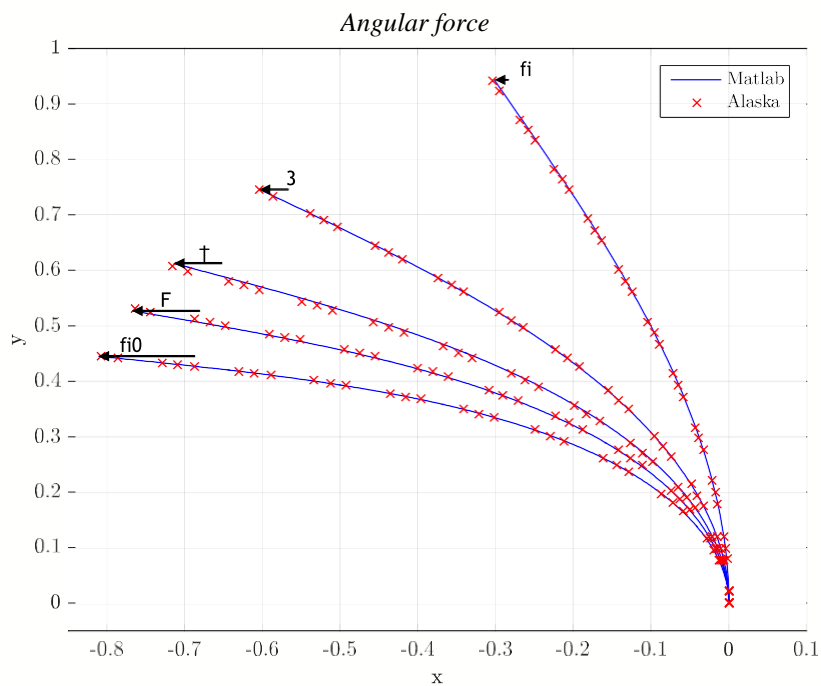


Figure 5.11: Deformation with directional force, force amplitude varied.

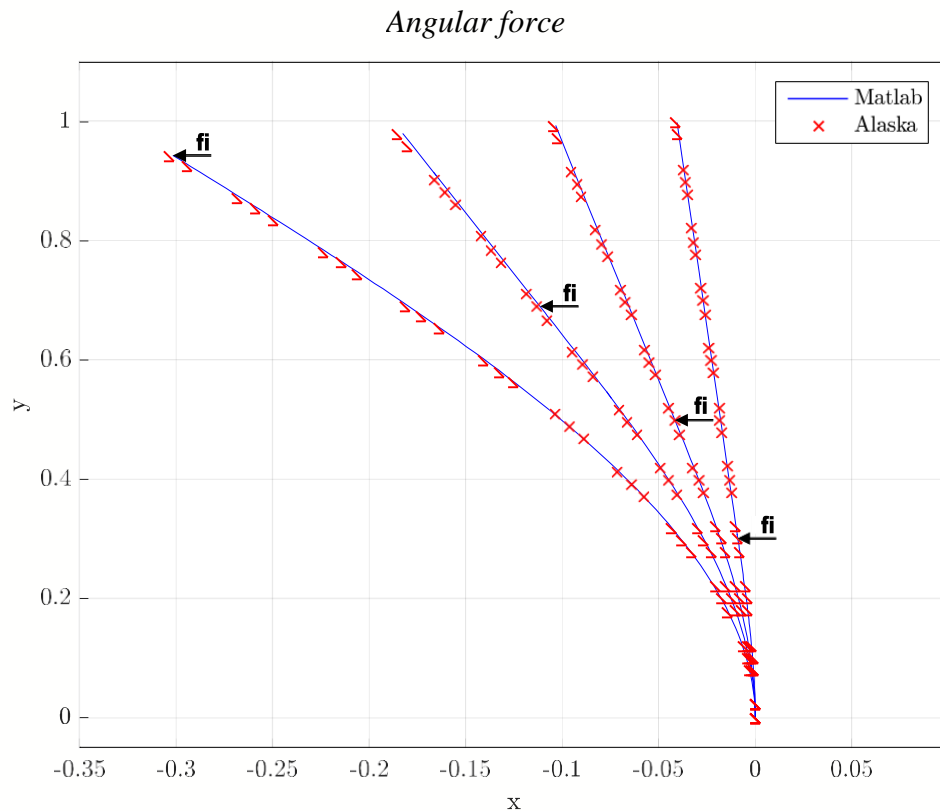


Figure 5.12: Deformation with directional force, point of force application varied.

When comparing the results, it is obvious that the deviations are small. These can be attributed to small dynamic effects and deviation due to the discretization in *ALASKA*. Furthermore, a minimal change in length of the vibrissa was simulated in *ALASKA*. The differences in the resulting bearing reactions between the two simulation methods are minor and can also be attributed to the effects described. The individual forces and moments can be read in the form of a table B in the appendix.

Furthermore, a circular object was scanned for verification purposes and its deformations and bearing reactions were compared with the results of [Eck20].

For the object scanning a movement of the vibrissa is necessary. This is imprinted in the clamping or bushing. For the first simulations, which are used for verification, a plane movement along an object contour $g(x)$ is specified. For this the guide „Prismatic“ is used. In addition to the initial position, this requires a motion profile with associated velocity and acceleration profiles. In this paper the position $Trans$ is specified. Here a constant velocity $TransVel$ is to be specified to minimize dynamic effects due to accelerations $TransAcc$. Furthermore, the speed is to increase slowly until the target value is reached in order to reduce acceleration effects here as well. The actual scanning process takes place after the constant speed has been reached. For this purpose the equations 5.2 in *ALASKA* were implemented. The equations 5.2 contain the following variables:

Table 5.1: Parameters for Prismatic.

Variable	Meaning
t	running parameters of time
t_{step}	time of acceleration process
t_{End}	time of motion
v	speed of movement

$$Trans = -((t < t_{Stieg})? \frac{v}{t_{Stieg}} - t^2) : ((t < t_{End})?(v - t) : 0)$$

$$TransVel = -((t < t_{Stieg})? \frac{v}{t_{Stieg}} - t) : ((t < t_{End})?v : 0) \quad (5.2)$$

$$TransAcc = -((t < t_{Stieg})? \frac{v}{t_{Stieg}}) : ((t < t_{End})?0 : 0)$$

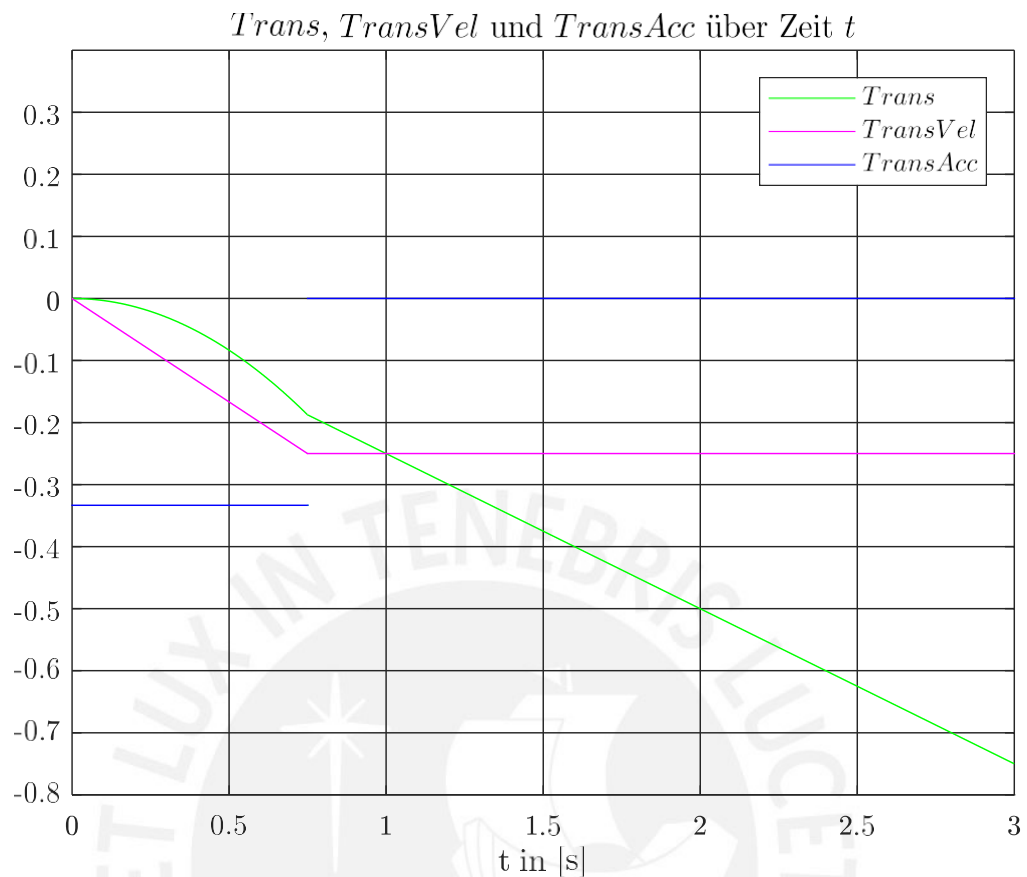


Figure 5.13: Displacement *Trans*, speed *TransVel* and acceleration *TransAcc* over time *t*.

For the object contour $g(x)$ a circle with the radius $R_k = 0.2\text{m}$ and a center position $x_k = -0.24\text{m}$, $y_k = 1.0\text{m}$ was chosen. This has a strictly convex shape. This means that there is only one contact point during the entire scan. Furthermore, the figure 5.14 shows the scanning of the object with a beam. Several contact scenarios are shown as K at different times t .

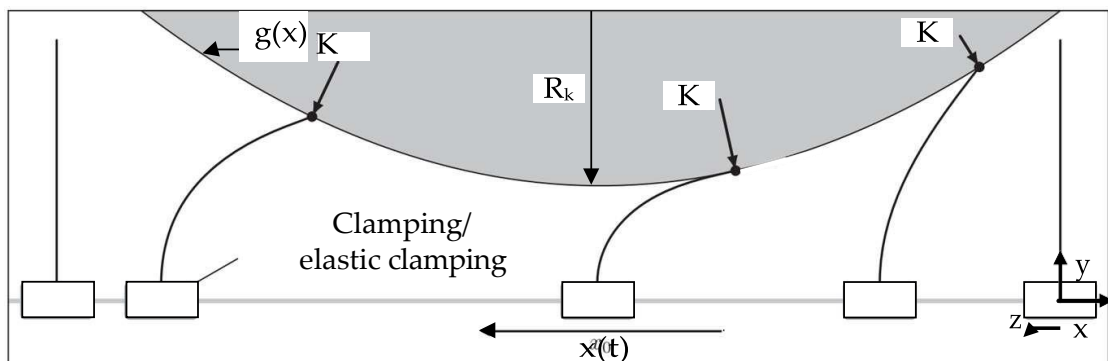


Figure 5.14: Schematic structure of a translatable object scanning according to [WBS17].

For the comparison with the work of [Eck20], the friction effects were neglected in *ALASKA* and a low speed of the base point with $v = 0.25 \frac{m}{s}$ was chosen. This has an important advantage - the minimization of dynamic effects (like z.B. bouncing). The deformation states shown in Figure 5.15 show only small deviations due to dynamic effects. From this it can be concluded that both simulation models are comparable.

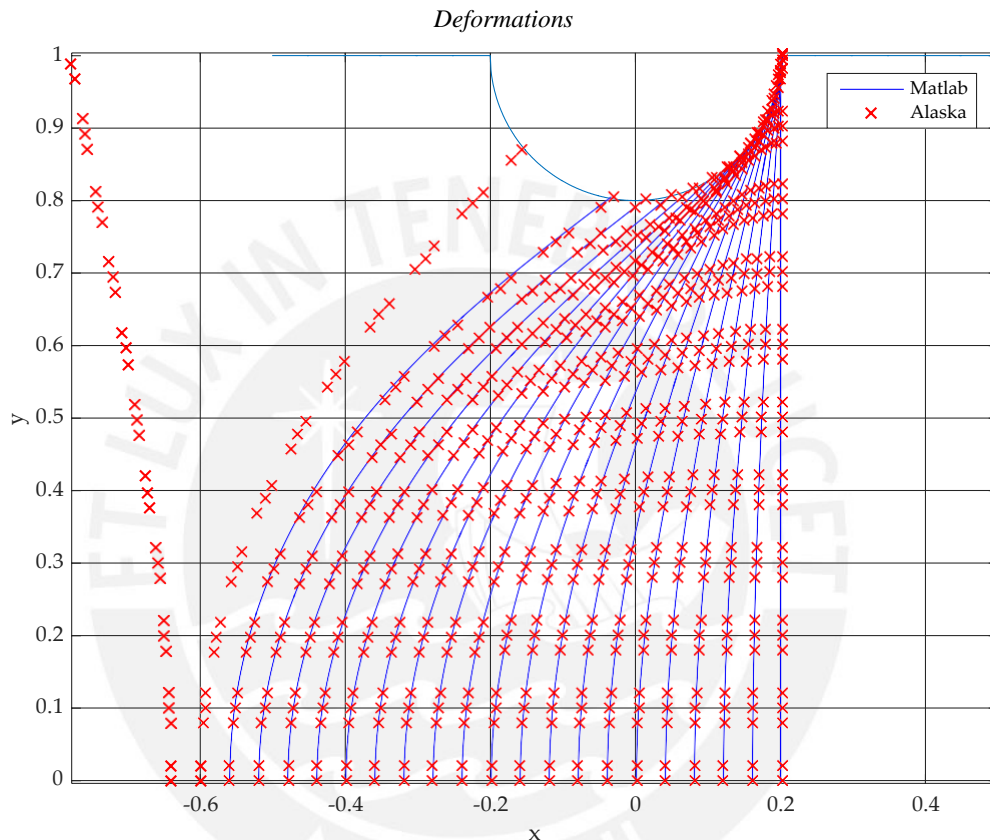


Figure 5.15: Comparison of the deformations of the vibrissae while scanning a circle contour [WBS17].

Also when comparing the bearing reactions, the dynamic effects can be seen in figure 5.16. In the *ALASKA* simulation these can be recognized in the range from $x_v = 0.2$ to $x_v = 0.19$ by a bounce of the contact point.

Furthermore, the jumping off of the beam is delayed during the simulation using *ALASKA*. The delay results, among other things, from the use of the beam model, which takes into account a change in the length of the beam.

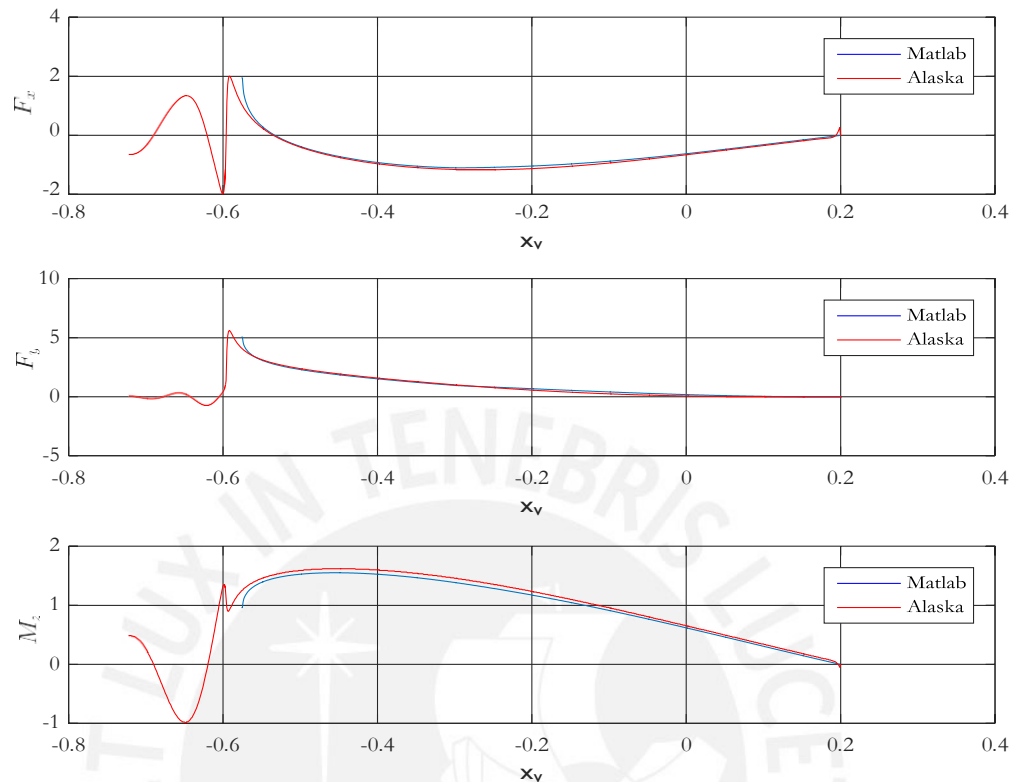


Figure 5.16: Comparison of the bearing reactions at the vibrissa while scanning a circle contour.

As a final verification, the bearing reaction during object scanning with an elastic support is to be compared with the work arising in parallel. Figure 5.17 shows the results of object scanning with a spring circuit. In *ALASKA* this is realized by a „Bushing“ with the stiffness $0.3 \frac{N}{m}$, in *MATLAB* it is implemented by adjusting the system equations. The graphs contain the bearing reactions of the beam. When comparing the graphs it can be seen that both models tend to have the same course. The difference of both can be explained by dynamic effects and length changes in the shear joint. As in the previous figures, *ALASKA* can be used to detect the jumping of the beam from the surface to be scanned.

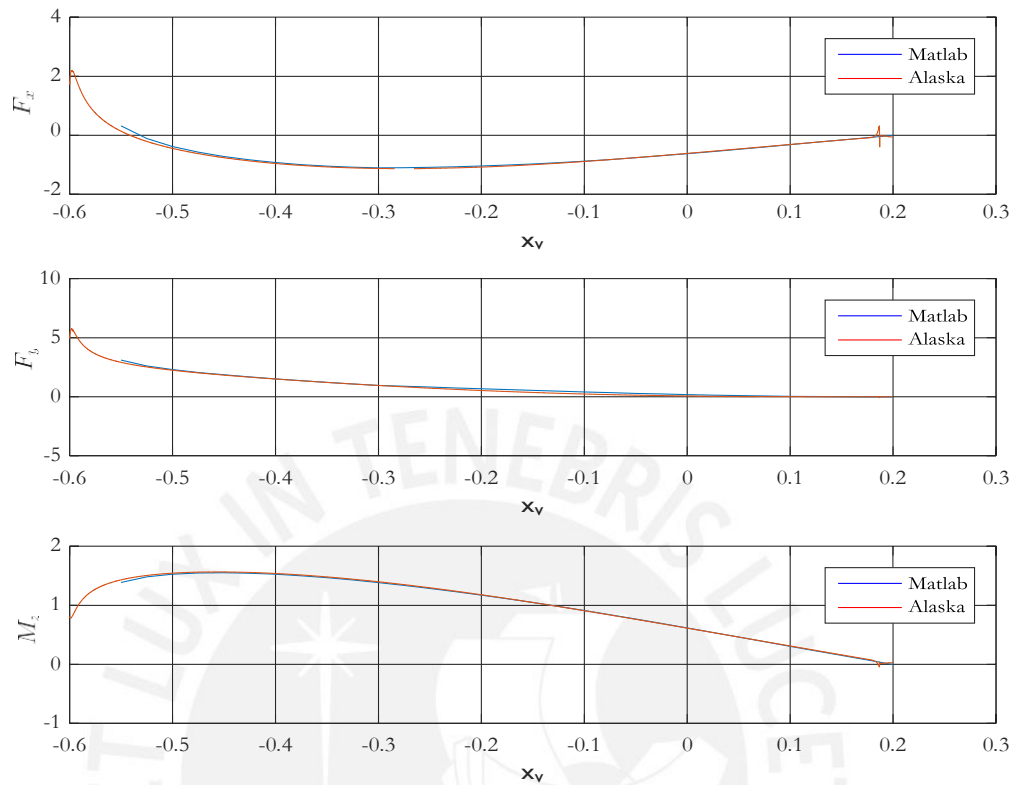


Figure 5.17: Comparison of bearing reactions on the vibrissae science while scanning a circle contour.

In summary, the two system models independently deliver similar results. It can therefore be assumed that the resulting model represents a realistic state.

A comparison of the deviation between the model of the numerical simulation by means of *MATLAB*, as well as the simulation performed with the multi-body system program *ALASKA* followed. The fact that the results do not agree 100 percent is due to the deviation caused by the discretization in *ALASKA*. This could be minimized by a large number of beam elements. Furthermore, in the MKS modeling, a thrust joint is also implemented per beam, which was not taken into account in the numerical simulation. This can lead to further deviations.

Results

Within the scope of this chapter, parameter studies to investigate the coefficient of friction, vibrissae mounting, vibrissae properties, object distance and surface slope are performed and evaluated.

First of all, it is tested whether the results of the simulations show a change for several cycles of the trajectory. Then the bearing reactions are evaluated by varying the individual parameters (ground distance, coefficient of friction of the surface, the angle of attack of the beam against the beam mounting and angle of inclination of the contact surface). These are displayed and evaluated using the coordinate system of the clamping (see fig. 5.5 and 5.6). The structure and parameters for the two models used (fixed and elastic restraint) are described in the chapter 5.

6.1 Reproducibility of motion

At the beginning, it was tested whether the movement path and the corresponding bearing reactions can be reproduced. For this purpose, three runs of the trajectory are plotted on top of each other in *MATLAB* (see figure 6.1). In the exemplary detailed view of F_x (see fig. 6.2) only small deviations in the range of only $1 - 10^{-4}N$ between the runs are visible. For

this reason and to minimize the simulation time, all continuous simulations are evaluated with only one run and the simulation time is set to $t_{end} = 5.0s$.

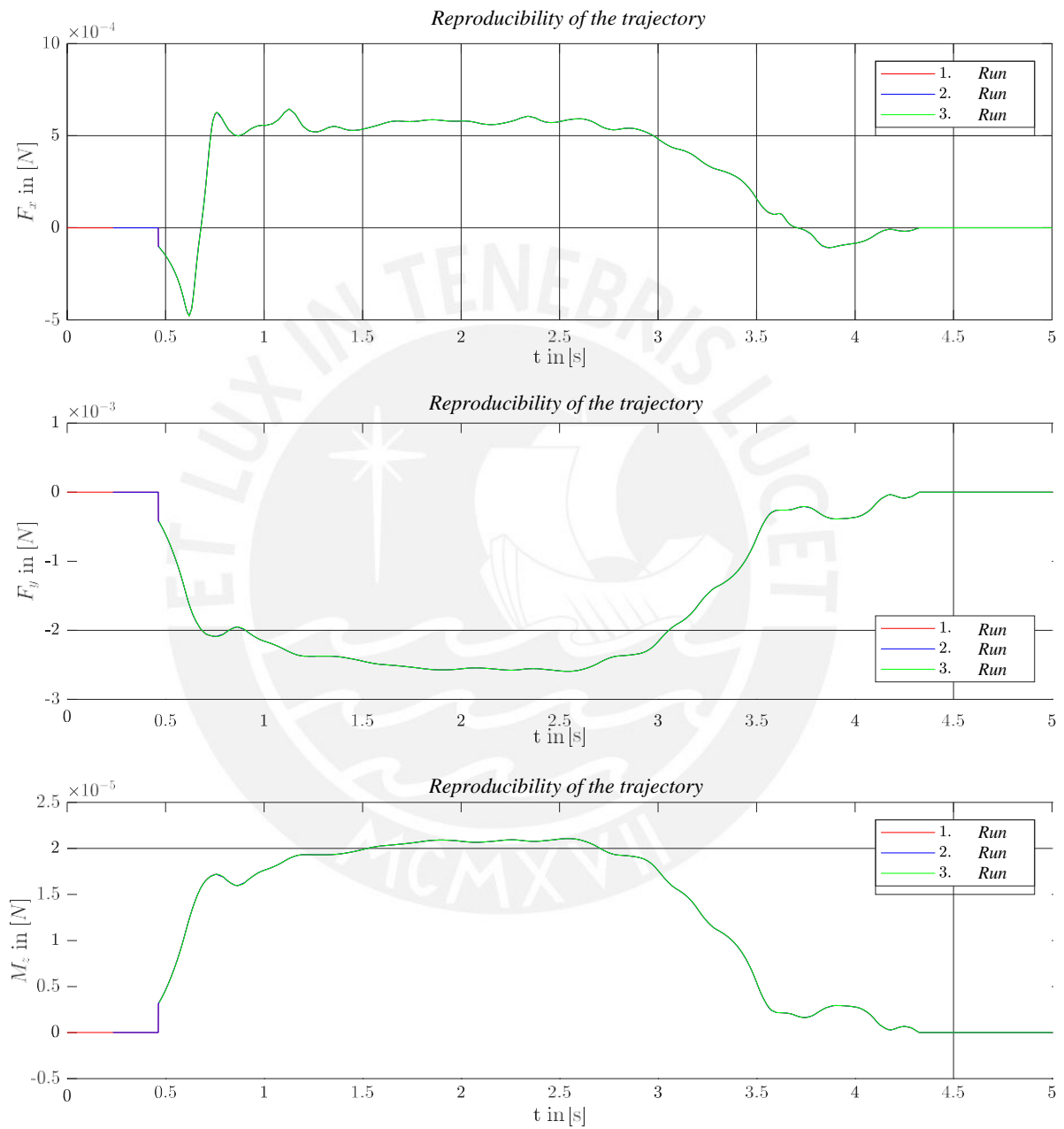


Figure 6.1: Comparison of three runs on reproducibility.

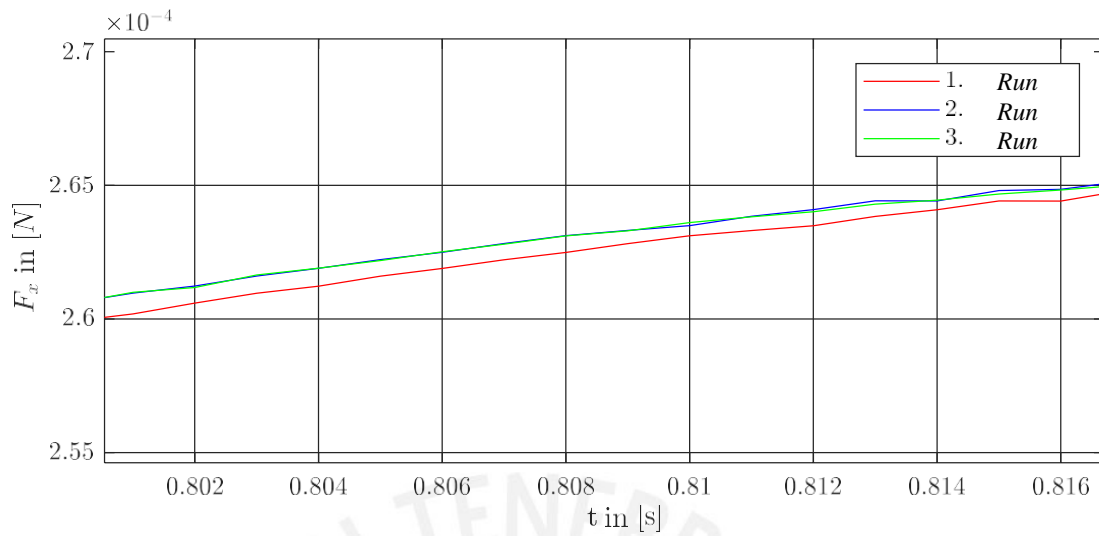


Figure 6.2: Detail view: Comparison of three runs for reproducibility.

6.2 Surface scanning with fixed clamping

In the following, the results of the simulations of the model with fixed clamping are examined (see section 5.4). For this purpose, first basic effects of object scanning are discussed and then parameter studies are carried out to determine the influences of the friction coefficient, vibrissa clamping, object distance, surface slope and beam properties.

Figure 6.3 shows the coordinates of the points of clamping (x_E, y_E) and contact (x_{Kp}, y_{Kp}) over time. The following important events are marked:

1. Initial contact of the vibrissa with the surface.
2. Reversal of motion in x direction.
3. Deviation of the change in the rise of the motion in the y -Direction.
4. Area where the vibrissae are in contact with the surface (sampling period).
5. Increase of the clamping of the beam (paw).
6. Reversal of the movement in x -direction.
7. Minimum change of position of the clamping in y -direction.
8. Detachment of the vibrissae from the surface.

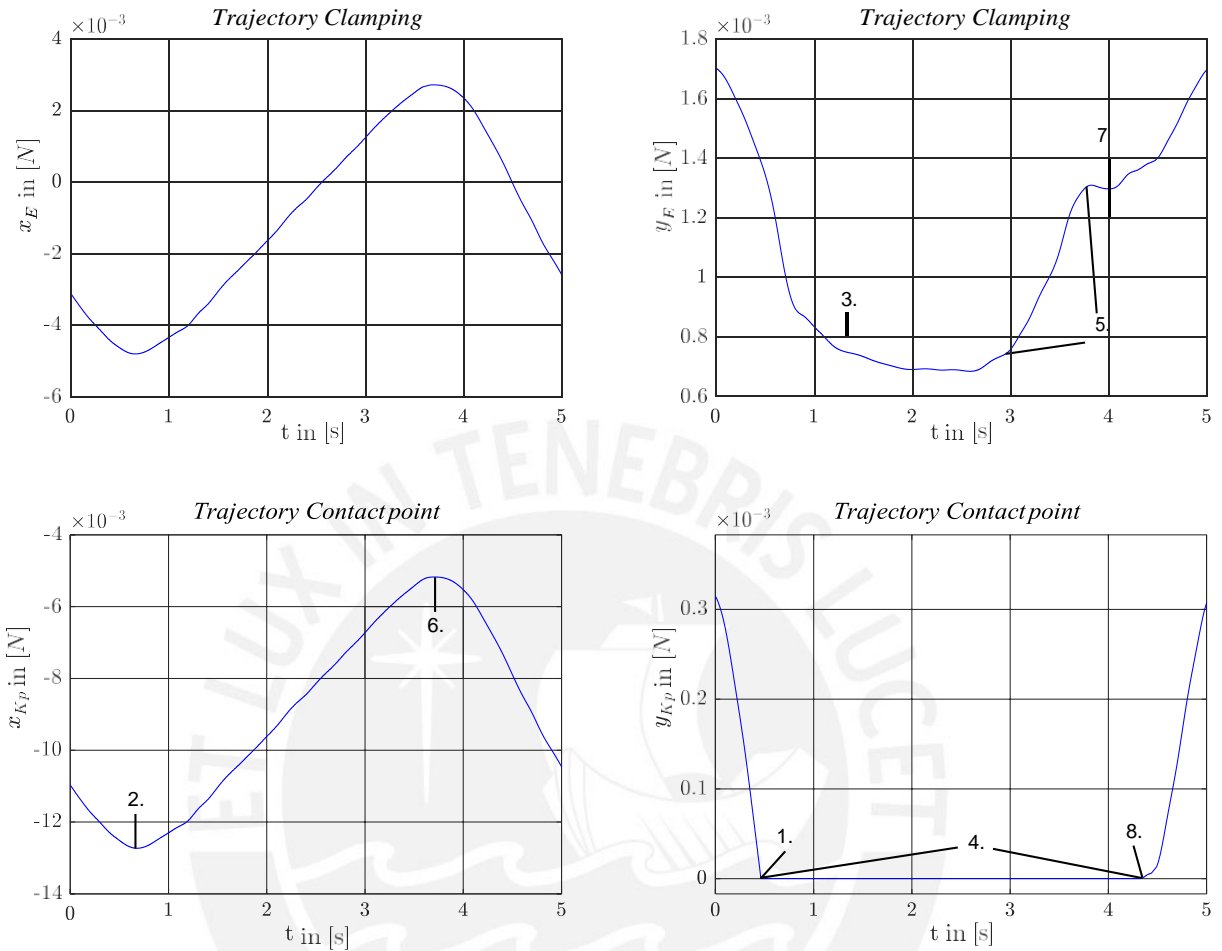


Figure 6.3: Trajectory of clamping (x_E , y_E) and contact point (x_{Kp} , y_{Kp}).

The figure 6.4 shows the course of the bearing reactions of a surface scan by means of a fixed beam with a given movement trajectory. The corresponding parameters are shown in section 5.2. References to the trajectory from figure 6.3 are established for this point.

In all bearing reactions the deflection of the signals starts at the first contact between beam and surface $g(x)$ (1.). The negative area following in the x component is caused by the negative direction of movement of the contact point in x direction and ends by the change of direction of the movement (2.). This results in a change in the load in the bar from compression to tension, which can be recognized by a change in the sign of the force. During the continuous scanning process (4.) the x -component of the force is positive in x -direction until the direction is reversed again.

The local maxima occurring in F_x at the times $t \approx 0.5s$ and $t \approx 1.15s$ can be traced back to the change in increase in y direction (3.). Here the contact point is pressed against the direction of movement by further lowering of the clamping. Meanwhile, the contact point is pulled further due to the movement specification. This results in a reduction of the force in x -direction. The decrease in bearing reactions occurring in the time range from $t \approx 3s$ to $t \approx 3.6s$ is due to the lifting of the clamping in y direction (5.). The subsequent negative range of the force F_x is again explained by a reversal of the direction of movement in x -direction (6.) and again leads to a change in load in the bar from tension to compression. The minimal change in position of the clamping in y -direction (7.) in the time range from $t \approx 3.55s$ to $t \approx 4.35s$ leads to a plateau, especially in the area of the force F_y and the moment M_z . Finally, all bearing reactions show the detachment of the vibrissae from the surface (8.) by the drop to zero.



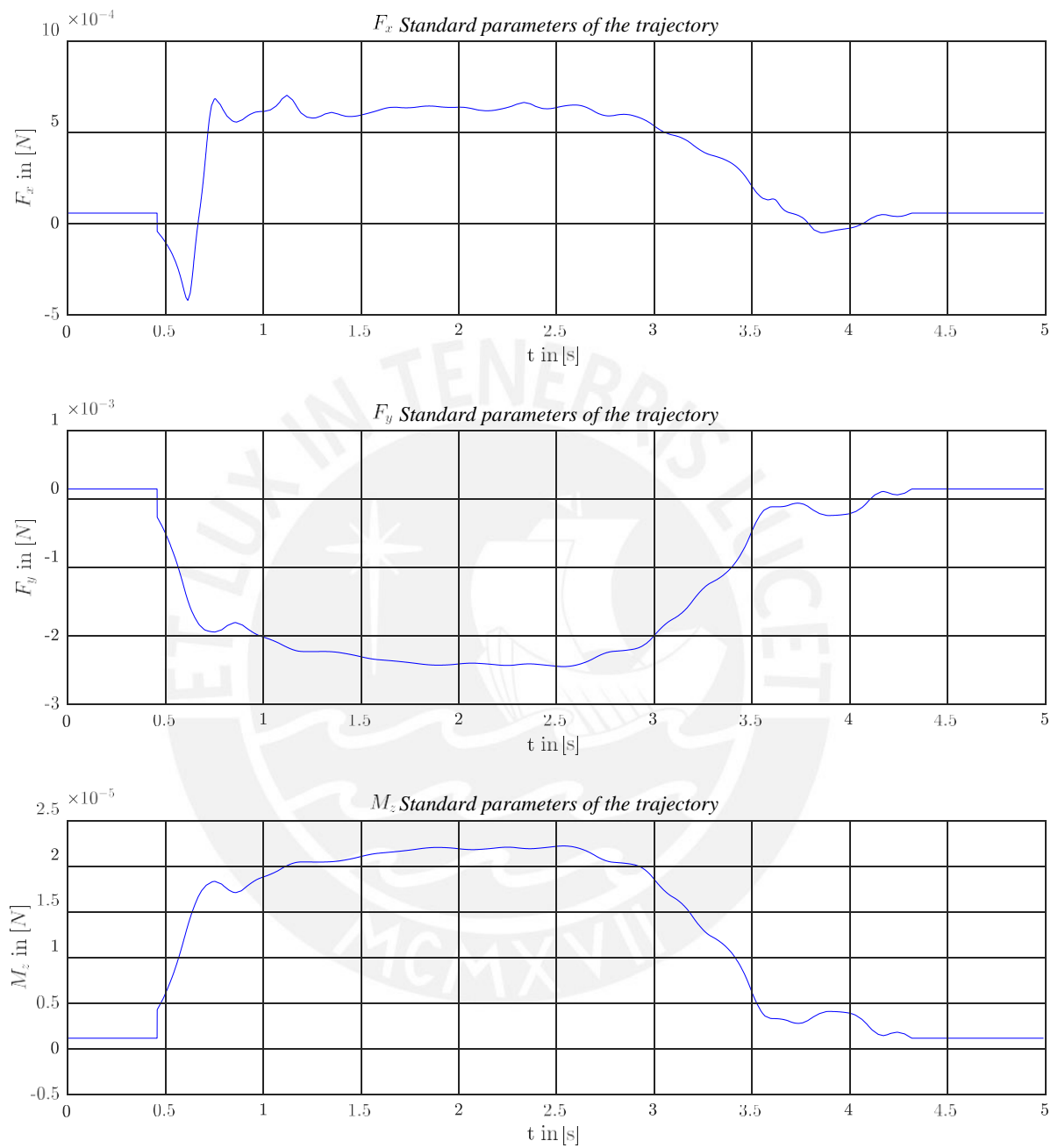


Figure 6.4: Bearing reaction over time t for the model with clamping with standard parameter.

6.2.1 Variation of the coefficient of friction

In the following, the coefficient of friction μ is varied. The remaining parameters are used according to chapter 5. In *ALASKA* the friction coefficient μ is divided into a coefficient for kinetic friction μ_{kin} and one for static friction μ_{sta} . In the following, only the kinetic factor is adjusted. The static factor is calculated internally in *ALASKA* by the standard configuration in the form of a factor of 1.5.

In figure 6.5 the corresponding bearing reactions are shown. It is noticeable that a variation of the friction coefficient mainly influences the contact force in x -direction; in the force component in F_y -direction and the moment in z -direction only a minimal change is visible. The reason is that the coefficient of friction μ only has an influence on the friction force. This acts against the direction of movement of the contact point, which can only move in x -direction due to contact with the surface. The relatively small changes in the other two bearing reactions are based on the minimal change in length of the beam, which is simulated by the thrust joint.

The friction coefficient μ has a linear influence on the contact force. This can also be seen in the bearing reactions; for example, an increase in amplitude can be observed with a simultaneous increase in the coefficient of friction μ . The basic form remains unchanged.

The common point of intersection at $t \approx 0.7s$ and $t \approx 3.75s$ remains unaffected by the variation of the coefficient of friction μ , since at this point the direction of the x movement is reversed and thus no movement exists which causes friction.

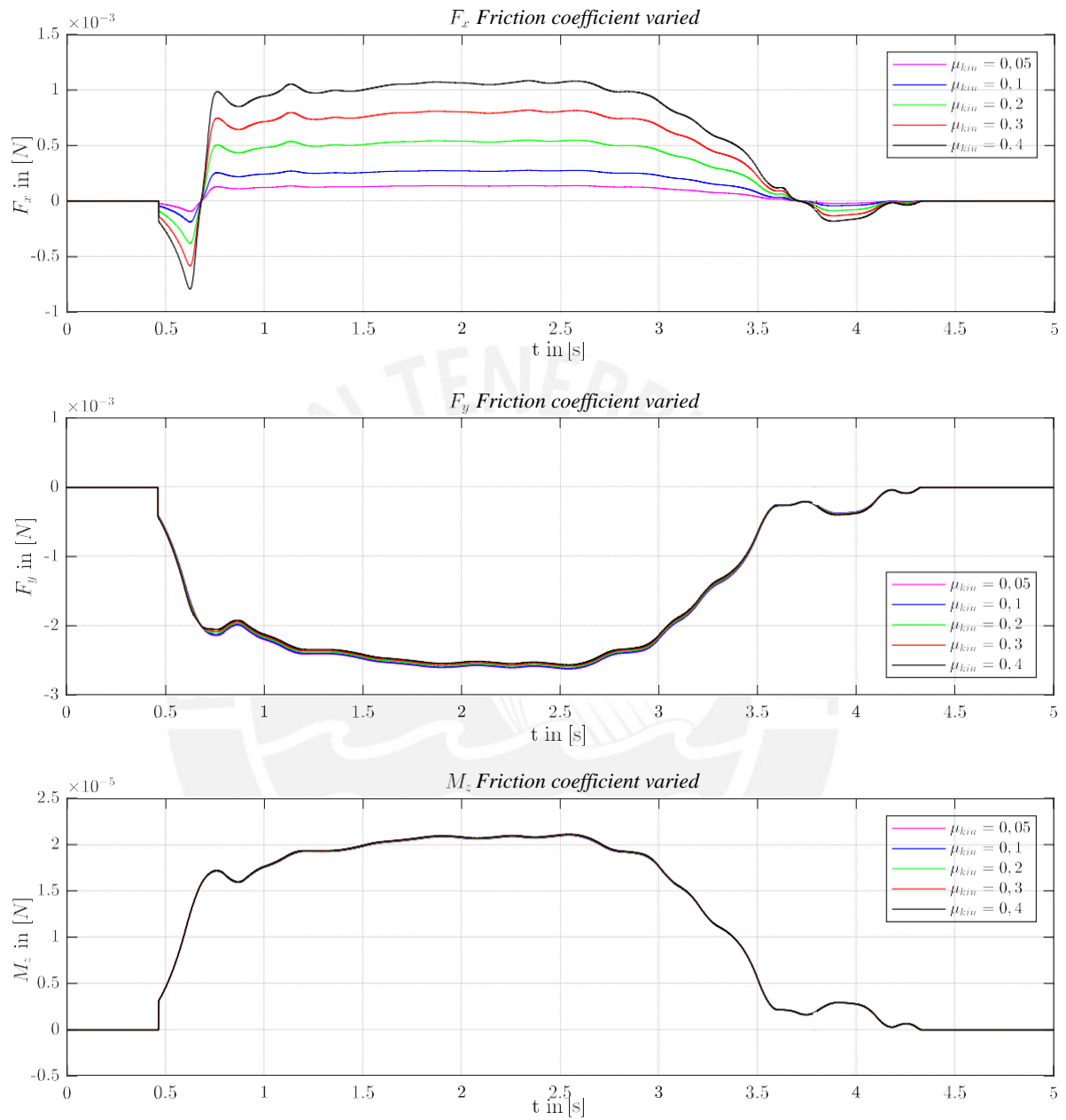


Figure 6.5: Bearing reaction over time t for the model with clamping with variation of the friction coefficient μ .

6.2.2 Variation of object distance

In the following section the object distance of the beam q is varied. The other parameters are selected as described in chapter 5.

Figure 6.6 shows the bearing reactions of this investigation. It can be seen that a variation of the object distance influences all three bearing reactions. Furthermore, a change of the signal strength is visible. Both mentioned effects can be explained by the change of the deformations due to the object distance variation. Thus an increase of the distance leads to a reduction of the bearing reactions.

Furthermore, a change in the contact time can be seen. If the distance is smaller, the time in which the beam is in contact with the object increases. In addition, with an object distance of $q = 0.0006m$ and $q = 0.0007m$ there is no negative range in the time range of $t \approx 4s$. This is because the beam is no longer in contact with the object at these distances when the trajectory specification causes a new reversal of motion. Furthermore, the common intersection point is maintained when the contact point reverses its movement in x direction.

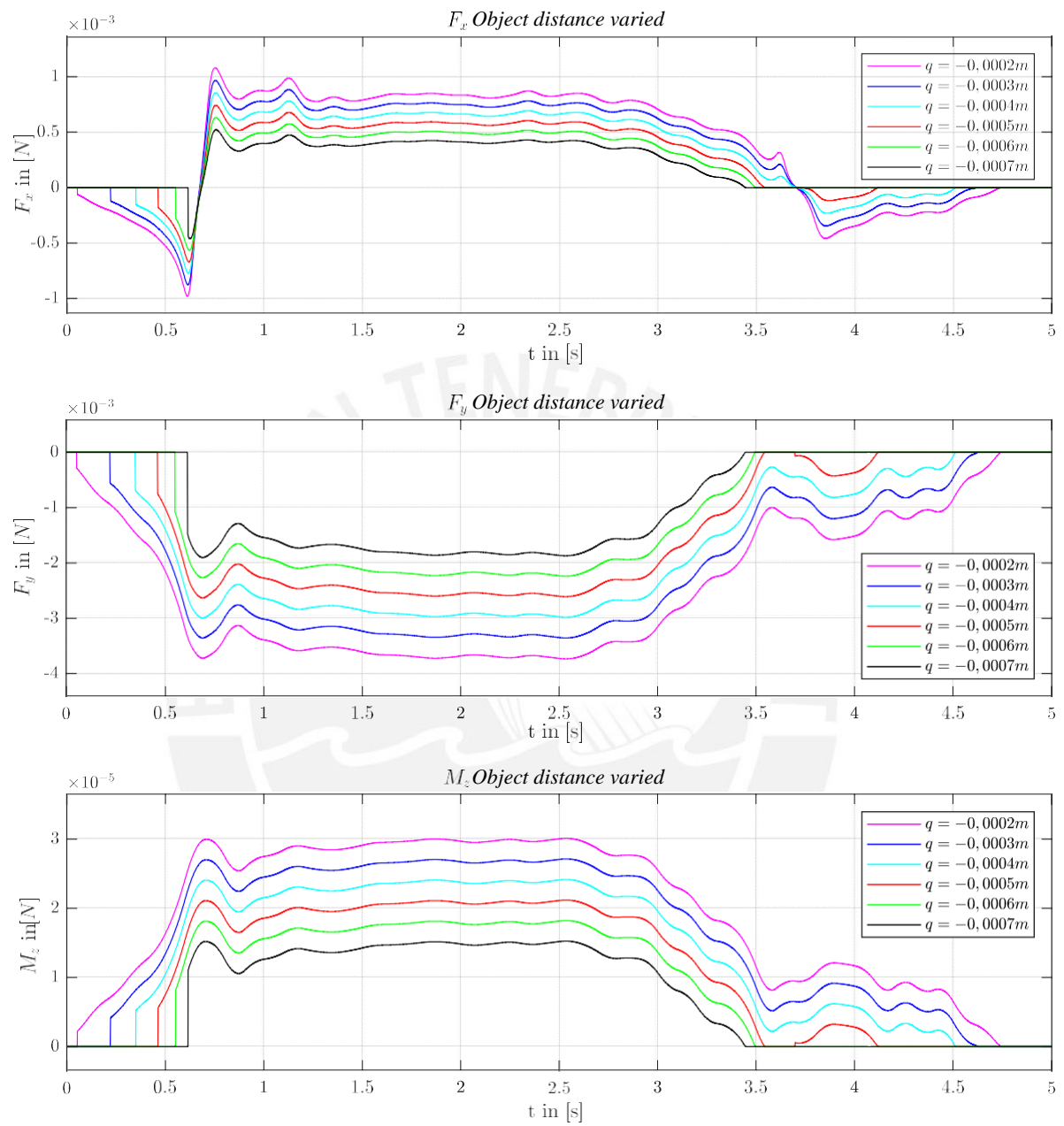
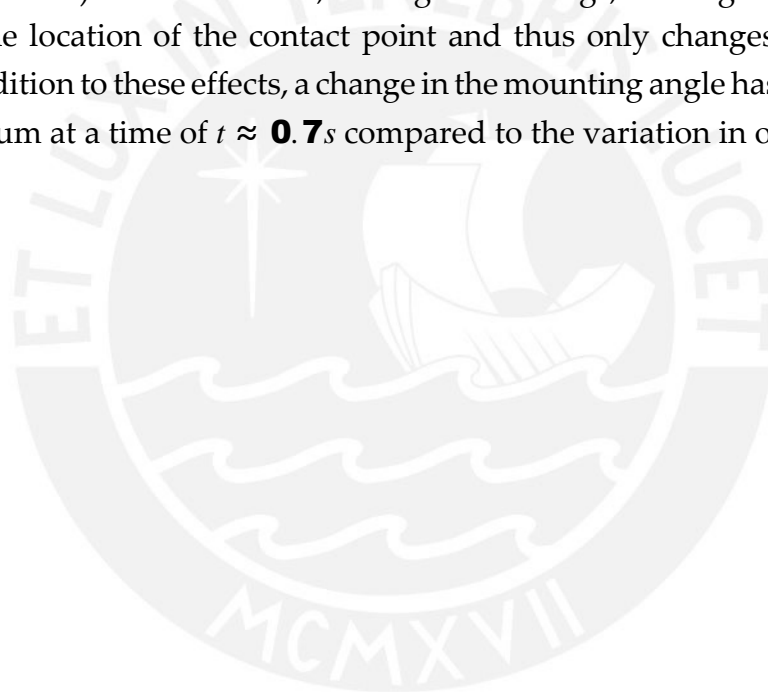


Figure 6.6: Bearing reaction over time t for the model with clamping by variation of the object distance q .

6.2.3 Variation of fixing angle

In the following, the angle of the beam is varied at the clamping β , the other parameters are selected as in chapter 5. The variation takes place in the range $\beta = 168^\circ - 172^\circ$. An angle larger than this range will prevent the beam from coming into contact with the surface. If you choose an angle smaller than this range, a contact within the surface already exists at the beginning of the simulation. This leads to an increased simulation effort. This was waived for a first investigation.

Figure 6.7 shows the bearing reactions of this investigation. It can be seen that a variation of the mounting angle has the same effects and causes as a variation of the object distance q (see section 6.2.2). This is because, among other things, a change in the angle causes a change in the location of the contact point and thus only changes the distance to the object. In addition to these effects, a change in the mounting angle has a more pronounced local maximum at a time of $t \approx 0.7$ s compared to the variation in object distance.



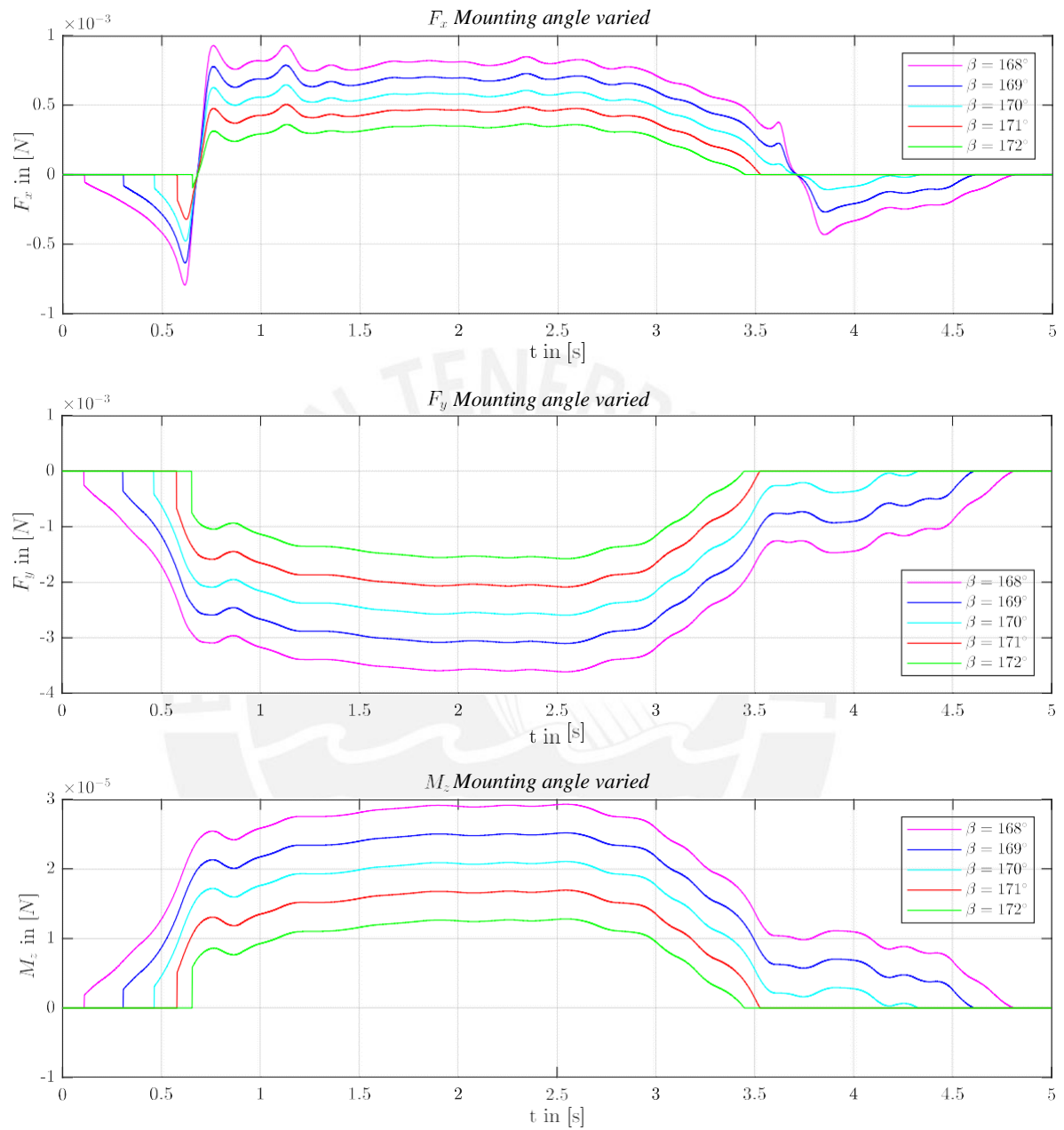


Figure 6.7: Bearing reaction over time t for the model with clamping by variation of the fixing angle β .

6.2.4 Variation of surface slope

In the following, a variation of the surface slope is examined. For this purpose, the contact surface is rotated at the point $x_{Abstand} = -0.009m$ by the angle ϕ .

Figure 6.8 shows the bearing reactions for a variation of the surface slope ϕ . Again, effects occur in all bearing reactions. First of all, it is noticeable that the beam comes into contact with the surface earlier at a negative angle and also detaches earlier. Furthermore, as with the variation of the object distance (see section 6.2.2), there is no negative range at an angle of $\phi = -2^\circ$ at the time of $t \approx 4s$. Again, this is due to the fact that the contact is missing after the reversal of motion in x direction. The points of intersection due to the reversal of motion are still present in the force F_x .

In all three bearing reactions an additional intersection point is noticeable. For the force F_y and the moment M_z this is at a time of $t \approx 2.15s$. At this time, the contact point is at the tipping point of the surface (see Fig. 6.3 at a time of $t \approx 2.15s$ corresponds to a value of $x_{Abstand} = -0.009m$) With the force F_x this intersection point is reached earlier ($t \approx 1.25s$). This is due, among other things, to the thrust joints and the trajectory specification, where a x and y movement occurs simultaneously.

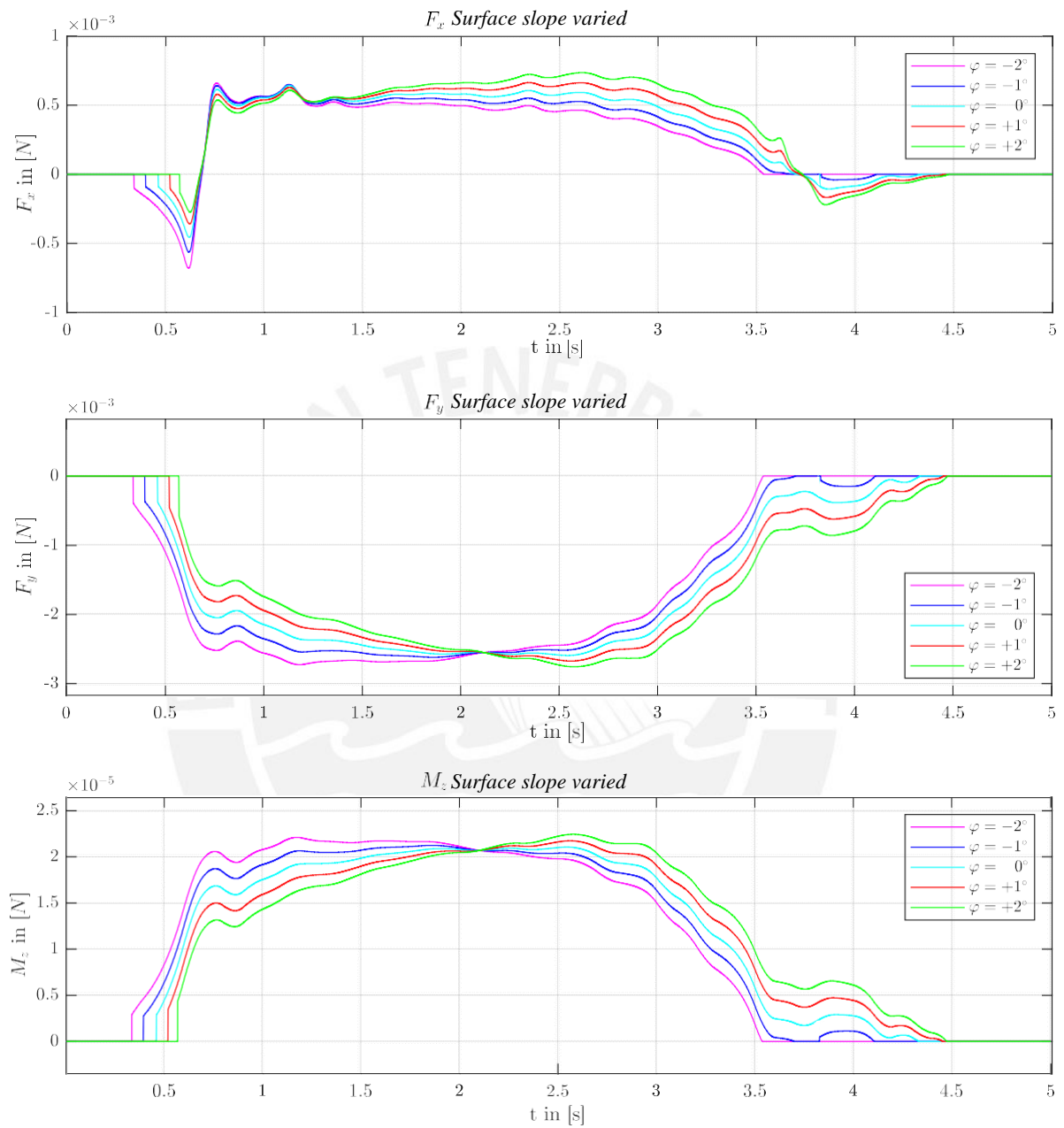


Figure 6.8: Bearing reaction over time t for the model with clamping by variation of the surface slope ϕ .

6.2.5 Variation of Young's Modulus

A variation of Young's modulus E only leads to a signal strength change of the bearing reactions (see fig. 6.9). As a result, the bearing reactions increase when the Young's modulus is increased. The sampling period as well as the common intersection points in F_x are unaffected.

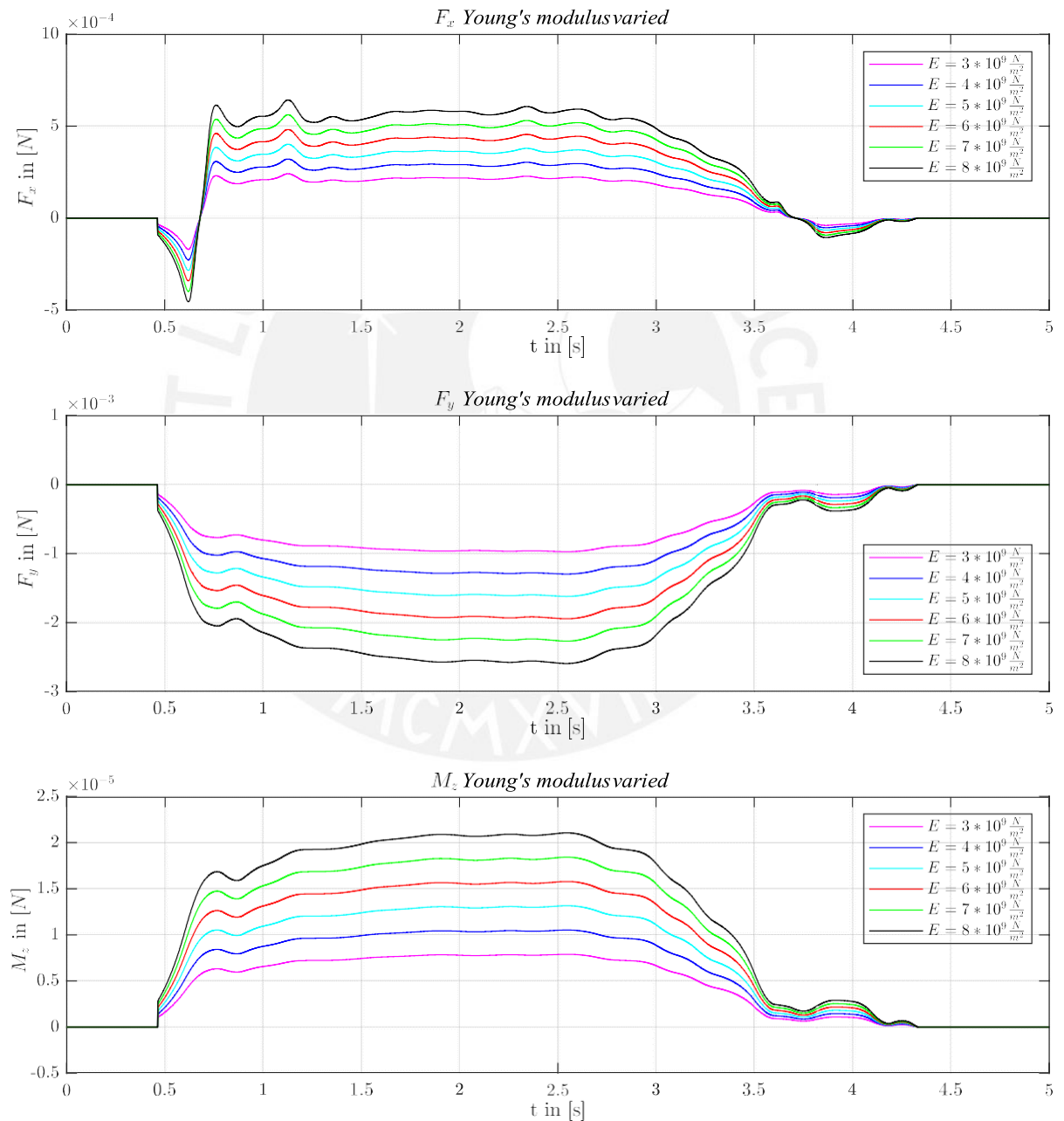


Figure 6.9: Bearing reaction over time t for the model with restraint by variation of the Young's modulus E .

6.3 Surface scanning with elastic bearing

In nature, the support of vibrissae is not to be regarded as a restraint, as previously investigated, because the paw tissue, in which the vibrissa are rooted, has elastic properties. Therefore, in the following a surface scan with an elastically clamped beam is carried out under specification of the movement trajectory. Parameter studies are carried out to investigate the coefficient of friction, the vibrissae clamping, the object distance, the ground rise and the properties of the beam. The adjustment parameters of the elastic support are modelled on nature [SBH⁺10] and, in addition to the other parameters necessary for the simulation, are presented in the chapter 5.2.

Figure 6.10 shows a comparison of the bearing reactions of both models (clamping and elastic support). A significantly lower signal strength in the simulation with elastic support (bushing) is noticeable, because in the comparison the beam is less deformed due to the elastic effect of the support. Furthermore, a shift of the signals in positive x direction is visible, which occurs due to the delayed scanning by the elasticity. This also includes the intersection point of the zero line at the force F_x , which is caused by the reversal of motion. The initial contact between beam and object remains unchanged due to a missing force on the elastic elements. Also the detachment happens almost at the same time, because the force shortly before detachment is also very low here. This causes a minimal deflection of the elastic elements.

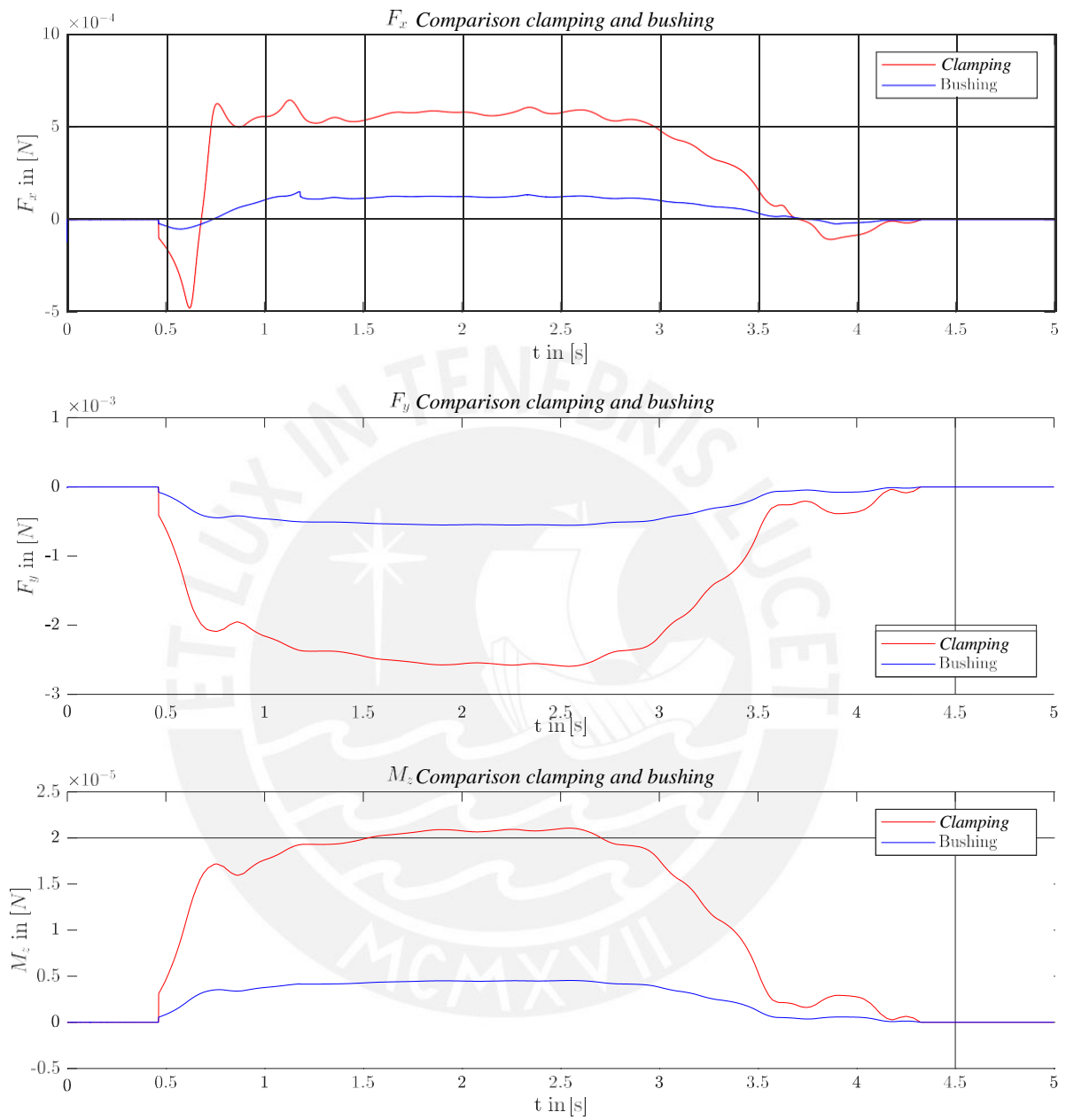


Figure 6.10: Bearing reaction over time t in comparison for the model with restraint and elastic support with standard parameters.

6.3.1 Variation of spring stiffness

In the following, the spring stiffness is varied in x and y direction of the elastic support (c_x , c_y). The variation of both parameters is done simultaneously. The proportionality factor of 10 between the stiffnesses is maintained. In the legend of the figure 6.11 only the spring stiffness c_x is shown for clarity. With the variation of the spring stiffness, a change in the signal strength is visible in all bearing reactions. As in section 6.3, this is due to the lower deformation caused by the elastic displacement of the beam restraint. Thus a reduction of the spring stiffness leads to a reduction of the signal strength in the bearing reactions. The intersection point in the force F_x at a time of $t \approx 0.7s$, which occurs in the model with elastic support, is not present in the model with elastic support, since the time delay of the signal is directly influenced by the spring stiffness. Furthermore, a displacement of the signals in the direction of movement can be derived with a decrease of the spring stiffness c_x . This finding corresponds to simulation results existing in the literature [MBSZ19].



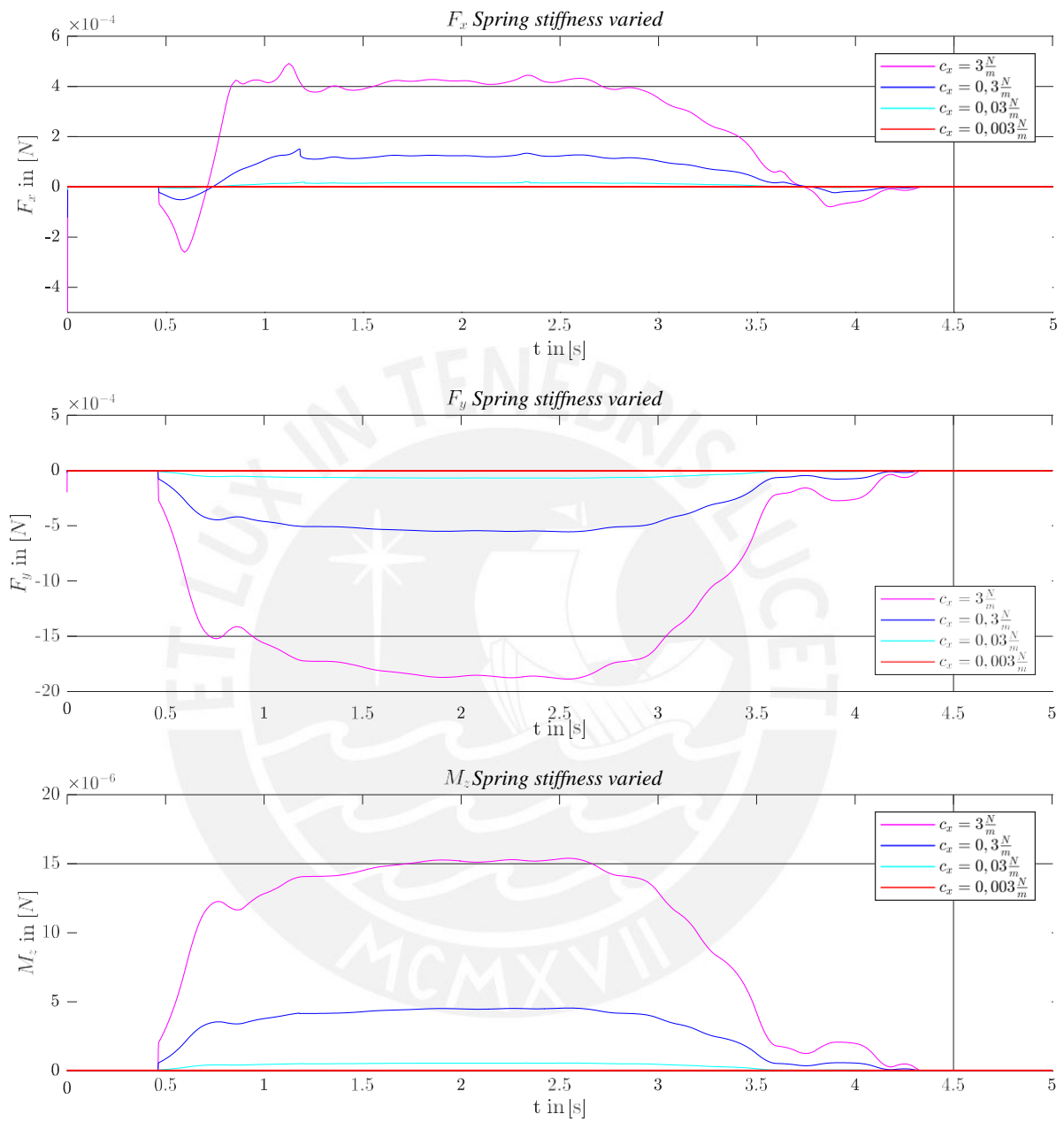


Figure 6.11: Bearing reaction over time t for the model with elastic support with variation of the spring stiffnesses c_x and c_y .

6.3.2 Variation of the coefficient of friction

A variation of the friction coefficient of the model with elastic support leads to largely the same findings as with the model with restraint (see section 6.2.1). However, the signal strengths of the individual bearing reactions are lower (see figure 6.13). Only the common points of intersection for the reversal of motion in x direction no longer exist.

The shape of the local maxima at $t \approx 1.3s$, $t \approx 1.6s$ and $t \approx 2.3s$ is also different in the model with elastic support. One hypothesis is that these jump points in the bearing force F_x result from a combination of different factors. Firstly, the velocity at the crack points changes, which is apparent in the form of an increase in the contact position in the x direction (x_{Kp}) (see Figure 6.12). This leads to the assumption that due to the friction, a delay occurs at the contact point. This leads to a change in the length of the bushing, which breaks loose when a threshold force is exceeded and causes an abrupt change in the position of the contact point and the forces. The fact that this effect occurs primarily in the x direction indicates that it has its origin in friction. It is also assumed that the specification of the movement trajectory also has an influence on the local maxima. The default motion does not have a straight line and, by changing the y coordinate, leads to a change in the contact force F_y and thus also to a change in the normal force F_N necessary for friction (see section 3.3).

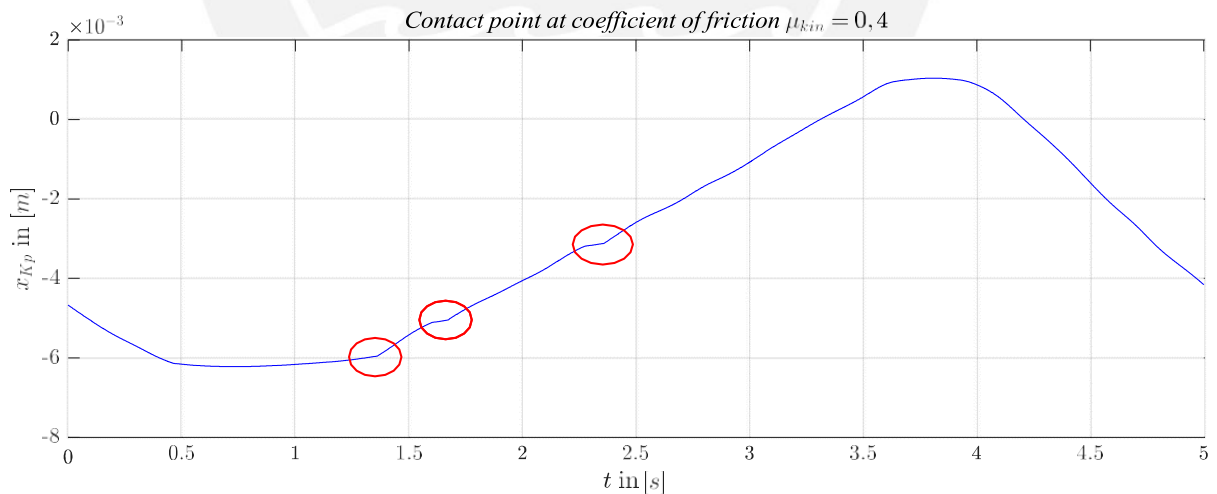


Figure 6.12: x -position of the contact point x_{Kp} over time t for the model with elastic support at the friction coefficient $\mu_{kin} = 0,4$.

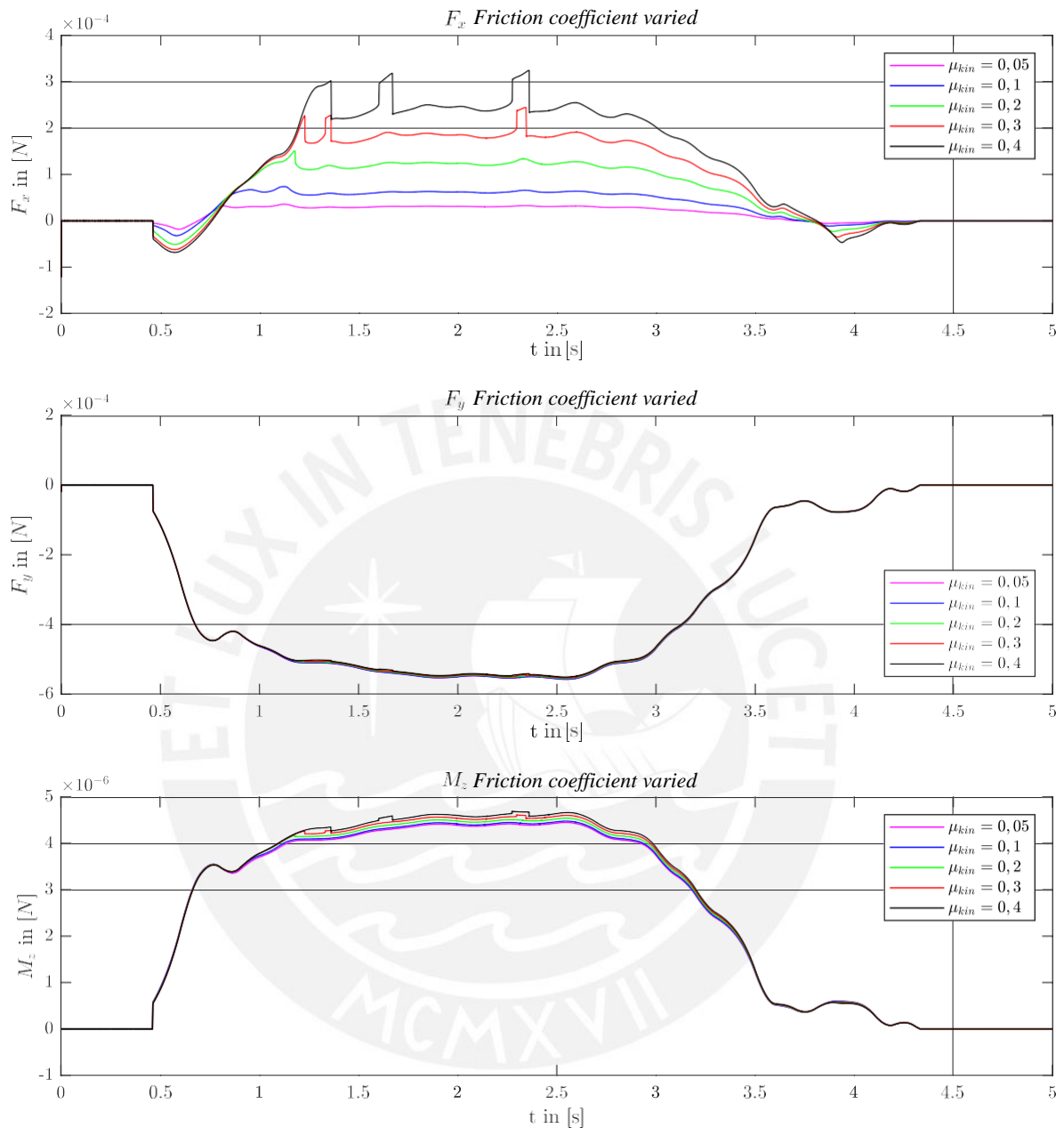


Figure 6.13: Bearing reaction over time t for the model with elastic support with variation of the friction coefficient μ_{kin} .

6.3.3 Variation of object distance

Figure 6.14 shows the support reactions of the model with elastic support with variation of the object distance. No new effects can be detected compared to the model with restraint (see section 6.2.2). The common intersection point for the reversal of motion due to the elastic support is also not present here. Furthermore, the local maxima are influenced by

the change of the object distance. The same hypotheses as for the variation of the friction coefficient are also conceivable here (see section 6.3.2). A change of the object distance leads to an increase of the normal force F_N , which results in an increase of the friction effects.

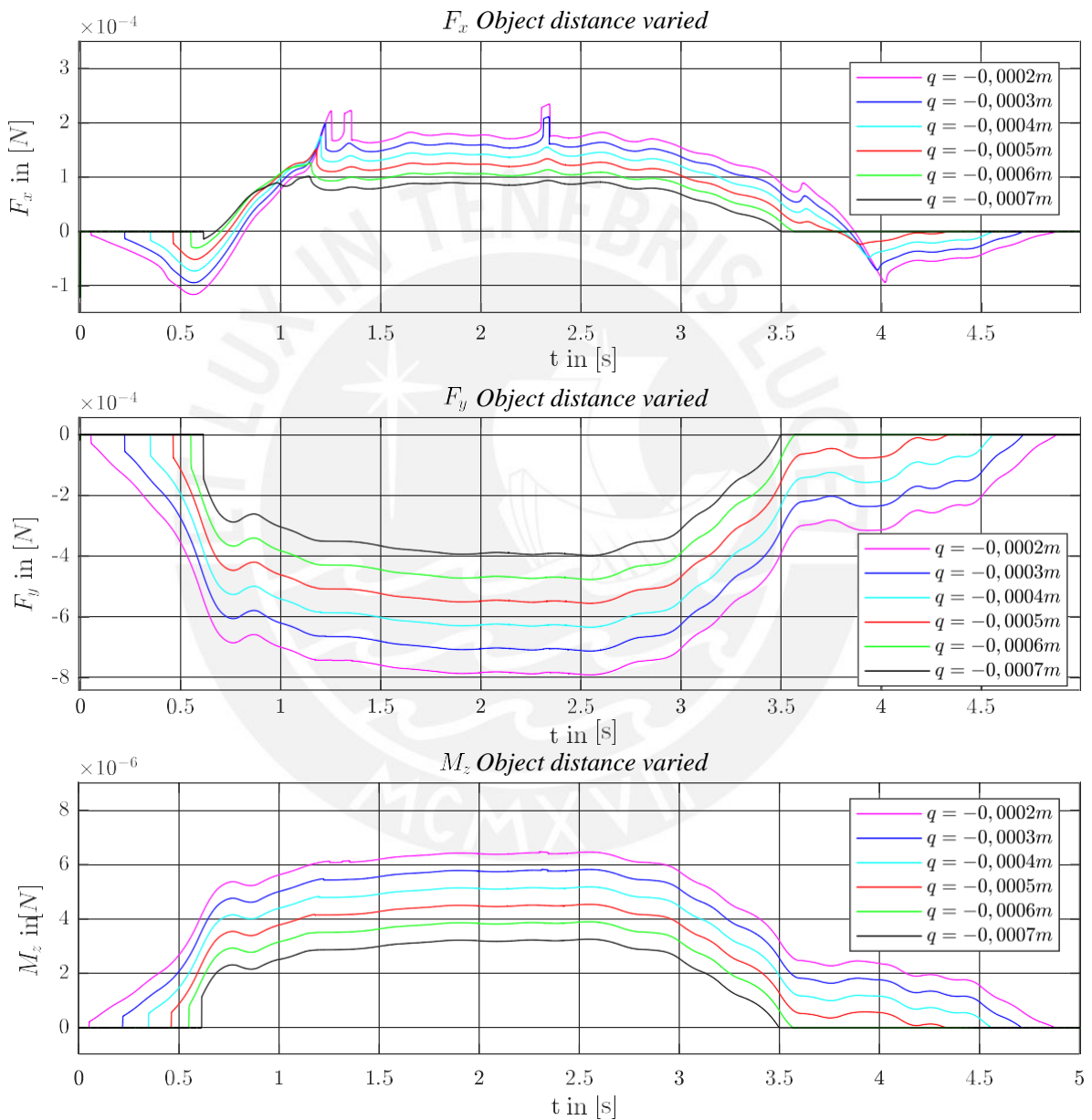


Figure 6.14: Bearing reaction over time t for the model with elastic support by variation of the object distance q .

6.3.4 Variation of fixing angle

A variation of the fixing angle β leads to a change in the object distance of the contact point on the beam, analogous to the section 6.2.3. Thus, even in the model with elastic support, no other effects can be observed in the support reactions (see Fig. 6.15) than those resulting from the variation of the object distance (see section 6.3.3). Furthermore, no common points of intersection are recognizable due to the reversal of motion in x direction.

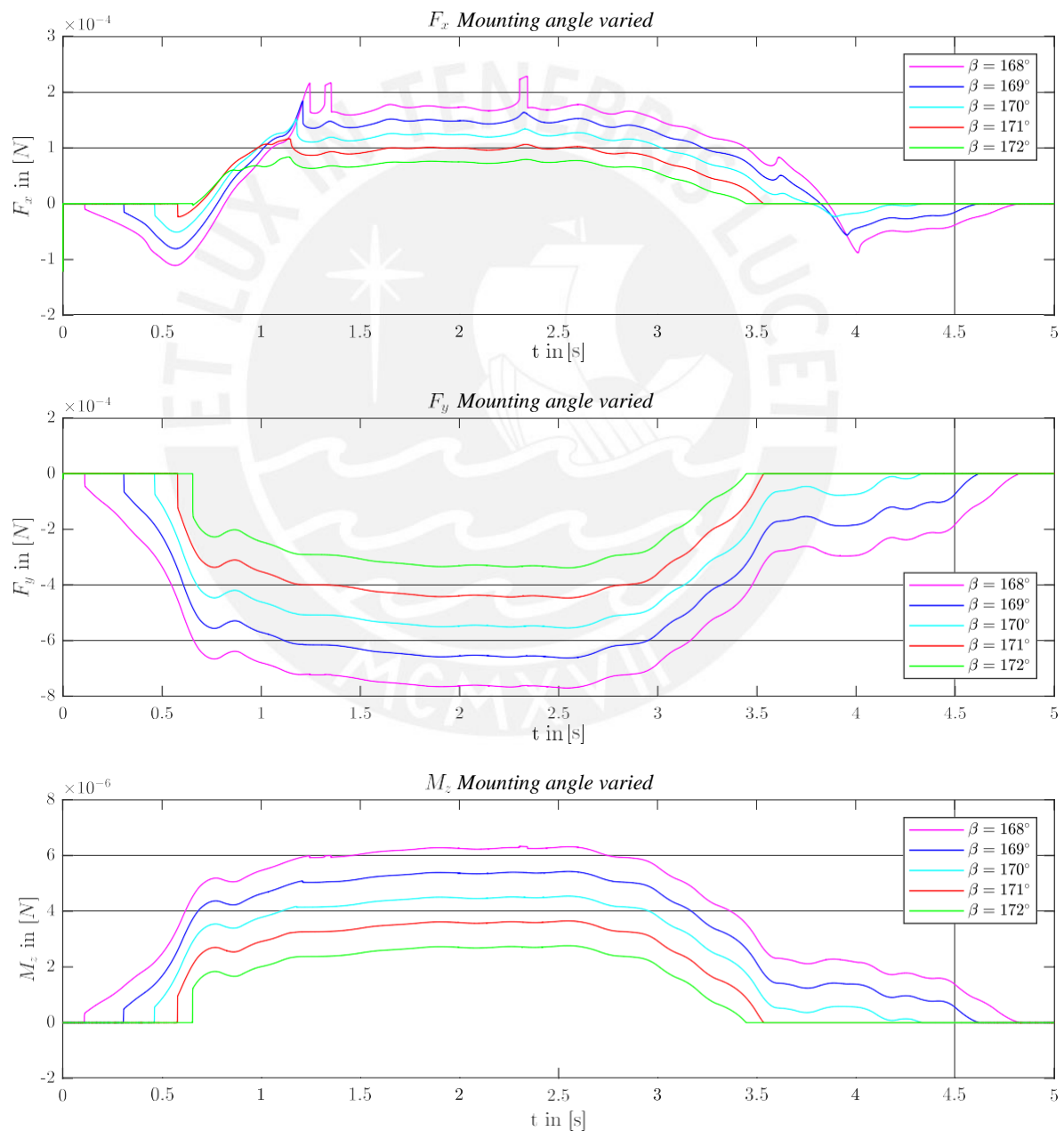


Figure 6.15: Bearing reaction over time t for the model with elastic support with variation of the fixing angle β .

6.3.5 Variation of surface slope

Figure 6.16 shows the bearing reactions with varied surface slope ϕ . Compared to the restraint model (see section 6.2.4), the effects are almost identical. The only difference is that in the model with elastic support there are no common points of intersection of the different signals at the force F_x due to the reversal of motion. The point of intersection, which results from the inclination of the surface, still exists and is therefore independent of the type of support

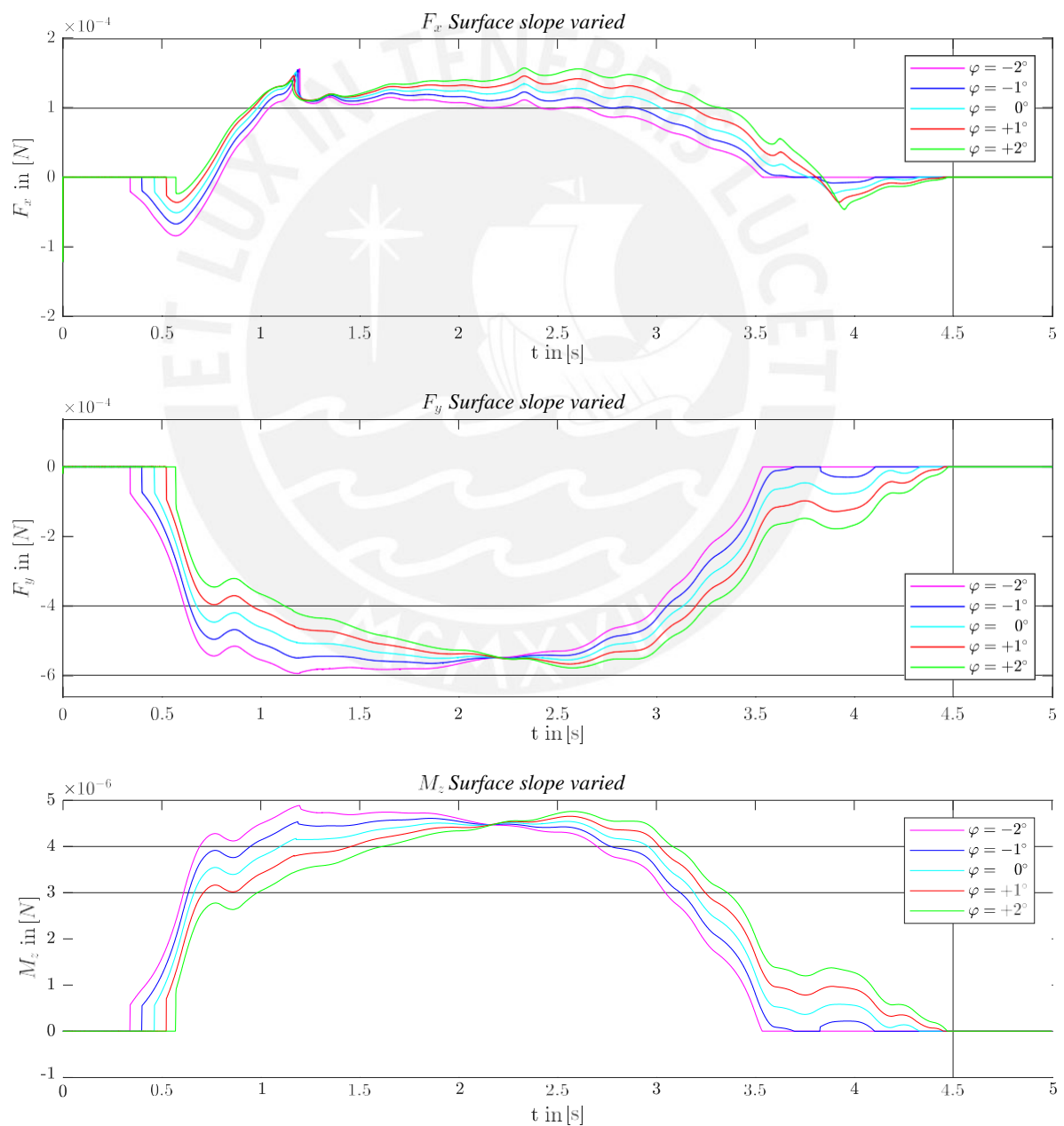


Figure 6.16: Bearing reaction over time t for the model with elastic support with variation of the surface slope ϕ .

6.3.6 Variation of Young's Modulus

Even a variation of Young's modulus does not provide any further insights in comparison to the section 6.2.5 (see fig. 6.17). The basic effects due to the elastic support - no common points of intersection, lower signal strength - are still evident.

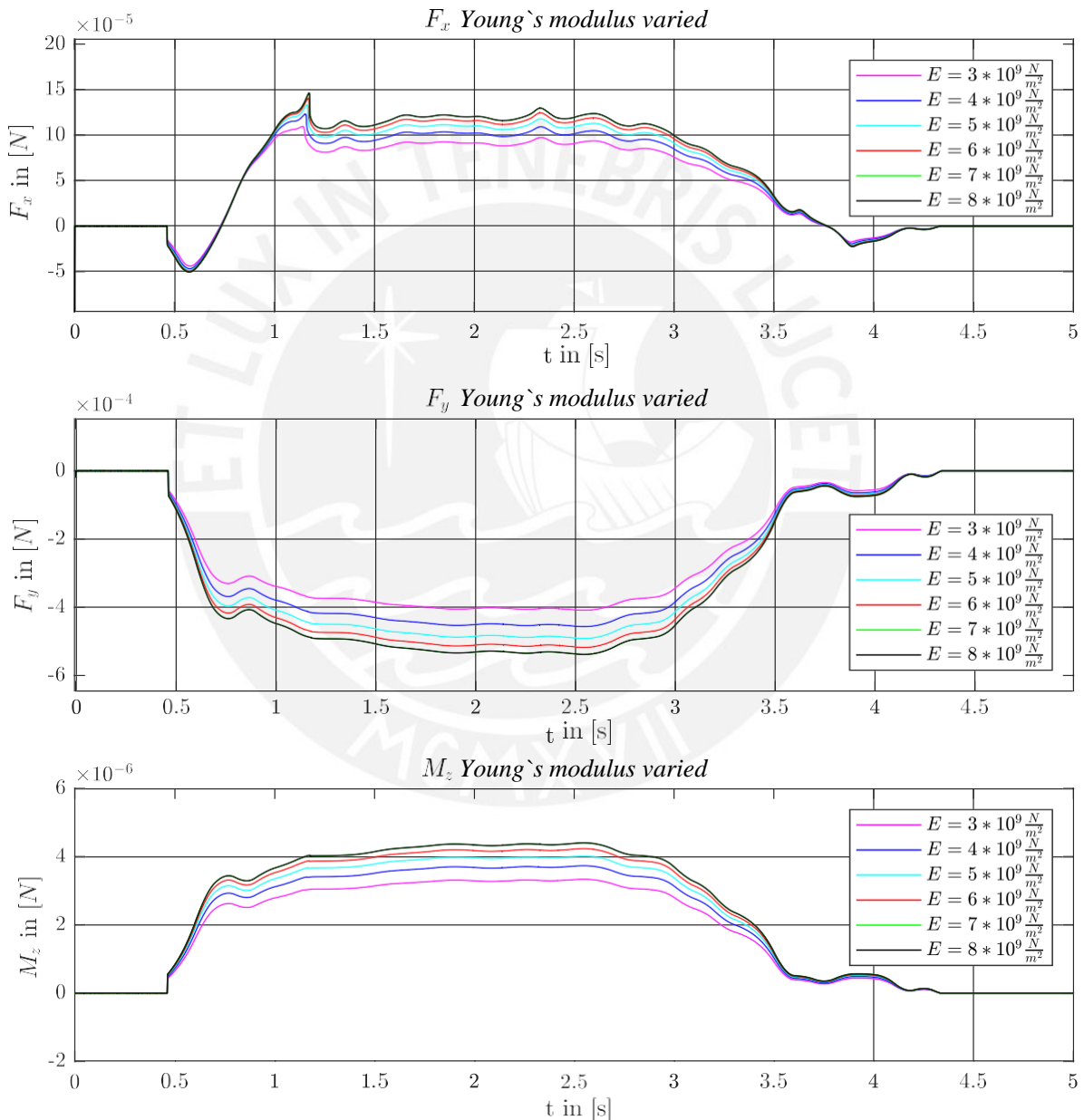


Figure 6.17: Bearing reaction over time t for the model with elastic support with variation of the Young modulus E .

6.4 Conclusion

In both simulated models (with restraint and with elastic support) three basic effects can be identified in parameter studies:

1. Signal strength change:

All variations of individual parameters carried out tend to lead to a change in signal strength in all bearing reactions. Only a modification of the friction coefficient leads to a change in signal strength in the force F_x ; the other two bearing reactions are largely unaffected. Here, an increase of the friction coefficient leads to a higher signal strength in the force F_x .

Furthermore, a reduction of the distance to the object leads to an increase in the bearing reactions. This can be seen by varying the object distance, the mounting angle and the object rise.

2. Contact time change:

When looking at the contact times between beam and object, two results can be concluded. On the one hand, a reduction of the distance between the beam and the object leads to an increase in the contact time. The reduction in distance can be caused by reducing the distance between the object or by reducing the mounting angle. On the other hand, a variation of the surface slope leads to a shift in the contact time. A negative slope angle of the object leads to a displacement in negative x direction and a positive slope angle leads to a displacement in positive x direction.

3. Intercept points in the bearing reactions:

For both models (with clamping and with elastic support), different intersections of the signals in the bearing reactions can be seen. For example, in the model with fixed support, when reversing the direction of the movement in x direction, intersections occur at the zero crossing of the force F_x . These are not present in the model with elastic support due to the elastic effect of the bearing.

On the other hand, when varying the surface slope, both models have an additional intersection point due to the same object distance at the point of object rotation.

In comparison between the two models, the model with elastic mounting shows a lower signal strength, which is due to the additional elastic effect in the mounting. Furthermore, the delay of the movement due to the modulated springs results in a time shift of the signals. The more elastic the bearing is designed, the greater is this delay.

With regard to the use as tactile sensors, the model with fixed mounting is better suited to scanning objects and thus to collect information about their properties due to the higher signal strength. If this model cannot be selected for other reasons, the elastic bearing should be designed as stiff as possible with regard to the signal strength. Furthermore, it should be noted that minimizing the object distance also leads to an increase of the signal strength.



Summary and Outlook

The present work complements research activities of the TU Ilmenau and the PUCP Lima in the field of tactile sensor technology based on the biological model of vibrissae (special tactile hairs). Here, an investigation of the signals of carpal vibrissae of a rat's locomotion is carried out to determine the influences of the friction coefficient, vibrissae attachment, vibrissae properties, object distance and surface slope.

With the aim of understanding the biological relationships that are necessary for modelling with subsequent analysis, the current state of knowledge about the vibrissae of a rat, the skeletal structure and the musculature of the extremities was analysed in the chapter 2. The following findings were thus obtained:

- Vibrissae are special hairs which are found on the extremities of rats, among others [Kla99].
- The hairs have a slender, long form, are pliable and elastic and serve as a conductor of stimuli [Kla99].
- Vibrissae are elastically mounted in the follicle-sinus complex, which also contains the mechanoreceptors [Kla99].

- Mammals that possess vibrissae use them to palpate surfaces and determine their properties [PMG11].
- Rats possess such vibrissae of a rat and can perform a variety of movements; the most common movement used for research purposes is walking [Sch01].
- During locomotion, areas of the extremities coupled by joints are moved relative to each other by means of targeted muscle contraction [BETV11, MF11, WHF97].

In the following chapter 3 the state of the art was presented with respect to the application of tactile sensors, the modelling of an artificial vibrissae, the friction theory according to Coulomb and existing simulation methods. This led to the specification of the task formulated in chapter 4, where it was determined that the simulations should be solved by means of multi-body simulation in the program *ALASKA*.

In chapter 5 the implementation of the model construction is described. A motion specification according to the trajectory of [Ber14] is implemented at the attachment point of the artificial vibrissa. The actual tactile hair is modelled as an Euler-Bernoulli beam and is attached to the paw simulated by the trajectory of motion by means of a clamping or elastic support. At the end of the chapter a verification of the created and implemented model was performed in Alaska. In order to verify the model, results of the beam deformations and the corresponding bearing reactions were compared with a directional or angular force application and with a parallel work generated during translational object scanning.

Within the framework of the parameter studies carried out in chapter 6 to investigate the influences of friction, beam attachment, object distance, vibrissae properties as well as surface slope, the results presented in the following provide A **change in signal strength** can be seen in the bearing responses when the object distance is changed by direct or indirect modification in the form of an adjustment of the mounting angle or surface slope. Furthermore, the coefficient of friction μ mainly influences the force F_x . The variation of the object distance leads to a **contact time change**, which again can be direct or indirect. In contrast, a modification of the surface slope leads to a **displacement of the contact time**. Furthermore, different **intersections in the bearing reactions** occur during object scanning. The intersection points occurring in the force F_x in the model with restraint result from the change of the direction of movement in x -direction, which determines the trajectory. These intersection points no longer exist in the model with elastic support due to the time delay caused by the elastic and damping effect. A further intersection point can be seen due to the variation of the surface slope.

The presented results of this work may form the basis for further investigations in the context of the investigation of signals of carpal vibrissae during object scanning under consideration of a motion trajectory. Already during the verification of the simulation models an influence of the scanning speed in the form of dynamic effects has been noticed. For example, a higher speed leads to an impact at the first contact between beam and object (see fig. 7.1). This also leads to a strong noise in the bearing reactions in figure 7.2. To assess the influences of the examined parameters at higher speeds, dynamic investigations should be carried out with regard to the problems shown.

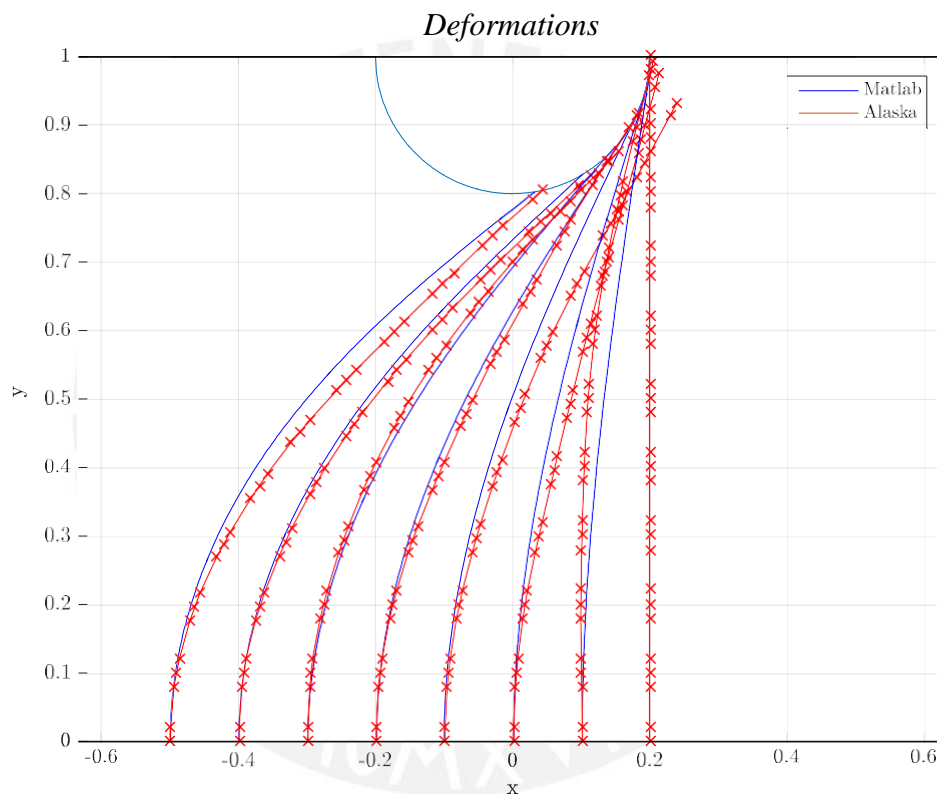


Figure 7.1: Comparing the deformations of the vibrissae when scanning a circle contour with dynamic effects.

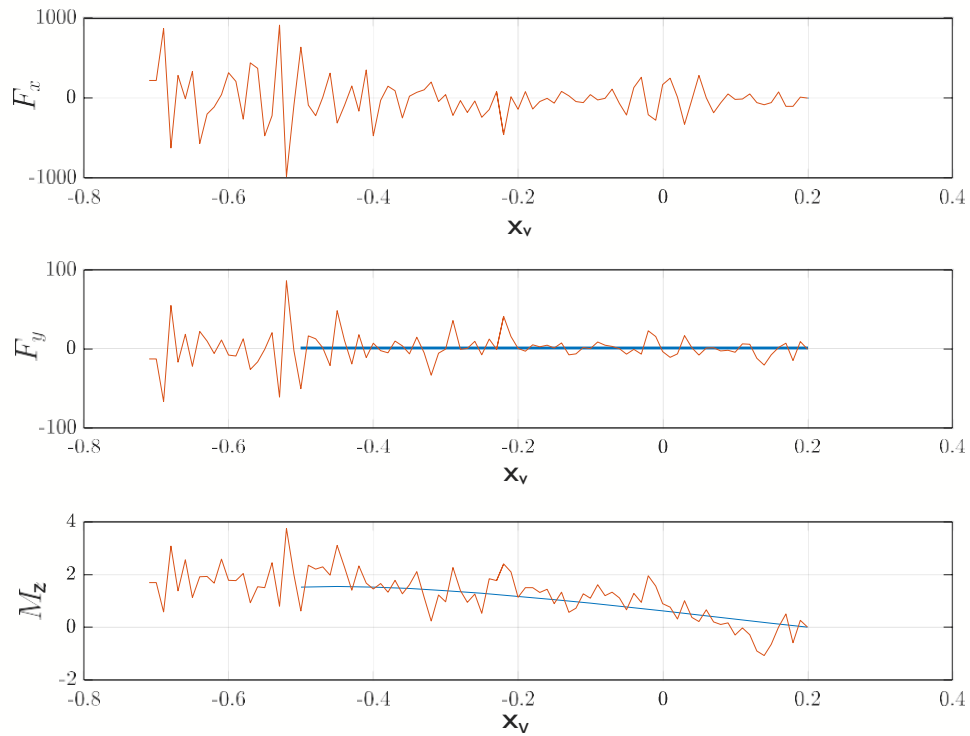


Figure 7.2: Comparison of the bearing reactions (dimensionless) at the vibrissae when scanning a circle contour with dynamic effects.

Furthermore, during the evaluation of the bearing reactions in the model with elastic restraint, a change in shape of the local maxima occurred during the variation of the friction coefficient or the object distance. In the present work, however, only hypotheses about its cause could be made (see section 6.3.2). For this reason, a more detailed investigation of this effect should be carried out.

Furthermore, the beam model should be adapted to the reality of the biological model by modification. Thus the conical shape of the vibrissa and the hollow area should be modelled after the medulla (see chapter 2). Figure 7.3 shows first approaches for this modification. The medulla can be simulated in a first approximation by a hollow beam model (see figure 7.3 (b)). For the first test an inner radius of $R_i = 0.00005m$ and an outer radius of $R = 0.0001m$ is selected. To simulate the conicity, the diameter of the individual beam elements can be reduced step by step in the direction of the bar ($R = [0.0001m; 0.00008m; 0.00006m; 0.00004m; 0.00002m]$) in the first level of abstraction (see Fig. 7.3 (c)). Furthermore, it is conceivable to combine these two models with R as in (c) and $R_i = [0.00005m; 0.00004m; 0.00003m; 0.00002m; 0.00001m]$ (see fig. 7.3(d)).

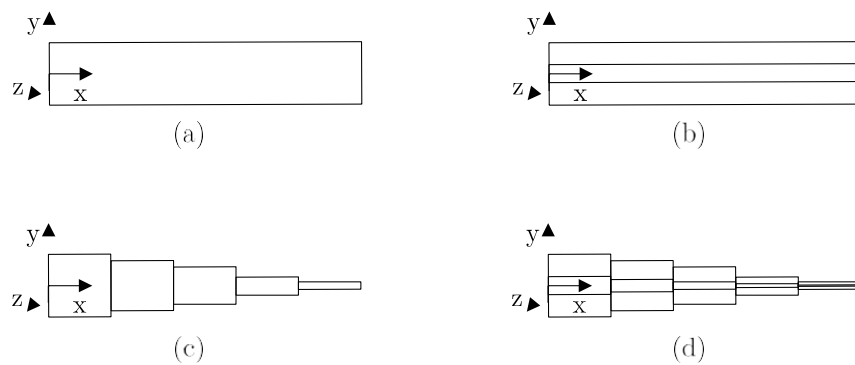


Figure 7.3: Modification levels of the beam model:

- (a) solid beam;
- (b) hollow beam to reproduce the medulla;
- (c) stepped solid beam to reproduce the conicity;
- (d) stepped hollow beam to reproduce the conicity and the medulla.

The bearing reactions of a first simulation of the presented modification stages are shown in Figure 7.4. Thereby an object scanning was performed with the model of a clamping for the different beam models. It becomes clear that a cavity in the beam leads to a reduction of the signal strength. Furthermore, a significantly reduced signal strength also occurs in the stepped beam. In this model, an additional cavity, as before, leads to a reduction in signal strength (see figure 7.5). Furthermore, the first simulation did not provide any new insights into the signal strength. However, some parameter studies should be performed for this bar modification to confirm the correctness of this statement.

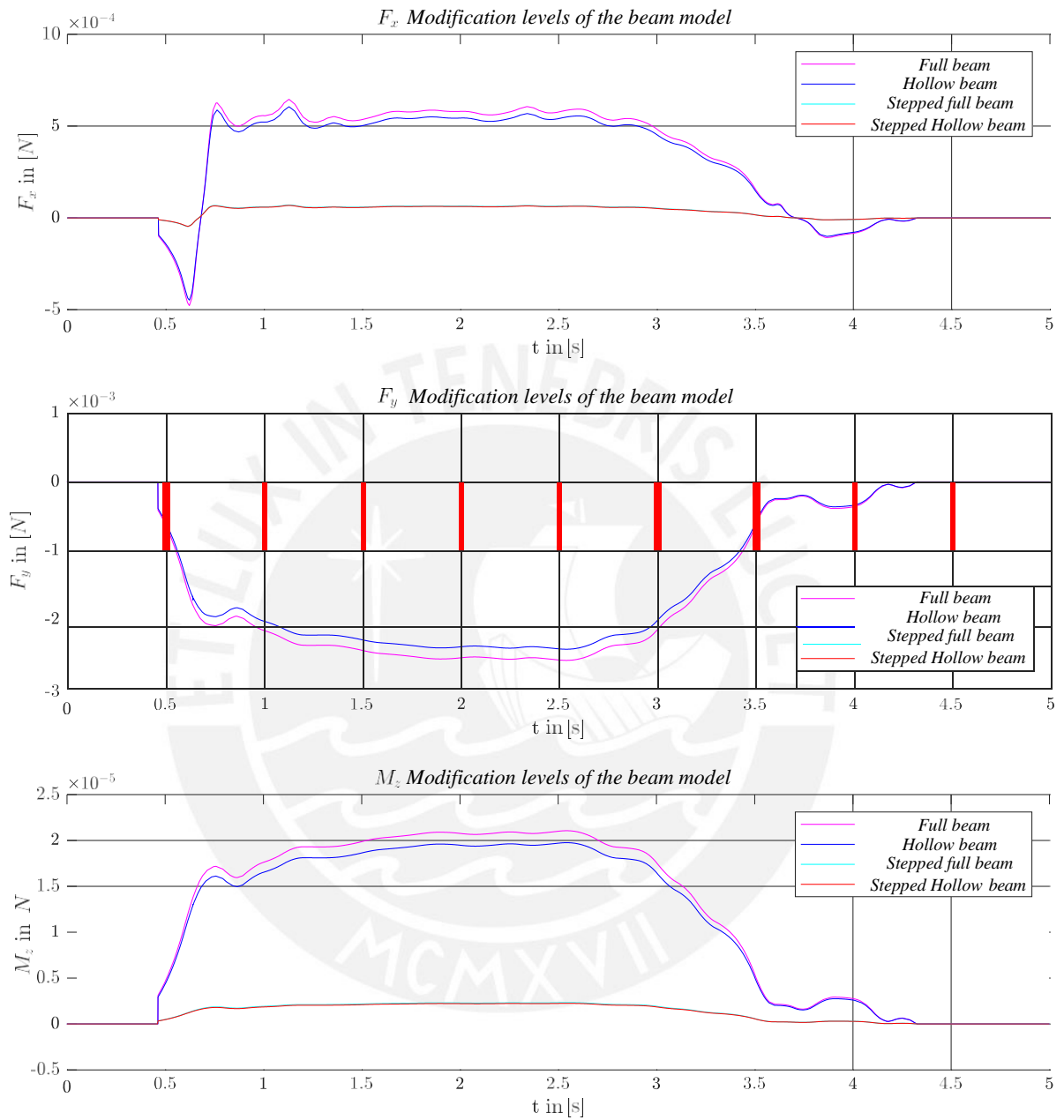


Figure 7.4: bearing reaction over time t for the model with restraint by variation of the modification levels of the beam model.

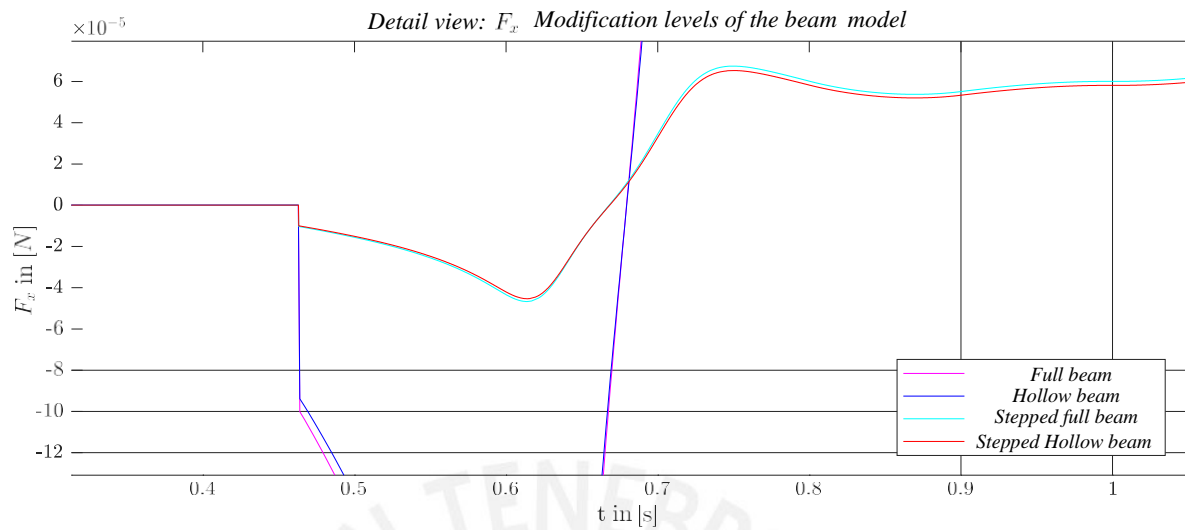


Figure 7.5: Detailed view of the force F_x of the bearing reaction over time t for the model with restraint while varying the modification levels of the beam model.

Since a surface on which the animals move is not always flat, further investigations should be carried out to determine the geometry of the surface. For this purpose, a first test as shown in figure 7.6 was simulated. A circular contour with the radius $R_k = 0.0002m$ at the position $x_{g1} = -0.012m$ and a ramp contour with an angle of rise of $\alpha_{g2,an} = 25^\circ$ and an angle of fall of $\alpha_{g2,ab} = 45^\circ$ at a center point position $x_{g2} = -0.01m$ from the object, which leads to a change of the contact point movement and thus to a change of the bearing reactions when scanning (see fig. 7.7). Differences in the signals can be seen, depending on the geometry. In order to be able to make a more precise statement about the behavior when scanning different objects, further simulations must be carried out.

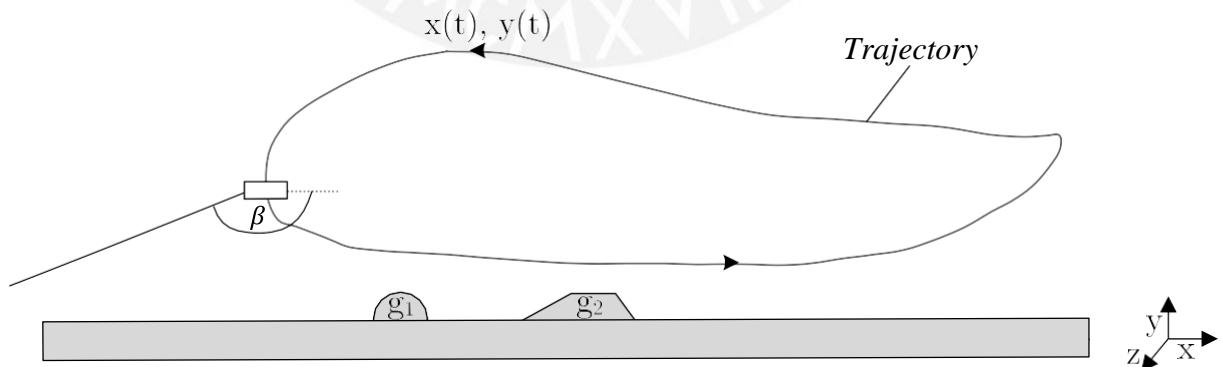


Figure 7.6: Path of motion with exemplary representation of different object contours g_1 and g_2 .

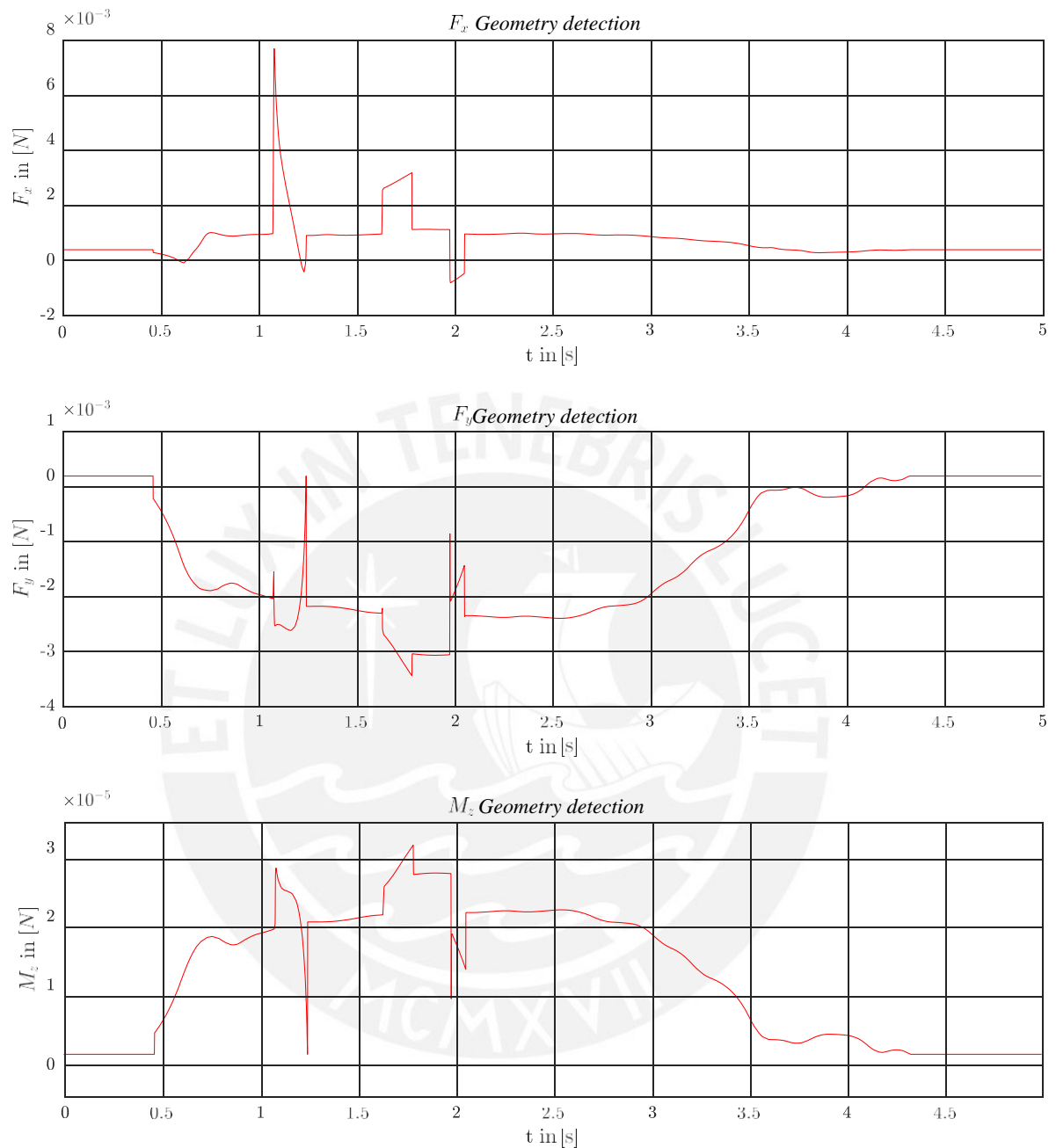


Figure 7.7: Bearing reaction over time t for the model with clamping when detecting circle contour g_1 and ramp contour g_2 .

In the following, further aspects are briefly described as an outlook for future investigations:

- **Consideration of the tangential contact:**

Within the scope of the investigations, only a single contact point at the tip has been implemented so far. Further contact points along the hair shaft should be considered, especially with regard to object scanning.

- **Extension of the simulation model by a pre-curvature of the vibrissae:**
In biology, vibrissae are pre-curved next to the conicity. This biological property should be considered in further investigations for a more realistic reproduction.
- **Optimize motion trajectory:**
Optimization potential can also be seen in relation to the movement trajectory. On the one hand, the simulations performed do not take into account any rotation of the paw when moving. In reality, however, there is an angle change of the vibrissae attachment. This should be considered for further investigations. On the other hand, the trajectory with a severed rat paw has been created. This trajectory should be updated by analysis of an animal motion sequence, using a live rat.
- **Extension of the model for a spatial problem:**
So far the model is limited to a flat problem. However, a three-dimensional scanning is desirable. Therefore the existing model for scanning should be extended to a spatial problem under consideration of a motion trajectory.
- **Extension of the model by further vibrissae:**
In the biological model of the rat, carpal vibrissae of a rat occur in groups of three tactile hairs on the paw. For this reason, further beams should be integrated into the model and coupled together following the example of nature.
- **Vibrissae angle to the scanning surface:**
Figure 7.8 shows the arrangement of three carpal vibrissae on one paw. It is obvious that the two outer hairs are at an angle to the path of motion. This angle leads to a change in the load on the hair and should therefore be considered in the simulation model.

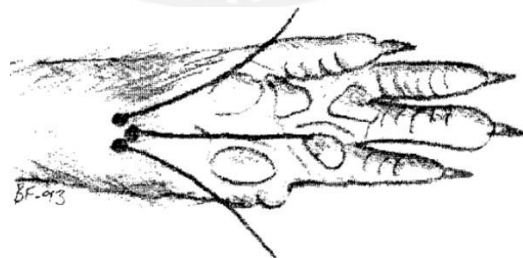


Figure 7.8: Arrangement of three carpal vibrissae on a rat's paw [ARF95].

Bibliography

- [AAC⁺17] AUMÜLLER, G. ; AUST, G. ; CONRAD, A. ; ENGELE, J. ; Kirsch, J.: *Duale Reihe Anatomie*. Bd. 4. Thieme, 2017. – ISBN 978-3-13-241752-6
- [AK11] AHISSAR, E. ; KNUITSEN, P. M.: Vibrissal location coding. In: *Scholarpedia* 6 (2011), Nr. 10, S. 6639. – revision #151626
- [ARF95] ARVIDSSON, J. ; RICE, F. L. ; FUNDIN, B. T.: Innervation of nonmystacial vibrissae in the adult rat. In: *The Journal of Comparative Neurology* 357(4) (1995), S. 501–512
- [Bau89] BAUMANN, W.: *Grundlagen der Biomechanik: 14. Studienbrief der Trainerakademie Köln des Deutschen Sportbundes*. Bd. 14. Hofmann, 1989. – ISBN 978-3-7780-8141-9
- [BAW⁺17] BEHN, C. ; ACKERMANN, L. ; WILL, C. ; HELBIG, T. ; STEIGENBERGER, J.: Vibrissa-Based design of tapered tactile sensors for object sensing. In: *59 th. Ilmenau Scientific Colloquium, Technische Universität Ilmenau, Deutschland, 11 - 15 September 2017* (2017)
- [BCD⁺17] Busch, M. ; CHOURBAJI, S. ; DAMMANN, P. ; FINGER-BAIER, K. ; GEROLD, S. ; HAEMISCH, A. ; JIRKOF, P. ; OSTERKAMP, A. ; OTT, S. ; PETERS, S. ; SPEKL, K.: Tiergerechte Haltung von Laborratten / Ausschuss für Tiergerechte Labortierhaltung. 2017. – Forschungsbericht
- [Ber14] BERG, M.: *Kinematik der räumlichen Führung carpaler Vibrissen*, Technische Universität Ilmenau, Bachelorarbeit, 2014

- [BETV11] BOMMAS-EBERT, U. ; TEUBNER, P. ; VOß, R.: *Kurzlehrbuch. Bd. 3: Anatomie und Embryologie*. Thieme, 2011. – ISBN 9783131355331
- [BK03] BERG, R. W. ; KLEINFELD, D.: Rhythmic whisking by rat: retraction as well as protraction of the vibrissae is under active muscular control. In: *Journal of Neurophysiology* 89(1) (2003), S. 104–117
- [BPM96] BRECHT, M. ; PREILOWSKI, B. ; MERZENICH, M. M.: Functional architecture of the mystacial vibrissae. In: *Behavioural Brain Research* 84(1-2) (1996), S. 81–97
- [Bra16] BRAND, M.: *FEM-Praxis mit SolidWorks: Simulation durch Kontrollrechnung und Messung verifizieren*. Bd. 3. Springer Vieweg, 2016. – ISBN 9783658093860
- [Car09] CARL, K.: *Technische Biologie des Tasthaar-Sinnessystems als Gestaltungsgrundlage für taktile stiftführende Mechanosensoren*, Technische Universität Ilmenau, Dissertation, 2009
- [CS90] CARVELL, G. E. ; SIMONS, D. J.: Biometric analyses of vibrissal tactile discrimination in the rat. In: *The Journal of Neuroscience* 10(8) (1990), S. 2638–2648
- [Dru18] DRUNK, G: Taktile Messtechnik. In: *Lexikon* (2018)
- [Eck20] ECKHARDT, S.: *Contribution to artificial tactile sensors for object contour recognition using coupled technical vibrissae*, Technische Universität Ilmenau, Masterarbeit, 2020
- [Elk16] ELKMANN, N: Mensch Roboter Kollaboration. In: *Fraunhofer IFF* (2016)
- [Eng17] ENGELHARDT, T: *Derating-Strategien für elektrisch angetriebene Sportwagen*. Bd. 1. Springer Vieweg, 2017. – ISBN 978-3-658-18207-6
- [FSS⁺02] FISCHER, M. S. ; SCHILLING, N. ; SCHMIDT, M. ; D., Haarhaus ; H., Witte: Basic limb kinematics of small therian mammals. In: *Institut für Spezielle Zoologie und Evolutionsbiologie* 205 (2002), S. 1315–1338
- [FSS16] FALLER, A. ; SCHÜNKE, M. ; SCHÜNKE, G.: *Der Körper des Menschen: Einführung in Bau und Funktion*. Bd. 17. Thieme, 2016. – ISBN 978-3133297172
- [GHSW19] GROSS, D. ; HAUGER, W. ; SCHRÖDER, J. ; WALL, W. A.: *Technische Mechanik: Statik*. Bd. 14. Springer Vieweg, 2019. – ISBN 978-3662591567

- [GIY73] GOTTSCHALDT, K. M. ; Iggo, A. ; YOUNG, D. W.: Functional characteristics of mechanoreceptors in sinus hair follicles of the cat. In: *Journal of Physiology* 235(2) (1973), S. 287–315
- [Har15] HARTMANN, M.: Vibrissa mechanical properties. In: *Scholarpedia* 10(5) (2015), S. 6636. – revision #151934
- [Hic08] HICKMAN, C.P.: *Zoologie*. Bd. 13. Pearson Studium, 2008. – ISBN 978–3827372659
- [HM86] HUTSON, K. A. ; MASTERTON, R. B.: The sensory contribution of a single vibrissa's cortical barrel. In: *JNP* 56(4) (1986), S. 1196–1223
- [HVN⁺14] HELBIG, T. ; VOGES, D. ; NIEDERSCHUH, S. ; SCHMIDT, M. ; WITTE, H.: The mechanics of carpal vibrissae of *rattus norvegicus* during substrate contact. In: *Shaping the Future by Engineering: Proceedings ; 58th IWK, Ilmenau Scientific Colloquium, Technische Universität Ilmenau, Deutschland, 8-12 September 2014* 58 (2014)
- [IB03] IONESCU, T. ; BÖGELSACK, G.: Terminology for the mechanism and machine science. In: *Pergamon Press* 38 (2003), S. 597–1111
- [Jen74] JENKINS, F. A.: The movement of the shoulder in clavicate and aclave mammals. In: *Journal of Morphology* 144 (1974), S. 71–84
- [Kla99] KLAUER, G. J.: *Vibrissen Analyse eines taktilen Sinnesorgans Band 1*, Universität Gesamthochschule Essen, Habilitationsschrift, 1999
- [Kle03] KLEIN, B.: *Grundgleichungen der linearen Finite-Element-Methode*. Vieweg+Teubner Verlag, 2003. – ISBN 978–3–8348–0296–5
- [KMB⁺01] KRUPA, D. J. ; MATELL, M. S. ; BRISBEN, A. J. ; OLIVEIRA, L. M. ; NICOLELIS, M. A. L.: Behavioral Properties of the Trigeminal Somatosensory System in Rats Performing Whisker-Dependent Tactile Discriminations. In: *The Journal of Neuroscience* 21(15) (2001), S. 5752–5763
- [KS09] KIENZLER, R. ; Schröder, R.: *Einführung in die Höhere Festigkeitslehre*. Bd. 1. Springer Berlin Heidelberg, 2009. – ISBN 978–3–540–89325–7
- [Leh99] LEHMANN, K.: Extremitäten. In: *Spektrum* (1999), S. 1–5
- [LM10] LYTLE, C.F. ; MEYER, J.R.: *Praktikum Allgemeine Zoologie*. Bd. 15. Pearson Studium, 2010. – ISBN 978–3868940350

- [MBSZ19] MERKER, L. ; BEHN, C. ; STEIGENBERGER, J. ; ZIMMERMANN, K.: Vibrissa-based sensor models with compliant support for object detection. In: *12th HSTAM International Congress on Mechanics Thessaloniki, Griechenland, 22 - 25 September 2019* (2019)
- [Mec19] MECHATRONIK, Institut für: *alaska 9: Modellierung und Simulation mechatronischer Systeme.* (2019)
- [MF11] MÜLLER, W. H. ; FERBER, F.: *Technische Mechanik für Ingenieure.* Bd. 4. Carl-Hanser-Verlag, 2011. – ISBN 9783446427693
- [MGA⁺11] MITCHINSON, B. ; GRANT, R. ; ARKLEY, K. ; RANKOV, V. ; PERKON, I. ; PRESCOTT, T.: Active vibrissal sensing in rodents and marsupials. In: *Philosophical transactions of the Royal Society of London. Series B, Biological sciences* 366(1581) (2011), S. 3037–3048
- [MH73] MARSHALL, P. T. ; HUGHES, G. M.: *Skelett, Muskulatur und Bewegung.* Bd. 17. Birkhäuser Basel, 1973. – ISBN 978-3-0348-5963-9
- [PMG11] PRESCOTT, T. J. ; MITCHINSON, B. ; GRANT, R. A.: Vibrissal behavior and function. In: *Scholarpedia* 6(10) (2011), S. 6642. – revision #189995
- [RS17] RILL, G. ; SCHAEFFER, T.: *Grundlagen und Methodik der Mehrkörpersimulation: Vertieft in Matlab-Beispielen, Übungen und Anwendungen.* Bd. 3. Springer Fachmedien Wiesbaden, 2017. – ISBN 978-3658160081
- [SBH⁺10] SIMONY, E. ; BAGDASARIAN, K. ; HERFST, L. J. ; BRECHT, M. ; AHISSAR, E. ; GOLOMB, D.: Temporal and spatial characteristics of vibrissa responses to motor commands. In: *The Journal of Neuroscience* 30(26) (2010), S. 8935–8952
- [Sch01] SCHLEIF, O.: *Ein Beitrag zur tiergerechten Haltung der Ratte anhand der Literatur,* Tierärztliche Hochschule Hannover, Diplomarbeit, 2001
- [Sch03] SCHIERLOH, A.: *Neuronale Netzwerke und deren Plastizität im Barrel-Kortex der Ratte,* Technischen Universität München, Diplomarbeit, 2003
- [Sen97] SENDLER, U.: *Neue Wege zur Produktentwicklung / Wissenschaftliches Forum für Produktentwicklung e. V.* 1997. – Forschungsbericht
- [SH16] SHABANA, A. A. ; HEINISCH, C.: *Einführung in die Mehrkörpersimulation.* Bd. 1. Wiley, 2016. – ISBN 978-3-527-33664-7

- [SK87] SOKOLOV, V. E. ; KULIKOV, A.: The Structure and Function of the Vibrissal Apparatus in some Rodents. In: *Mammalia* 51(1) (1987)
- [Sk111] SKLADNIKIEWITZ, M.: Taktil oder optisch: Welche Messtechnik bietet welche Vorteile? In: *Know-How* (2011)
- [Smi09] SMITH, C. U. M.: *Biology of sensory systems*. Bd. 2. Wiley-Blackwell, 2009. – ISBN 9780470518632
- [Ste13] STEIGENBERGER, J.: A continuum model of passive vibrissae. In: *Preprint / Technische Universität Ilmenau, Institut für Mathematik* (2013)
- [SWZ⁺14] SCHMIDT, M. ; WITTE, H. ; ZIMMERMANN, K. ; NIEDERSCHUH, S. ; HELBIG, T. ; VOGES, D. ; HUSUNG, I. ; VOLKOVA, T. ; WILL, C. ; BEHN, C. ; STEIGENBERGER, J. ; KLAUER, G. J.: Technical, non-visual characterization of substrate contact using carpal vibrissae as a biological model: an overview. In: *58th Ilmenau Scientific Colloquium, Technische Universität Ilmenau, Deutschland, 8 - 12 September 2014* (2014)
- [VCK⁺12] VOGES, D. ; CARL, K. ; KLAUER, G. J. ; UHLIG, R. ; SCHILLING, C. ; BEHN, C. ; WITTE, H.: Structural Characterization of the Whisker System of the Rat. In: *Sensors Journal, IEEE* (2012), S. 332–339
- [WBS17] WILL, C. ; BEHN, C. ; STEIGENBERGER, J.: Object contour scanning using elastically supported technical vibrissae. In: *ZAMM - Journal of Applied Mathematics and Mechanics* 98 (2017), S. 1–17
- [Wel18] WELSCH, B.: Neues gkf Projekt: Feine Antennen. In: *Info* 47 (2018)
- [WF19] WEDLER, G. ; FREUND, H.: *Lehr- und Arbeitsbuch Physikalische Chemie*. Bd. 1. Wiley-VCH Verlag GmbH, 2019. – ISBN 9783527334261
- [WHF97] WALKER, W. F. ; HOMBERGER, D. G. ; FINE, L.: *Anatomy and dissection of the rat*. Bd. 3. W. H. Freeman, 1997. – ISBN 978-0716726357
- [Zen14] ZENTNER, L.: *Nachgiebige Mechanismen*. De Gruyter, 2014

Bearing reactions for directional and angular forces

N : Numerical calculation

MKS: Multibody system calculation

Table A.1: Angular Force Amplitude Variation.

Angular force amplitude varies:	F_x	F_y	M_z
N: $F = 1N$	0,8795	0,4758	0,9755
MKS: $F = 1N$	0,9311	0,5075	1,0279
N: $F = 3N$	0,5139	2,9557	2,4313
MKS: $F = 3N$	0,5295	3,0606	2,5185
N: $F = 5N$	-2,5163	4,3207	2,9396
MKS: $F = 5N$	-2,6064	4,4662	3,0413
N: $F = 7N$	-5,9366	3,7091	2,7236
MKS: $F = 7N$	-6,0587	3,8178	2,8300
N: $F = 10N$	-9,8894	1,4833	1,7224
MKS: $F = 10N$	-9,9876	1,4674	1,8232

Table A.2: Angular Force Point Variation.

Angular force application point varies:	F_x	F_y	M_z
N: $S1 = 30\%$	0,9990	0,0450	0,2999
MKS: $S1 = 30\%$	1,0384	0,0477	0,3134
N: $S1 = 50\%$	0,9922	0,1246	0,4992
MKS: $S1 = 50\%$	1,0367	0,1320	0,5238
N: $S1 = 70\%$	0,9703	0,2421	0,6958
MKS: $S1 = 70\%$	1,0194	0,2593	0,7321
N: $S1 = 100\%$	0,8795	0,4758	0,9755
MKS: $S1 = 100\%$	0,9311	0,5075	1,0279

Table A.3: Directional force amplitude variation.

Directional scatter Force amplitude varies:	F_x	F_y	M_z
N: $F = 1N$	1	0	0,9437
MKS: $F = 1N$	1,0472	0,0035	0,9851
N: $F = 3N$	3	0	2,2367
MKS: $F = 3N$	3,1103	0,0026	2,3183
N: $F = 5N$	5	0	3,0619
MKS: $F = 5N$	5,2385	0,0674	3,2040
N: $F = 7N$	7	0	3,6895
MKS: $F = 7N$	7,2107	0,0477	3,8007
N: $F = 10N$	10	0	4,4500
MKS: $F = 10N$	10,3494	0,0190	4,6039

Table A.4: Directional force application point variation.

Directional scatter Force application point varies:	F_x	F_y	M_z
N: $S1 = 30\%$	1	0	0,2998
MKS: $S1 = 30\%$	1,0395	0,0005	0,3133
N: $S1 = 50\%$	1	0	0,4979
MKS: $S1 = 50\%$	1,0448	0,0006	0,5223
N: $S1 = 70\%$	1	0	0,6893
MKS: $S1 = 70\%$	1,0498	0,0041	0,7239
N: $S1 = 100\%$	1	0	0,9436
MKS: $S1 = 100\%$	1,0472	0,0035	0,9851

APPENDIX **B**

Muscles of the front extremity and their function

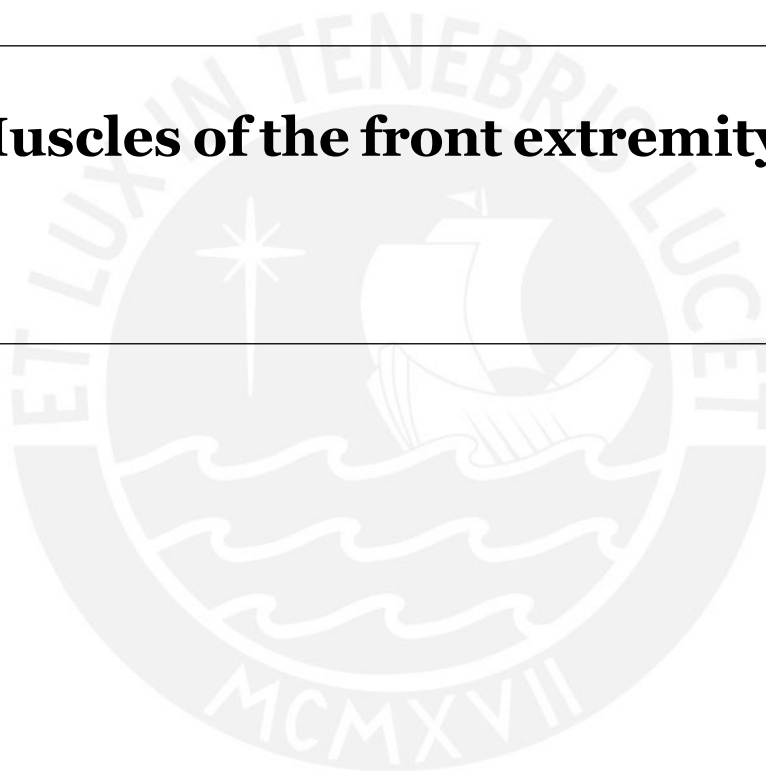


Table B.1: Muscles of the shoulder joint and their function [Ber14].

	<i>lat. Bezeichnung</i>	<i>Funktion</i>
Muskeln des Schultergelenks	M. trapezius	Stützen der Scapula
	Pars clavicularis	zieht Scapula und Clavicula nach vorne (anterior)
	Pars cervicalis	zieht die Scapula nach medial
	Pars thoracica	zieht die Scapula nach kaudal
	M. omotransversarius	zieht die Scapula nach vorne
	M. deltoideus	Zusammen bewirken die Partes eine Abduktion der Vordergliedmaße und verhindern eine Adduktion des Humerus
	Pars scapularis	laterale Gelenkstabilisierung, unterstützt Humerusretraktion
	Pars clavicularis (auch M. cleidobrachialis)	zieht den Arm nach vorne sowie schwach nach innen, Gelenkstabilisierung
	Pars acromialis	streckt und dreht den Humerus medial, Gelenkstabilisierung
	M. latissimus dorsi	streckt und zieht den Oberarm heran, zieht die Schulter nach hinten
	M. pectoralis profundus	Adduktion und Retraktion der Vordergliedmaße
	M. pectoralis superficialis	Adduktion und Retraktion der Vordergliedmaße
	M. teres major	dreht den Humerus caudoventral (Adduktion) und beteiligt sich am Rückführen des Armes
	M. teres minor	dreht den Humerus caudolateral und trägt zum Beugen des Schultergelenks bei und stützt dieses
	M. supraspinatus	zieht Humerus nach vorne; Verhindert passive Gelenkflexion während Stützphase
	M. infraspinatus	zieht Humerus nach hinten und dreht ihn leicht nach außen, Gelenkstabilisierung
	M. rhomboideus capitis	zieht die Scapula cranial
	M. rhomboideus cervicis	zieht die Scapula medial
	M. rhomboideus thoracis	zieht die Scapula medial
	M. serratus ventralis cervicis	zieht die Scapula nach vorne (Rückführen der Gesamtgliedmaße)
M. serratus ventralis thoracis	zieht die Scapula herab (Vorführen der Gesamtgliedmaße) und befestigt die Vorderextremität am Brustkorb	
M. subscapularis	Adduktion des Humerus und Stabilisierung der Schulter	

Fortsetzung auf nächster Seite

Table B.2: Muscles of the elbow joint and their function [Ber14].

	<i>lat. Bezeichnung</i>	<i>Funktion</i>
Muskeln des Ellenbogengelenks	M. triceps brachii	Extension des Unterarmes; Stützen und Stabilisieren des Armes während Stützphase; Fixator des Ellenbogengelenks
	Caput mediale	Extension des Ellenbogengelenks
	Caput laterale	Extension des Ellenbogengelenks
	Caput longum	beugt das Schultergelenk, bewirkt zusätzlich eine leichte Adduktion und Retroversion der Vordergliedmaße
	M. biceps brachii	Flexion des Ellenbogengelenks, Extension des Schultergelenks, Fixator des Schulter- und Karpalgelenks; verhindert Streckung am Ende der Bodenkontaktphase
	Caput longum	schwache Abduktion sowie leichte Innenrotation des Armes
	Caput breve	schwache Adduktion des Armes
	M. brachialis	beugt den Ellenbogen (Flexion)
	M. coracobrachialis	Fixierung des Humerus in der Gelenkpfanne, zudem Beteiligung an Adduktion, Anteversion und Innenrotation des Armes
	M. anconeus epitrochlearis	Extension des Unterarmes, Stabilisierung des Ellenbogens, zieht Ulna medial während der Supination
M. tensor fasciae antebrachii	Streckung des Ellenbogengelenks, Beugung des Schultergelenks, Spannen der Fascia antebrachii	
M. pronator teres	Pronation des Unterarmes, Flexion des Ellenbogengelenkes	
M. pronator quadratus	Pronation des Unterarmes, Flexion des Unterarms	
M. supinator	Supination des Unterarms, Stabilisieren des Unterarms	
<i>Fortsetzung auf nächster Seite</i>		

Table B.3: Muscles of the carpal joints and their function [Ber14].

	<i>lat. Bezeichnung</i>	<i>Funktion</i>
Muskeln der carpalen und digitalen Gelenke	M. flexor carpi radialis	bewirkt Flexion im Handgelenk und Radialabduktion, unterstützt Pronation
	M. extensor carpi radialis	Streckung und Fixation des Karpalgelenks
	M. flexor carpi ulnaris	Beugung des Handgelenks, Ulnarabduktion
	M. extensor carpi ulnaris	Extension des Handgelenks, Ulnarabduktion
	M. palmaris longus	Flexion des Handgelenks
	M. extensor digitorum communis	Streckung der Phalangen und des Handgelenks
	M. flexor digitorum profundus	Beugung der Phalangen und des Handgelenks, Fixierung des Karpalgelenks
	M. flexor digitorum superficialis	Beugung der Phalangen bis zum mittleren Fingerglied, Fixierung des Karpalgelenks
	M. extensor indicis proprius	Extension des Handgelenks
	Mm. interossei palmares	Adduktion der Fingergelenke, Träger des Körpergewichts im Stand
	Mm. interossei dorsales	Abduktion der Fingergelenke, Beteiligung an der Flexion der Phalangen in den Grundgelenken, Träger des Körpergewichts im Stand
	Mm. lumbricales	Flexion der Phalangen in den Grundgelenken und Extension in den Endgelenken, Stützfunktion im Stand
	M. extensor indicis proprius	Extension des Handgelenks, Stabilisierung während Stützphase
	M. extensor pollicis	Stabilisieren des Unterarms
	M. extensor digiti quarti	Extension des 4. Fingers, Stabilisierung während Stützphase
	M. extensor digiti quinti	Extension des 5. Fingers, Stabilisierung während Stützphase
		Eminentia hypothenaris (M. abductor digiti V, M. flexor digiti V)
	Eminentia thenaris (M. abductor pollicis, M. flexor pollicis brevis, M. adductor pollicis)	Bilden den Daumenballen und dienen der Beweglichkeit der gesamten Hand